POLITECNICO DI MILANO

SCUOLA DI INGEGNERIA INDUSTRIALE E DELL'INFORMAZIONE

DIPARTIMENTO DI ELETTRONICA, INFORMAZIONE E BIOINGEGNERIA

CORSO DI LAUREA MAGISTRALE IN INGEGNERIA BIOMEDICA

DESIGN AND VALIDATION OF A VISCOELASTIC MICROFLUIDIC DEVICE FOR SPERM CELLS RETRIEVAL FOR MALE INFERTILITY APPLICATIONS

Relatore:
Prof. Marco Rasponi

Co-relatore:

Prof. Simone Vesentini

Prof. Andrea Salonia

Prof. Ian Papautsky

Tesi Magistrale di:

Ludovica Barilla 919749

Anno Accademico: *2019-2020*

A mia nonna Anna,
ovunque tu sia

ACKNOWLEDGMENTS

As this university path comes to an end, the least I could do is thank all the people who made this journey possible; I would have bought a drink to everyone cited here, of course, but this pandemic makes it impossible logistically; maybe next graduation, maybe not.

First of all, a big thank you goes to my advisor, Professor Rasponi, who always supported me since the very beginning of my career, when as a student I shily submitted two different designs for the lab training and he wisely chose the Batman-logo one, till this last period of academic research and hard work. With his example, he taught me how to become a resourceful person and to cope with all the difficulties that I encountered. He also valued my opinions and encouraged me by giving me the possibility of conducting a whole research study without restrictions and allowing me to learn how to become independent and enterprising. I also have to express my gratitude to professor Vesentini, who patiently supported and bore all my crazy proposals, from the allegations about Ant-Man and its inconsistencies with quantum physics when I was just one of his students, to the very practical needs of this thesis research. He helped me through all the steps of this final journey with kindness and passion; he has to be thanked not only for making the collaboration with San Raffaele Hospital possible, but also because he showed me enthusiasm and empathy all the way.

A big thank you goes to prof. Papautsky, without whom this project would not have been possible; he allowed me to start the very first steps of this research while I was in Chicago and after I was not of his students anymore, he gave me the chance to participate in my very first conference, trusting my abilities and believing in my determination. I hope our paths will cross again.

My appreciation goes to professor Salonia, who welcomed me in its laboratory and team, and gave me the possibility to make this project feasible. Many thanks to Dr. Alfano for his prompt suggestions, and to Dr. Locatelli for her valuable assistance in the hospital lab. Another big thank you goes to Dr. Covino, who patiently helped me with my microscope work and complied with all my crazy requests.

I could not forget to thank all my lab mates who helped me and shared with me an important part of my life; in particular, Erika: thank you your guidance and relentless support; thank you Sara for our long

conversations about everything and nothing, which made me feel part of something bigger; and thank you Fahrad for the beautiful friendship born from common miseries and arrived at shared lunch and chat about life; I will miss our adventures.

Of course, not all the support I received came to the academic world and since this pandemic made everything a challenge, I really have to express all my thankfulness to all the people that helped me day through day.

I would like to thank my Red Cross team of emergency rescuers: they are a second family to me and their presence, support, and cheering during every shift gave me the strength to cope with this awful sanitary emergency while working and studying.

A big thank you goes to my big and loud family: aunt Rosella, uncle Giuseppe, Serena, Samuela, Sonia, Cecè, and Sofia; our lunches, dinners, and time spent together were the breaths of fresh air I needed in this particular time. Thanks for loving me despite my moods.

Thank you Mahaut for our long-distance friendship; even though it has been a year since we last saw each other in person, you always found time to call me, to check on me, and update one another with our life. I cannot wait to see you again and have dinner together with a white glass of wine.

Thank you Francesco (AKA Fratm): I did not expect our friendship to last even without eating deep pizza or tiramisu together. But yet, here we are. Thanks for bearing every stupid thing and proposal that come out of my mouth and for being there when I needed you.

Thank you Francesca, our friendship is one of the oldest ones I have and, even though months could go by without speaking to each other, I know I can always count on you and it always feels like no time has passed. I wish we grow old and become very annoying together, eventually.

My long-time appreciation goes to Marta and Gebba: your presence in time of need never failed and our times together will not be forgotten. Thank you, I'm looking forward to our next reunion.

A big thank you to my Lonatesi friends: Valeria, Johnny, Serena e Much; even thought this pandemic didn’t allow us to see each other, I know you were always there and ready to share good news and happy thoughts in this sad time.

A lot of gratitude goes to my Giropasta or Topini friends: Alessandro, Chiara M., Chiara T., Giulia, Laura, Marco, Paolo, Stefano, Roberta, and Serena; you were always by my side and no pandemic could stop our friendship. We always found a way to spend time together even if it meant playing a super silly online Nome, Cose e Città or just leaving a note or a little gift on the gate. I really cannot way to hug you all again and re-join our adventures together (no helicopter this time, I promise).

A big grazie to my aunt Maria, who still doesn't know what I am studying, why I had to go all around the world to get my degree or why I do have to work all the time. But you make me frittelle and meatballs anyway and this is the fuel I need for everything I do.

Here we are to the final part, where you may have to get a tissue: otherwise you could wet my thesis and, since it was expensive to print, I prefer you not to ruin it; so, watch out. A thank you to my parents is never enough. This is the third time I have to express my feeling of gratitude and appreciation for you, and I still don’t know where to start. I said thousands of times I could not be where I am without you and it is always true. You gave me everything, from the material possibility to go to Chicago and to become the independent and strong woman I am today, to every little encouragement for my job and my life. Even if I keep on challenge you with my problems, you always find a way to get me up again and face all my problems head-on, no matter what. I do not know what I would do without your support and love. I could not be luckier to have such a wonderful and supportive family. Thank you, for real. I would like to thank you Giovanni, my little brother: you are not little anymore, and you will probably resent me for keep saying it. You are a lovely young man who care a lot about me, even though you don't show it very much; you help me with all the things that matter (for sure going downstairs to pick up things from the basement is not one of them, but it’s okay). Life without you would be so much boring.

Last but not least, a lot of appreciation goes to Tommaso. Despite my particular character you are able to bear me and love me, even after 9 years, a high school exam, and three degrees. Not only do you help me with statistics, grammar corrections, or prescriptions, but you also patiently comply with all my craziness, stubbornness, and paranoia while still being able to support me no matter what and love me matter what. You are the apple of my eyes, my fellow companion, and I wish to spend as many other years of lifetime adventures with you by my side.

Just kidding, he was not the last. The real thank you and true love go to my parrots Rio and Paco (and Tokyo, wherever you are with grandma). The endless cuddles and affection you are showing me are making my heart exploding with joy for having you in my life. Cannot way to teach you how to say bad words and to call me Ing.

L.B.

TABLE OF CONTENT

LIST OF TABLES

LIST OF FIGURES

LIST OF ACRONYMS

PDMS = Polydimethylsiloxane

PS = Polystyrene

RBC = Red Blood Cells

WBC = White Blood Cells

PBMC = Peripheral Blood Mononuclear Cells

PEO = Polyethylene Oxide

PVP = Polyvinylpyrrolidone

PAM = Polyacrylamide

AR = Aspect Ratio

BR = Blockage Ratio

PEB = Post-Exposure Bake

FWHM = Full Width at Half Maximum

MESA = Microsurgical Epididymal Sperm Aspiration

PESA = Percutaneous Epididymal Sperm Aspiration

TESA = Testicular Sperm Aspiration

TESE = Testicular Sperm Extraction

IVF = In-Vitro Fertilization

ART = Assisted Reproductive Technologies

WHO = World Health Organization

ROS = Reactive Oxygen Species

OS = Oxidative Stress

ICSI = Intracytoplasmic Sperm Injection

BF = Bright-Field

ABSTRACT

Introduction

Infertility is defined as the inability to conceive after one year of regular sexual intercourse without the use of contraceptives[1], and it has been estimated to affect more than 70 million couples around the world[2]. In particular, male infertility is recognized as the cause of more than half of the cases of global childness[1,2]. This pathologic state is always associated with health issues that must be taken into consideration. Indeed, the male-factor may occur due to several different reasons; among others, leukospermia, azoospermia, and hematospermia are serious pathologies with a similar effect[3-5], *i.e.* the presence in the semen of non-sperm cells such as white blood cells (WBCs) and/or red blood cells (RBCs) that could affect the fertilization ability of the spermatozoa and, in many cases, could be also correlated to sperm defects or can cause DNA fragmentation[3-5]. For all of these pathological conditions, which are recognized as the main causes of male infertility, there exist several methods used to obtain the separation of spermatozoa from all the other cells, such as the swim-up method and the density gradient centrifugation[1-5]. These techniques used to separate these cells from sperm cells are just the main ones, and along with the fact that they could only retrieve motile sperm cells and could require complicated equipment, they also need elevated time to perform, have an extremely high cost, but most of all they could increase the spermatozoa damage by eliminating the antioxidant factors that prevent and exaggerated the reactive oxygen species production; this latter is the major issue when we realize that the damage caused by WBCs in semen is done by elevated ROS levels. This is where microfluidics takes over and it can potentially overcome all the enumerated drawbacks: it has the potential to separate sperm cells from others by just implementing a sorting by shape and size, it does not require a labeling system or external forces, it would not eliminate the antioxidant factors, it can also recover less motile and non-motile sperm cells, and last but not least, it would be a cheaper and less time-consuming procedure[6]. Indeed, microfluidics can offer an easy, fast, efficient, cost-effective, operator-independent, and clinically feasible way to separate sperm cells from all the other cells present in the retrieved biopsy[7]. Furthermore, the microfluidic channel

can exploit the viscoelastic fluid to dilute and avoid the clogging of the device while assuring a compatible environment for the cells and eliminating the need for the mechanic or enzymatic additions to ensure a high-performance separation. To perform the separation by size and shape, viscoelastic microfluidic is exploited[9-13] and, specifically, the synergic effect of the inertial[8] and the elastic forces enable the displacement of bigger particles near the sidewalls while the smaller one focus at the center of the channel[9-13] (figure 1).

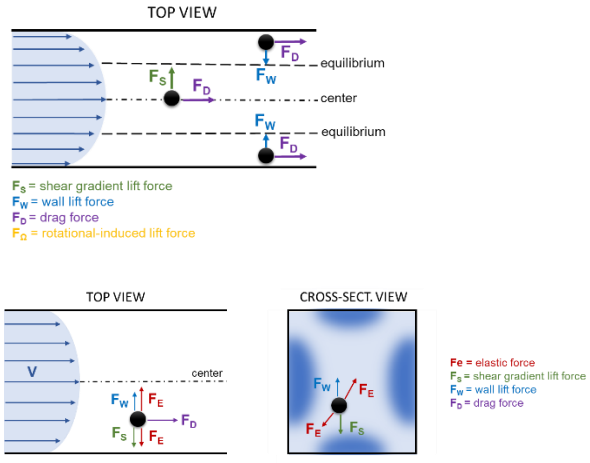

Figure 1 - Top and cross-section views of the forces acting on particles in a viscoelastic fluid.

The scope of this thesis project is to create a passive microfluidic device consisting of a straight channel with a rectangular cross-section that is able to perform the separation between spermatozoa and other cells that can be found in the semen or the biopsy fluid of a male testicle by exploiting the viscoelastic effect of the medium. In particular, the thesis has three main objectives: at first, to find the optimal conditions for sorting microparticles (with a size similar to target cells) based on their dimensions; secondly, to separate spermatozoa from leukocytes in order to obtain a pure sample of sperm cells for their subsequent use in in-vitro fertilization procedures; lastly, to achieve the optimal separation of spermatozoa from all the cells that could be found in the supernatant, so in the biopsy's tissues collected, such as red blood cells, leukocytes, cells debris, etc. This latter is needed to obtain a valuable device that supports clinicians after different procedures, such as testicular sperm extraction or just from samples of leukocytospermic patients, and permits pure spermatozoa extraction for optimized assisted reproductive procedures.

Materials and Methods

Two different straight microfluidic channels with a rectangular cross-section (figure 2) were produced using classic soft-lithography techniques. Both channels have a height of 30 µm, a length of the main straight body of 3cm,

and 3 different branches of 1.5cm before the outlets. The difference between the two channels is the width which is 50µm and 75µm for the first and the second channel, respectively. The aspect ratio (AR) of the channels is 1.67 for the 50µm x 30µm and 2.5 for the 75µm x 30µm channel. The open outlets' configuration (figure 2), with different ramifications after the main body and its expansion, was chosen to answer the necessity of controlling and adjusting the sorting cutoff, the fluid resistance, and resistance ratio so that the purity and separation efficiency can be changed and regulated by just changing the position of the punched outlets without having to redesign and refabricate the entire device.

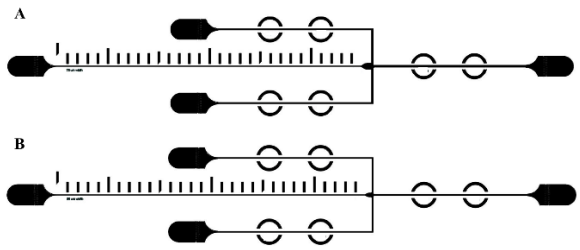

Figure 2 - Two different straight microfluidics channels with a rectangular cross-section. A) 75 µm x 30 µm channel, B) 50 µm x 30 µm channel.

The microfabrication process started with the creation of the microfluidic channels on AutoCAD, then the chosen pattern was transferred to a silica wafer of 4 inches by using laser inscription. The soft-lithography technique (figure 3) was used to create the PDMS devices but since the increasing of the production rate was necessary, before proceeding with the production, copies of the master were made with epoxy resin. The device production consisted of mixing PDMS monomer and curing agent with a ratio of 10:1; the mixture was then poured over the replica mold, degassed in a vacuum chamber for at least 20 min, and finally baked at 65°C for 2h. After this, PDMS replicas were peeled off from the mold, and the inlets and outlets were created with a puncher. Finally, the device was bonded to a glass slide by treating the surfaces with plasma oxygen; to ensure the bonding, the device was baked once again at 65°C for 1 h.

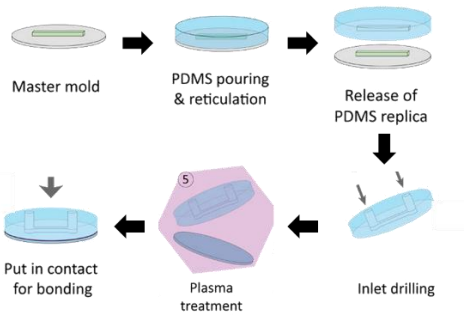

Figure 3 – Soft-lithography procedure: from the master mold to the final devices.

The viscoelastic medium for our project was created by diluting Poly(ethylene oxide) (PEO) (MW = 2 x 106 Da) in phosphate-buffered saline (PBS) to create a viscoelastic solution of

1000ppm that could match the osmolarity required by cells (290 mOsm/kg). To replicate the cells' behavior polystyrene microbeads were used; we decided to employ 4µm (~4.19µm), 7µm (~7.32µm), and 15µm (~15.25µm) particles because it has been shown that RBCs have a discoid shape with a mean diameter of 7-8µm[9], leukocytes are more spherical and have a mean diameter of 15µm while the spermatozoa have a much more complicated shape, which includes a tail and a head, but the most relevant dimension is our case is the head that has a flat ellipsoid shape of about 4µm x 3µm. The biological samples used, which were seminal fluid, spermatozoa, red blood cells, and leukocytes, were obtained from the waste of samples collected from healthy subjects that underwent a periodical check-up at Centro Scienze della Natalità of San Raffaele Hospital. The isolated spermatozoa were obtained by centrifuging the semen, the seminal fluid was simply diluted in our viscoelastic solution, and the erythrocytes were recovered from whole blood with the density gradient centrifugation. Unfortunately, the leukocytes could not be fully retrieved due to the massive presence of the RBCs and thus could not be used in the experiments. Finally, the solutions of spermatozoa mixed with RBCs or with the 15µm particles were created by following the specific procedure already explained and were just added together to obtain a concentration of about 3 x 10^6 cells/mL for the spermatozoa, 6 x 10^6 cells/mL for the erythrocytes and 2.5 x 10^6 particles/mL for the 15µm beads. The experimental procedure consists in pumping the sample solution into the microfluidic device using a syringe pump; then, the fluorescence images for the particles and the bright-field images for the biological samples were captured with An Inverted Phase Contrast Fluorescence Microscope (Zeiss Axio Observer Z1, Zeiss, Germany) fitted with a digital EMCCD camera (Hamamatzu, EM-CCD C9100, Japan). The analysis of data was possible thanks to different software: Volocity allow us to capture the images from the Zeiss Axio Observer Z1 Microscope, ImageJ, Excel, Origin Lab, R, and MatLab were used to perform the post-process analysis and to convert what we could observe qualitatively in quantitative data that could be analyzed.

Results and Discussion

To understand the influence of the different forces on the behavior of the corpuscles, we

compared the dynamics and analyzed the performances in our microchannel by considering the dimensionless parameters, such as Reynolds number (*Re*), which is defined as the ratio of the inertial force to the viscous force, Weissenberg number (*Wi*), which is the ratio between two different time constants, and Elasticity number (*El*), which measures the relative importance of elasticity to inertia.

The different sizes of polystyrene microbeads were firstly tested one at a time in the 50µm x 30µm channel; in particular, the behavior of the particles was investigated at different flow rates, from 5µL/min to 50µL/min, and the relative images acquired were then analyzed to obtain quantitative data of the intensity values and the focusing efficiencies. The equilibrium position of the 4µm PS microbeads in AR = 1.67 channel is achieved at the centerline for all flow rates with a focusing efficiency > 95% from 10µL/min to 25µL/min (figure 4). Also, the 7µm microbeads tend to focus on the center of the channel for every flow rate, and the performances of efficiency are higher than 93% for every flow rate > 5µL/min (figure 4). The 15µm beads, instead, reach in general two different focusing positions located near the sidewalls of the channel with a focusing efficiency always between 97% and 100%.

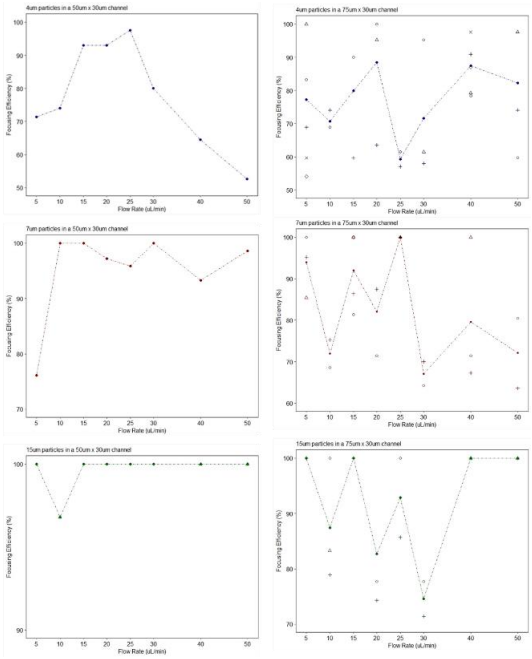

Figure 4 – Focusing efficiency values calculated for each flow rate and each particle size for the 50µm x 30µm.

Analogous experiments were performed in the 75µm x 30µm channel; this time the 4µm beads showed multiples streamlines gathered at the center of the channel; this affected the focusing efficiency values that were calculated, making them fluctuate between 60% and 90% (figure 4). The 7µm beads had similar behavior and could be found in the central 30-40µm while forming multiple streamlines; the focusing efficiency remained between 70% and 100% (figure 4). The 15µm particles, instead, formed most of the time two streamlines near the channel walls and three streamlines as the flow

rate increases but their focusing efficiency values were between 75% and 100%, with the majority of the values around 90% (figure 4).

Since the final aim of the project is sorting the different types of cells, the different behavior of the different particles in the same channel at the same flow rate was compared, as showed in figure 5 and 6. This allows a better understanding of the simultaneous equilibrium positions and thus, the visualization of the potential sorting. In the 50µm x 30µm channel (figure 25), from 5µL/min till 30µL/min, with the only exception of 10µL/min, the sorting of 4µm and 7µm particles from the 15µm particles could be feasible, while in the 75µm x 30µm channel the separation could be reached from 10µL/min to 30µL/min because the 4µm and 7µm particles streamlines can be usually found in the space between the two different equilibrium positions of the 15µm particles.

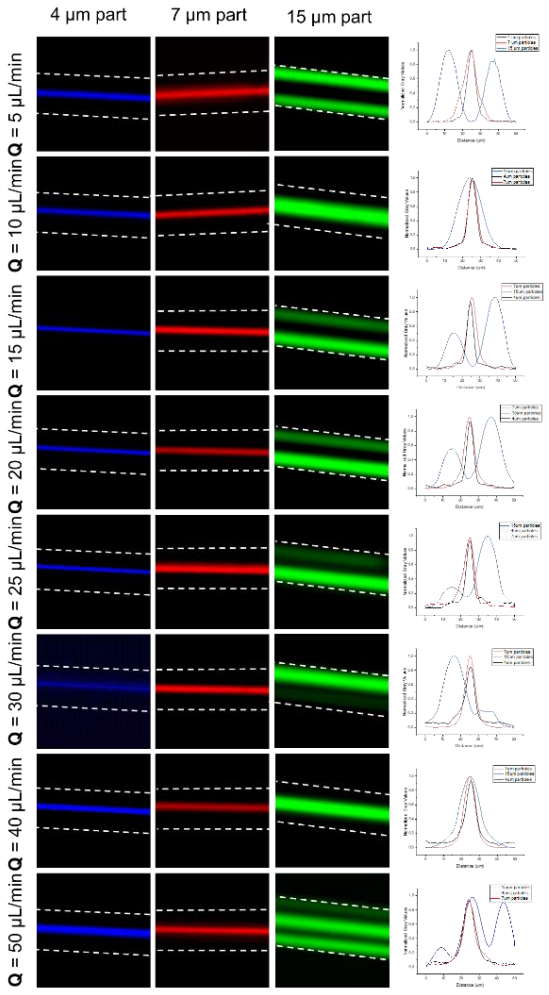

Figure 5 – Fluorescence images of 4 µm (blue), 7 µm (red), and 15 µm (green) PS particles in 1000ppm PEO in PBS solution in 50 µm x 30 µm channel at different flow rates along with their superimposed intensities values profiles for each flow rate tested.

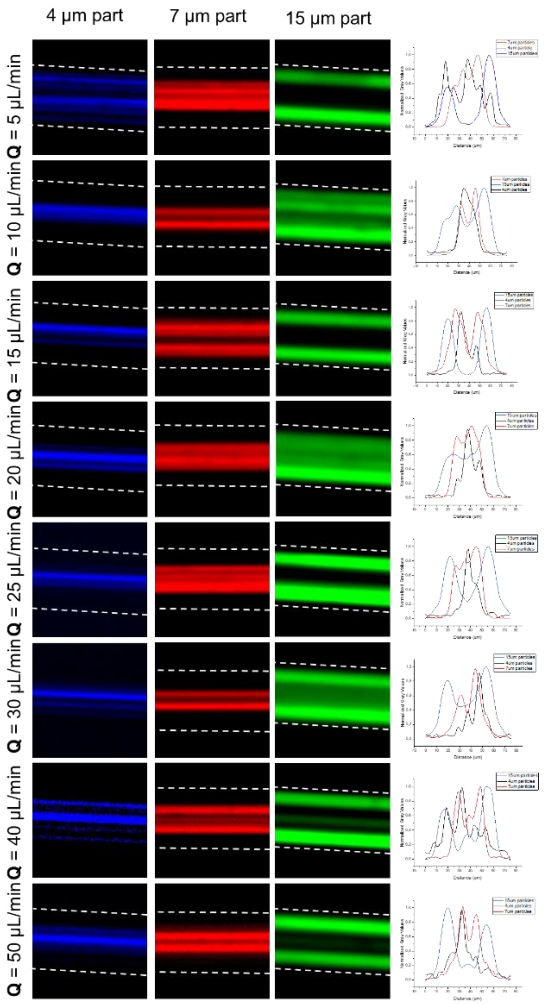

Figure 6 – Fluorescence images of 4 µm (blue), 7 µm (red), and 15 µm (green) PS particles in 1000ppm PEO in PBS solution in 75 µm x 30 µm channel at different flow rates along with their superimposed intensities values profiles for each flow rate tested.

The next experiments were performed with a mixture of 4µm and 15µm particles to find the optimal configuration, which was created by changing the distance of the side outlets, to achieve the best separation possible. The data obtained were only qualitative, but it allowed us to discard configuration #3 and exploit configuration #1 and #2 for further experiments with the biological samples. Specifically, this decision was made considering our final clinical application where we need to obtain a perfectly pure sample of spermatozoa to further process with IVF procedures and get rid of all the other cells. In configuration #3, even the bigger particles could be collected in the central outlet, making this configuration unsuitable for our application, but the remaining two allow us to gather all the unwanted cells into the side outlets.

Since our expectations were fulfilled, we started the experiments with the biological samples. We started by testing the spermatozoa alone, then the diluted seminal fluid, and finally the erythrocytes. No leukocytes were tested because we could not retrieve the WBCs from the whole blood samples that were provided. But, given the fact that those cells are perfectly round, very regular in dimension, and have a mean diameter of 15µm beads, we considered this latter as substitutes of the real white blood cells. The isolated spermatozoa and diluted seminal fluid gave us similar results, with actually better performances registered for the latter. The spermatozoa could be focused in a central area of about 28µm in the AR = 1.67 channel and of about 43µm in the AR = 2.5

channel. The location of sperm cells became tighter when diluted semen was used; in particular, the area occupied by the cells was 3µm smaller for the 50µm x 30µm channel and 8µm smaller for the 75µm x 30µm channel (figure 7). It must be noticed that, due to the very different shape from the 4µm beads, a perfect focusing was not reachable and some of the spermatozoa could be lost in the side outlets but still the majority of them could be collected from the central one. Moreover, without spoiling anything yet, the fact that some of the spermatozoa could be lost in the side outlets will turn out to be essential for the coming sorting step.

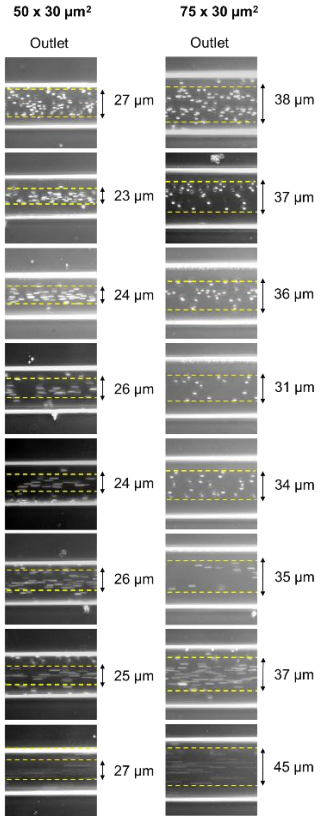

Figure 7 – Bright-field images of diluted seminal fluid captured at the outlet for both AR = 1.67 and AR = 2.5 channels.

The RBCs behaved exactly as predicted by the 7µm beads: they focused in a central area of the channel and were even able to form two different streamlines in some cases. Overall, the focusing zone became smaller with the increasing of the flow rate and the mean values attained were 12µm for the AR = 1.67 channel and 29 for the AR = 2.5 channel (figure 8).

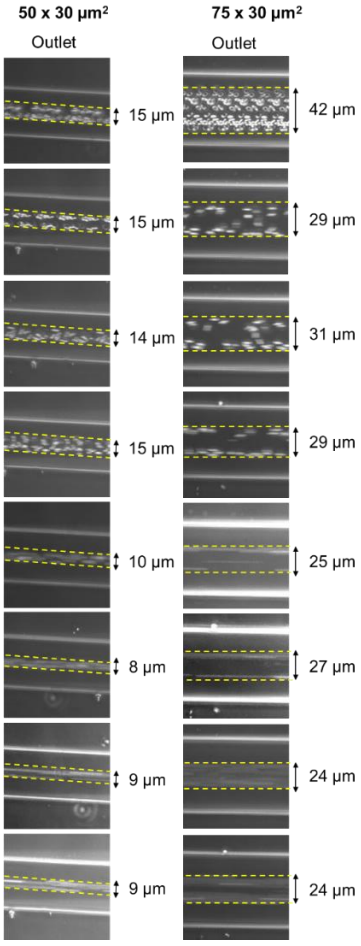

Figure 8 – Bright-field images of erythrocytes captured at the outlet for both AR = 1.67 and AR = 2.5 channels.

Last but not least, the experiments with the mixtures of spermatozoa and other corpuscles

were performed. The mixture of spermatozoa and 15µm particles was tested in both the AR channel and in configurations #1 and #2. In general, a successful outcome was achieved for all the condition tested but only the main accomplishment will be reported (figure 10): the best conditions were found at 15µL/min, with configuration #1 in the 50µm x 30µm channel and at 20µL/min, always in configuration #1 in the 75µm x 30µm channel. In both cases the separation efficiency for the 15µm beads and the purity of the spermatozoa sample was 100%; the only thing that changed was the separation efficiency for the spermatozoa, which means the number of spermatozoa retrieved with respect to the total number of sperm in the initial sample, that was 64% for the first case and 56% for the second one (figure 9).

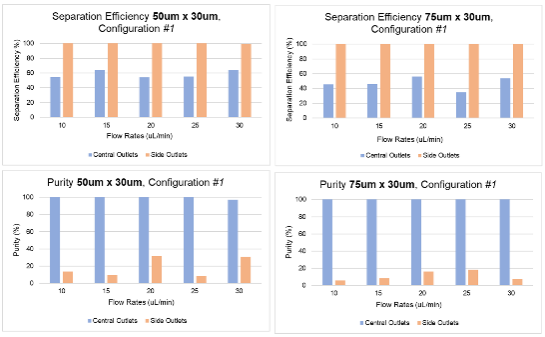

Figure 9 –Separation efficiency and Purity values calculated for all the flow rates and for both AR = 1.67 and AR = 2.5 channels in configuration #1.

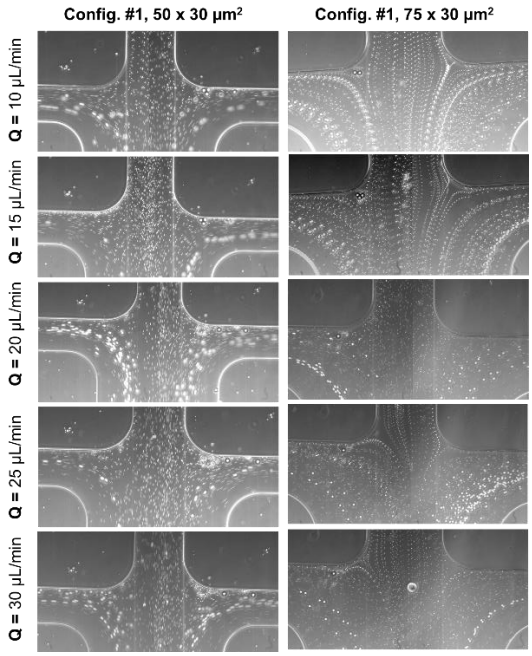

Figure 10 – Bright-field images of spermatozoa and 15µm beads captured at the expansion for both AR = 1.67 and AR = 2.5 channels in configuration #1.

The mixture of spermatozoa and RBCs was also tested in both our channels and in both valid configurations. In the beginning, we did not expect to achieve this separation because both sperm and red blood cells focused on the central area of the channel. But, luckily, what we considered to be a disadvantage at first, turned out to be the only option for separation. Indeed, as said before, while the erythrocytes were tightly focused on the center of the channel and could even form streamlines, the spermatozoa were more randomly distributed in a central area and some of them would escape the central outlet and could be collected by the side ones (figure 11). This happened only with AR = 1.67

channel because in the bigger one two streamlines of RBCs could be seen and thus, they could be collected from all three outlets, making that specific channel unsuitable for our final application. The best conditions found were only in the 50µm x 30µm channel; in configuration #1 at 20µL/min the separation efficiency of RBCs and the purity of the spermatozoa collected were 100% and the separation efficiency of the spermatozoa, thus the number of spermatozoa retrieved from the initial values, was 72%. Analogously happened in configuration #2 at 30µL/min; the only difference is the separation efficiency for the spermatozoa that reached 70% (figure 12).

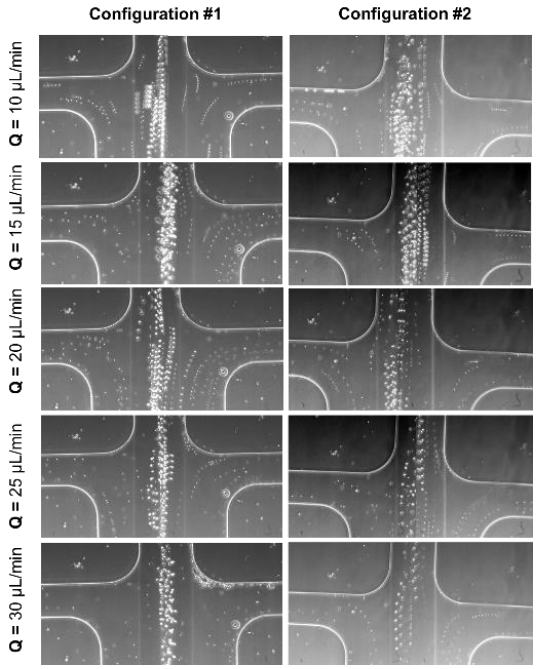

Figure 11 – Bright-field images of spermatozoa and erythrocytes captured at the expansion for AR = 1.67 channel in both configurations, #1 and #2.

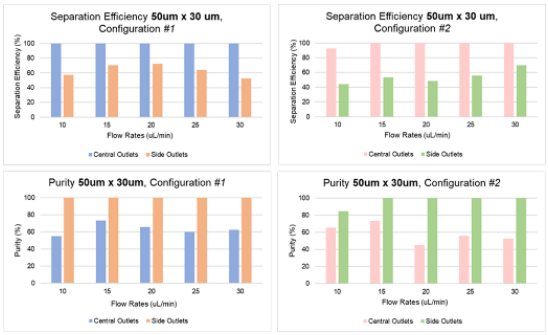

Figure 12 –Separation efficiency and Purity values calculated for all the flow rates and for AR = 1.67 in both configurations, #1 and #2.

Conclusions

The main purpose of this thesis project was the creation of a passive microfluidic device able to perform the separation between spermatozoa and the other cells, such as leukocytes and erythrocytes, that can be found in the semen of pathologic patients. With our research we were proudly able to demonstrate the retrieval of a pure sperm cells sample to use for further in vitro fertilization procedures, to allow fatherhood even to men that have a pathology that, in the past, precluded the possibility of having babies. Specifically, since the number of spermatozoa needed in IVF procedure is between 100 000 and 10 000 spermatozoa per oocyte[14] and our initial concentration of sperm in the used solutions is about 3 x 10^6 sperm cells/mL, with our separation efficiency values always between 60% and 70%, we would be able to achieve the pure retrieval of enough

sperm cells in less than 30 minutes for both mixtures, thus eliminating successfully both leukocytes and erythrocytes from the initial solution.

Of course, there were some issues encountered during this path, among which it is worth citing the formation of clusters and the device clogging, that could be resolved by coating the internal channel with a hydrophobic solution before the usage, and by adding surfactants to the solutions; the necessity of testing real leukocytes and real pathologic samples or biopsies in the channel that could validate once and for all the performances of our device; the testing of the remaining configurations to explore if the eventual change in distance of the central outlet could provide better efficiency and purity values; and finally the fact that different viscoelastic fluids could be taken into consideration because the PEO showed shear-thinning effects which causes a focusing decrease at high flow rates, limiting the maximum flow rate usable and thus, the throughput of the device. Overall, our proposed device is able to provide an easy, fast, efficient, cost-effective, and feasible way to perform the spermatozoa sorting from all the different cell types, and it has all the potentials to become a valid alternative to the current standards methods.

Bibliography

1. Fathalla, M. F. Reproductive health: a global overview. Early Hum. Dev. 29, 35–42 (1992)
2. Cao, X. W., Lin, K., Li, C. Y. & Yuan, C. W. A review of WHO Laboratory Manual for the Examination and Processing of Human Semen (5th edition). *Zhonghua Nan Ke Xue* 17, 1059–1063 (2011)
3. Jung, J. H. et al. Treatment of Leukocytospermia in Male Infertility: A Systematic Review. World J. Mens. Health 34, 165 (2016).
4. De Bellabarba, G. A. et al. Non-sperm cells in human semen and their relationship with semen parameters. Arch. Androl. 45, 131–136 (2000)
5. Wosnitzer, M., Goldstein, M. & Hardy, M. P. Review of Azoospermia. Spermatogenesis 4, e28218 (2014).
6. Whitesides, G. M. The origins and the future of microfluidics. Nature 442, (2006).
7. Samuel, R. et al. Microfluidic-based sperm sorting & analysis for treatment of male infertility. Transl. Androl. Urol. 7, S336–S347 (2018)
8. Zhou, J. & Papautsky, I. Fundamentals of inertial focusing in microchannels. Lab Chip 1121–1132 (2013). doi:10.1039/c2lc41248a
9. Li, D., Lu, X. & Xuan, X. Viscoelastic separation of particles by size in straight rectangular microchannels: A parametric study for a refined understanding. Anal. Chem. 88, 12303–12309 (2016)
10. Fan, L. L. et al. Enhanced viscoelastic focusing of particle in microchannel. Electrophoresis 1–10 (2020). doi:10.1002/elps.201900397
11. Liu, C. et al. Size-Based Separation of Particles and Cells Utilizing Viscoelastic Effects in Straight Microchannels. Anal. Chem. (2015). doi:10.1021/acs.analchem.5b00516
12. Yuan, D. et al. Sheathless separation of microalgae from bacteria using a simple straight channel based on viscoelastic microfluidics. Lab Chip 19, (2019).
13. Lu, X., Zhu, L., Hua, R. mao & Xuan, X. Continuous sheath-free separation of particles by shape in viscoelastic fluids. Appl. Phys. Lett. 107, (2015)
14. Kim, Y. Y. et al. Use of the total motile sperm count to predict pregnancy outcomes in in vitro fertilization. Fertil. Steril. 100, S448 (2013)

SOMMARIO

Introduzione

L'infertilità è definita come l'incapacità di concepire dopo un anno di rapporti sessuali regolari senza l'uso di contraccettivi[1], ed è stato stimato che colpisca più di 70 milioni di coppie in tutto il mondo[2]. In particolare, l'infertilità maschile è riconosciuta come la causa di oltre la metà dei casi di infertilità globale[1,2]. Questo stato patologico è sempre associato a problemi di salute che devono essere esaminati approfonditamente. Infatti, l'infertilità maschile può verificarsi a causa di diversi motivi; tra i più frequenti si trovano la leucospermia, l'azoospermia e l'ematospermia, le quali sono gravi patologie accumunate dalla presenza nello sperma di cellule non spermatiche[3-5], quali globuli bianchi (WBC) e /o globuli rossi (RBC) che potrebbero influenzare la capacità di fecondazione degli spermatozoi e, in molti casi, potrebbero anche essere correlati a difetti dello sperma o causare la frammentazione del DNA[3-5]. Per tutte queste condizioni patologiche, riconosciute come le principali cause di infertilità maschile, esistono diversi metodi utilizzati per ottenere separare gli spermatozoi da tutte le altre cellule presenti ma indesiderate, come ad esempio il metodo swim-up e la centrifugazione a gradiente di densità[1-5]. Queste tecniche utilizzate per eliminare tutto ciò che non sia spermatozoo sono solo le principali; purtroppo però permettono unicamente il recupero di spermatozoi mobili, richiedono l'utilizzo di attrezzature complicate utilizzabili unicamente da personale specificatamente addestrato, impiegano molto tempo per eseguire la separazione, hanno un costo estremamente elevato, ma soprattutto potrebbero aumentare il danno agli spermatozoi eliminando i fattori antiossidanti che impediscono l'esagerata produzione delle specie reattive ossidative (ROS); queste, infatti, rappresentano il principale problema della presenza di leucociti nel liquido seminale poiché i danni causati nello sperma sono proprio dovuti ad elevati livelli di ROS. È qui che la microfluidica può subentrare e può potenzialmente superare tutti gli svantaggi appena elencati: ha la capacità di separare le cellule spermatiche dalle altre presenti semplicemente implementando uno suddivisione per forma e dimensione, non richiede l'utilizzo di un sistema di marcatura o forze esterne, non eliminerebbe i fattori antiossidanti, può permettere anche il recupero di spermatozoi meno motili o non motili e,

ultimo ma non meno importante, sarebbe una procedura più economica e meno dispendiosa in termini di tempo[6]. In effetti, la microfluidica può offrire un modo semplice, veloce, efficiente, economico, indipendente dall'operatore e clinicamente fattibile per separare le cellule spermatiche da tutte le altre cellule presenti nel liquido seminale o nella biopsia prelevata[7]. Inoltre, il nostro canale microfluidico può sfruttare il fluido viscoelastico per diluire ed evitare l'intasamento del dispositivo garantendo al contempo un ambiente chimicamente e fisicamente comparabile per le cellule ed eliminando la necessità di aggiunte meccaniche o enzimatiche per garantire una separazione ad alte prestazioni. Per eseguire la separazione per dimensione e forma, si sfrutta la microfluidica viscoelastica[9-13] e, in particolare, l'effetto sinergico delle forze inerziale ed elastiche, le quali consentono lo spostamento delle particelle più grandi vicino alle pareti laterali mentre di quelle di dimensione minore al centro del canale[9-13] (figura 1).

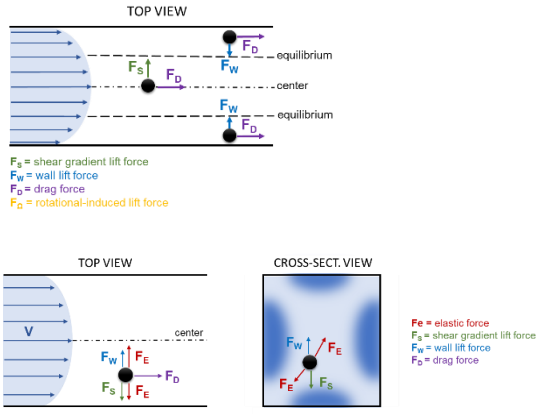

Figura 1 - Viste superiore e trasversale delle forze che agiscono sulle particelle in un fluido viscoelastico.

Lo scopo principale di questo progetto di tesi è la creazione di un dispositivo microfluidico passivo costituito da un canale dritto a sezione rettangolare in grado di eseguire la separazione tra spermatozoi e altre cellule che si possono trovare nel liquido seminale o nel fluido ricavato dalla biopsia di un testicolo, sfruttando l'effetto viscoelastico della soluzione. In particolare, l'obiettivo principale di questa tesi può essere suddiviso in tre sotto obiettivi: in un primo momento, trovare le condizioni ottimali per la separazione delle microparticelle (con una dimensione simile alle cellule bersaglio) in base alle loro dimensioni; in secondo luogo, separare gli spermatozoi dai leucociti al fine di ottenere un campione puro di spermatozoi per il loro successivo utilizzo in procedure di fecondazione in vitro; infine, per ottenere la separazione ottimale degli spermatozoi da tutte

le cellule che potrebbero essere trovate nel supernatante e/o tessuti della biopsia raccolti, quali globuli rossi, leucociti, detriti cellulari, ecc. Quest'ultimo è indispensabile per dimostrare l'ottenimento di un dispositivo in grado di supportare i medici dopo le diverse procedure perpetuate per estrarre gli spermatozoi necessari da utilizzare nelle procedure riproduttive assistite.

Materiali e metodi

Due diversi canali microfluidici dritti con una sezione trasversale rettangolare (figura 2) sono stati prodotti utilizzando le classiche tecniche di soft-litografia. Entrambi i canali hanno un'altezza di 30 μm, una lunghezza del corpo rettilineo principale di 3 cm e 3 diversi rami di 1,5 cm ciascuno. La differenza tra i due canali risiede nella larghezza che è 50μm e 75μm rispettivamente per il primo e il secondo canale. L'aspect-ratio (AR) dei canali è pari a 1,67 per il canale 50μm x 30μm e 2,5 per il canale 75μm x 30μm. La configurazione "open outlets" (figura 2), con diverse ramificazioni dopo il corpo principale e l'espansione, è stata scelta per rispondere alla necessità di controllare e regolare il cutoff, la resistenza del fluido e il rapporto di resistenza in modo che la purezza e l'efficienza di separazione possano essere modificate e regolate semplicemente cambiando la posizione degli outlets senza dover ridisegnare l'intero dispositivo.

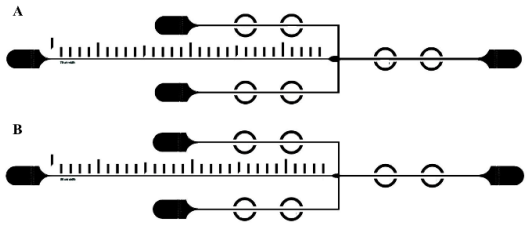

Figura 2 – I due diversi canali dritti di microfluidica a sezione trasversale rettangolare. A) Canale da 75 μm x 30 μm, B) canale da 50 μm x 30 μm.

Il processo di micro-fabbricazione è iniziato con la creazione dei canali microfluidici su AutoCAD, quindi il modello scelto è stato trasferito su un wafer di silicio di 4 pollici utilizzando l'iscrizione laser. La tecnica della soft-litografia (figura 3) è stata utilizzata per creare i dispositivi in PDMS, ma poiché un aumento del tasso di produzione era necessario, prima di procedere con la produzione, alcune copie del master sono state realizzate con resina epossidica. La produzione del dispositivo consisteva nel mescolare il monomero del PDMS ed il suo agente polimerizzante con un rapporto di 10:1; la miscela è stata quindi versata sopra la replica dello stampo, degassata in una camera sottovuoto per almeno 20 minuti e infine polimerizzata a 65 °C per 2 ore in forno.

Successivamente, le repliche di PDMS sono state staccate dallo stampo e gli inlet ed outlet sono stati creati con un perforatore apposito. Infine, il dispositivo è stato chiuso con un vetrino grazie all'utilizzo di un trattamento con l'ossigeno al plasma per sigillare le superfici; per garantire la tenuta ermetica, il dispositivo è stato nuovamente infornato a 65°C per 1 h.

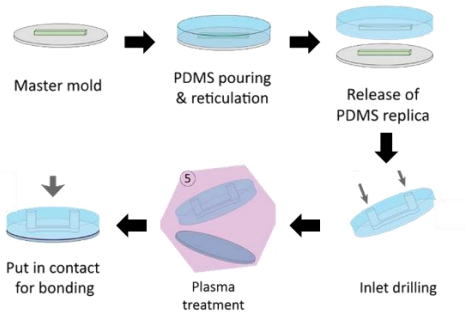

Figura 3 – Procedure di soft-litografia: dalla produzione del master fino al dispositivo finale.

Il mezzo viscoelastico per il nostro progetto è stato creato diluendo l'ossido di etilene (PEO) (MW = 2 x 106 Da) in una soluzione salina tamponata da fosfati (PBS) per creare una soluzione viscoelastica di 1000pppm che fosse in grado di ricreare l'osmolarità richiesta dalle cellule (290 mOsm/kg). Per replicare il comportamento delle cellule sono state utilizzate micro-sferette di polistirene; abbiamo deciso di impiegare particelle da 4µm (~4,19µm), 7µm (~7,32µm) e 15µm (~15,25µm) perché è stato dimostrato che i globuli rossi hanno una forma discoidale con un diametro medio di 7-8µm[9], i leucociti hanno una forma perfettamente sferica con un diametro medio di 15µm mentre gli spermatozoi hanno una forma molto più complicata, che include una coda e una testa, ma la dimensione più rilevante nel nostro caso è la testa che ha una forma ellissoide piatta di circa 4µm x 3µm. I campioni biologici utilizzati, che erano fluidi seminali, spermatozoi, globuli rossi e leucociti, sono stati ottenuti dallo scarto di campioni biologici raccolti da soggetti sani che si sottoponevano a controlli periodici presso il Centro Scienze della Natalità dell'Ospedale San Raffaele. Gli spermatozoi isolati sono stati ottenuti centrifugando lo sperma; il liquido seminale è stato semplicemente diluito nella nostra soluzione viscoelastica, e gli eritrociti sono stati recuperati da sangue intero con la centrifugazione a gradiente di densità. Sfortunatamente, non siamo riusciti a recuperare i leucociti a causa della massiccia presenza dei globuli rossi e quindi non sono stati usati negli esperimenti. Infine, le soluzioni di spermatozoi mescolate con RBCs o con le particelle da 15µm sono state create seguendo la procedura specifica già spiegata per il loro

isolamento, e sono state aggiunte nella stessa soluzione per ottenere una concentrazione di circa 3 x 10^6 cellule/mL per gli spermatozoi, 6 x 10^6 cellule/mL per gli eritrociti e 2,5 x 10^6 particelle/mL per le particelle da 15µm. La procedura sperimentale consiste nel pompare le nostre soluzioni di particelle o cellule nel nostro dispositivo microfluidico utilizzando una pompa a siringa; quindi, le immagini a fluorescenza per le particelle e le immagini in campo luminoso per i campioni biologici sono state catturate con un microscopio a fluorescenza a contrasto di fase invertito (Zeiss Axio Observer Z1, Zeiss, Germania) dotato di una fotocamera EMCCD digitale (Hamamatzu, EM-CCD C9100, Giappone). L'analisi dei dati è stata possibile grazie a diversi software: Volocity è stato quello utilizzato per catturare le immagini dal microscopio Zeiss Axio Observer Z1; ImageJ, Excel, Origin Lab, R e MatLab sono stati utilizzati per eseguire l'analisi post-processo e per convertire le immagini in dati quantitativi che potevano essere analizzati.

Risultati e discussione

Per comprendere l'influenza delle diverse forze agenti sui diversi corpuscoli, abbiamo confrontato le dinamiche e analizzato le prestazioni nel nostro micro-canale considerando i numeri adimensionali, come il numero di Reynolds (Re), che è definito come il rapporto tra la forza inerziale e la forza viscosa, il numero di Weissenberg (Wi), che è il rapporto tra due diverse costanti di tempo, e il numero di elasticità (El), che misura l'importanza relativa dell'elasticità all'inerzia. Le diverse dimensioni delle micro-sferette di polistirene sono state prima di tutto testate una alla volta nel canale 50µm x 30µm; in particolare, il comportamento delle particelle è stato studiato a diversi flussi, da 5µL/min a 50µL/min, e le relative immagini acquisite sono state poi analizzate per ottenere dati quantitativi sui valori di intensità, la loro posizione e sulle efficienze di focalizzazione. La posizione di equilibrio delle particelle da 4µm nel canale con AR = 1,67 si raggiunge esattamente al centro per tutti i flussi studiati, con un'efficienza di focalizzazione > 95% per flussi da 10µL/min a 25µL/min (figura 4). Anche le sferette da 7µm presentano la tendenza di posizionarsi al centro del canale qualsiasi sia la portata, e le prestazioni di efficienza sono superiori al 93% per ogni flusso > 5µL/min (figura 4). Le particelle da 15µm, invece, raggiungono in

generale due diverse posizioni di equilibrio situate vicino alle pareti laterali del canale con un'efficienza di focalizzazione sempre compresa tra il 97% e il 100%.

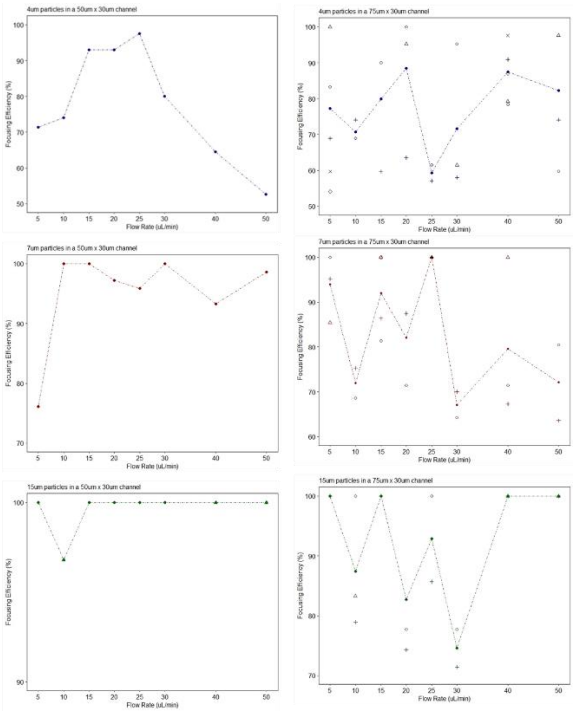

Figura 4 – Valori dell'efficienza di focalizzazione calcolati per ogni flusso e ogni particella di diversa dimensione all'interno del canale da 50µm x 30µm.

Esperimenti analoghi sono stati eseguiti nel canale da 75µm x 30µm; questa volta le particelle da 4µm mostravano multiple posizioni di equilibrio, comunque localizzate al centro del canale; ciò ha però influito sui valori di efficienza, facendoli oscillare tra il 60% e il 90% (figura 4). Le sferette da 7µm hanno mostrato un comportamento simile e sono state trovate nei 30-40µm centrali del canale; l'efficienza di focalizzazione è rimasta compresa tra il 70% e il 100% (figura 4). Le particelle da 15µm, invece, formavano la maggior parte delle volte due posizioni di equilibrio vicino alle pareti del canale, le quali diventavano tre all'aumentare della portata; comunque, i loro valori di efficienza sono sempre rimasti tra il 75% e il 100%, con la maggior parte dei valori intorno al 90% (figura 4). Poiché l'obiettivo finale del progetto è quello di separare i diversi tipi di cellule, il diverso comportamento delle diverse particelle nello stesso canale alla stessa portata è stato confrontato, come mostrato nelle figure 5 e 6. Ciò consente una migliore comprensione delle posizioni di equilibrio simultanee e quindi la visualizzazione del potenziale smistamento. Nel canale da 50µm x 30µm (figura 25), da 5µL/min a 30µL/min, con l'unica eccezione di 10µL/min, la separazione di particelle da 4µm e 7µm dalle particelle da 15µm potrebbe essere fattibile, mentre nel canale da 75µm x 30µm la separazione potrebbe essere ottenuta fra 10µL/min e 30µL/min perché le particelle da 4µm e 7µm si collocano solitamente nello spazio tra le due diverse posizioni di equilibrio delle particelle da 15µm.

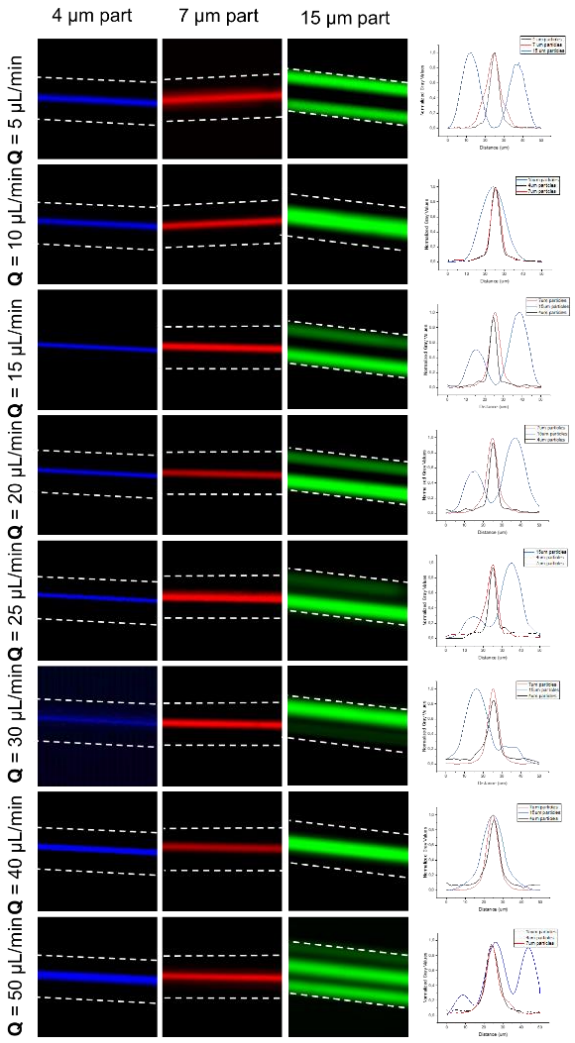

Figura 5 –Immagini a fluorescenza di particelle di PS da 4 µm (in blu), 7 µm (in rosso) e 15 µm (in verde) nella soluzione di PEO in PBS da 1000 pppm per il canale da 50 µm x 30 µm a diverse portate; si riportano anche i loro profili di intensità sovrapposti per ogni portata testata.

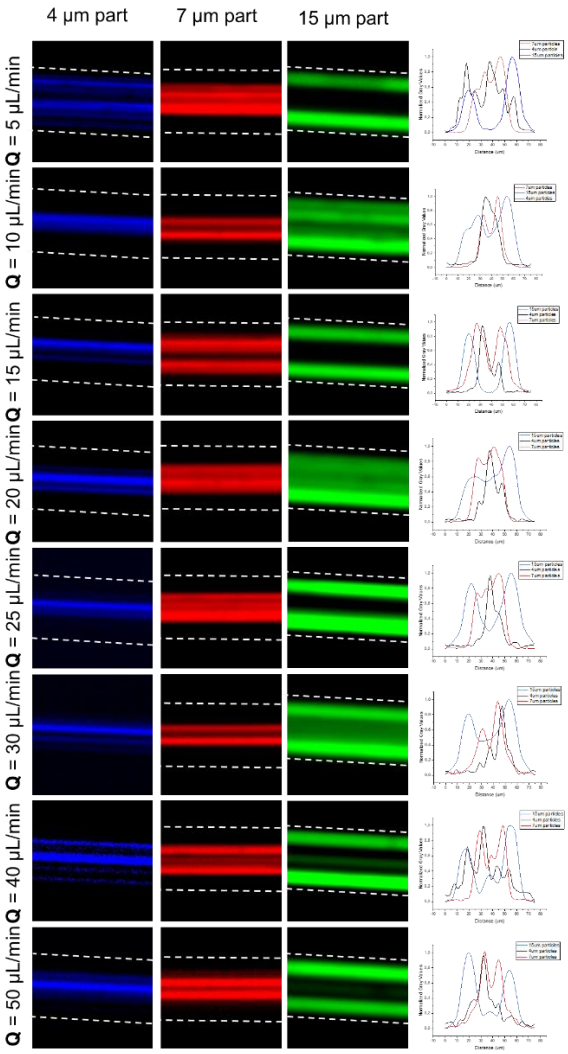

Figura 6 – Immagini a fluorescenza di particelle di PS da 4 µm (in blu), 7 µm (in rosso) e 15 µm (in verde) nella soluzione di PEO in PBS da 1000 pppm per il canale da 75 µm x 30 µm a diverse portate; si riportano anche i loro profili di intensità sovrapposti per ogni portata testata.

Gli esperimenti successivi sono stati eseguiti con una miscela di particelle da 4µm e 15µm per trovare la configurazione ottimale, investigata cambiando la distanza degli outlet laterali, per ottenere la migliore separazione possibile. I dati ottenuti erano solo qualitativi, ma ci hanno permesso di scartare la configurazione #3 e di studiare ulteriormente la configurazione #1 e #2 per gli esperimenti con

i campioni biologici. In particolare, questa decisione è stata presa considerando la nostra applicazione clinica finale in cui abbiamo bisogno di ottenere un campione perfettamente puro di spermatozoi da elaborare ulteriormente con le procedure di fecondazione in vitro, eliminando tutte le altre cellule. Nella configurazione #3 anche le particelle più grandi venivano raccolte nella outlet centrale, rendendo perciò questa configurazione inadatta alla nostra applicazione; invece, le altre due configurazioni ci permettono di raccogliere tutte le cellule indesiderate negli outlet laterali. Poiché le nostre predizioni ed aspettative sono state soddisfatte, abbiamo iniziato gli esperimenti con i campioni biologici. Abbiamo iniziato testando gli spermatozoi da soli, poi il liquido seminale diluito e infine gli eritrociti. Nessun leucocita è stato testato perché, come detto prima, non siamo stati in grado di recuperarli dai campioni di sangue intero forniti. Ma, dato che queste cellule sono perfettamente rotonde, hanno dimensioni molto regolari, e hanno un diametro medio di 15μm, abbiamo considerato le particelle di quel diametro come sostituti dei veri globuli bianchi. Gli spermatozoi isolati e il liquido seminale diluito ci hanno dato risultati simili, anzi abbiamo ottenuto prestazioni migliori con quest'ultimo. Gli spermatozoi si sono riusciti a focalizzare in un'area centrale di circa 28μm nel canale con AR = 1,67 e di circa 43μm nel canale con AR = 2,5. La posizione di equilibrio degli spermatozoi diviene più stretta quando si utilizza il liquido seminale diluito; in particolare, l'area occupata dalle cellule era più piccola di 3μm per il canale da 50μm x 30μm e di 8μm più piccola per il canale da 75μm x 30μm (figura 7). Va notato che, a causa della forma molto diversa dalle particelle da 4μm, una focalizzazione perfetta non era raggiungibile e alcuni spermatozoi si sono persi negli outlets laterali; nonostante ciò, la maggior parte di essi è stata raccolta da quello centrale. Inoltre, senza fare spoiler, il fatto che alcuni spermatozoi possano essere persi negli outlets laterali, sarà essenziale per la buona riuscita della separazione in alcuni specifici casi.

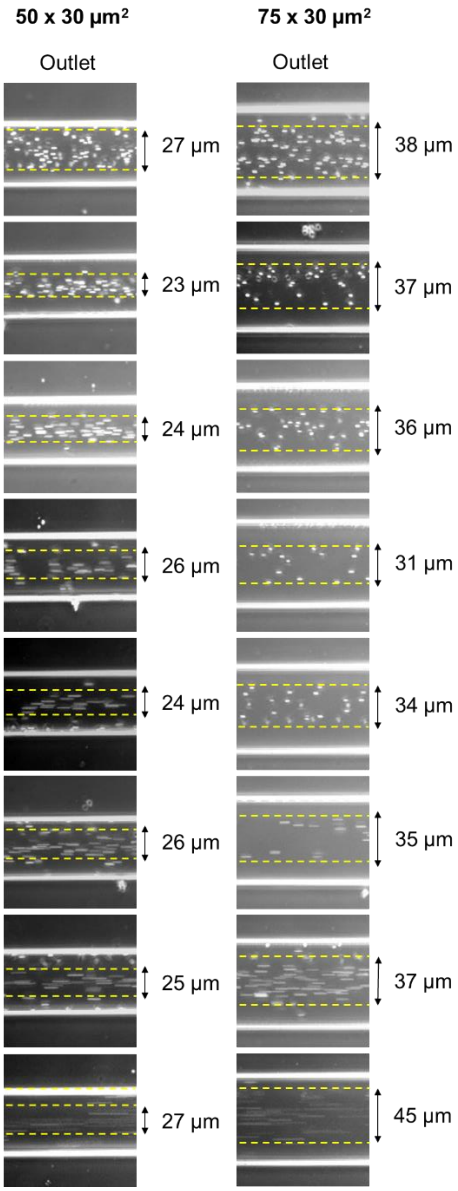

Figura 7 – Immagini in campo chiaro di liquido seminale diluito catturate all'uscita sia del canale con AR = 1,67 che di quello con AR = 2,5.

Gli eritrociti si sono comportati esattamente come previsto dalle particelle da 7µm: si sono posizionate in un'area centrale del canale e in alcuni casi erano persino in grado di formare due diverse posizioni di equilibrio. Complessivamente, la zona di focalizzazione diventa più piccola all'aumentare del flusso ed i valori medi raggiunti sono stati di 12µm per il canale con AR = 1,67 e di 29 µm per il canale con AR = 2,5 (figura 8).

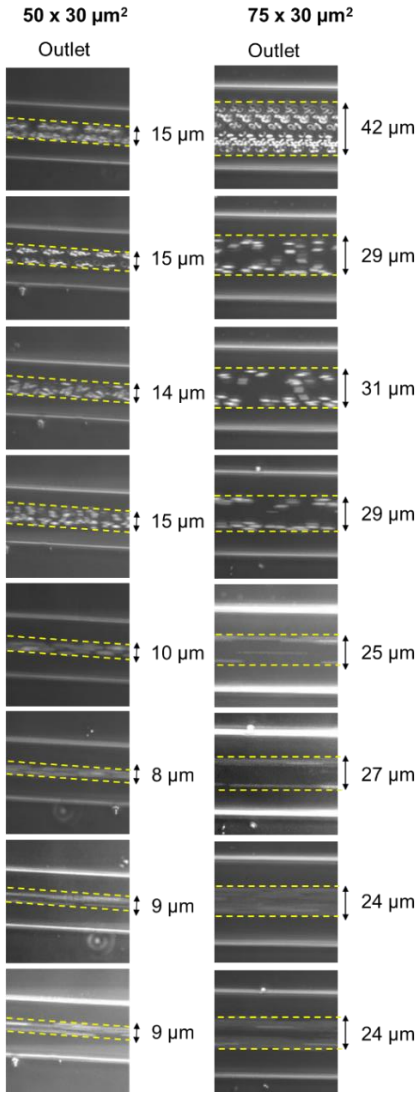

Figura 8 – Immagini in campo chiaro di eritrociti catturate all'uscita sia del canale con AR = 1,67 che di quello con AR = 2,5.

Per ultimi, ma non meno importanti, sono stati eseguiti gli esperimenti con le soluzioni di spermatozoi e altri corpuscoli. La soluzione di spermatozoi e particelle da 15µm è stata testata sia nei diversi canali che nelle configurazioni

#1 e #2. In generale, è stato raggiunto un risultato positivo per tutte le condizioni testate, ma verranno riportati solo i risultati principali (figura 10): le migliori condizioni sono state trovate a 15µL/min, con la configurazione #1 nel canale da 50µm x 30µm e a 20µL/min, sempre in configurazione #1 nel canale da 75µm x 30µm. In entrambi i casi l'efficienza di separazione per le particelle da 15µm e la purezza del campione di spermatozoi era del 100%; gli unici valori differenti sono stati quelli di efficienza di separazione per gli spermatozoi (cioè il numero di spermatozoi recuperati rispetto al numero totale di spermatozoi nel campione iniziale) che erano del 64% per il primo caso e del 56% per il secondo (figura 9).

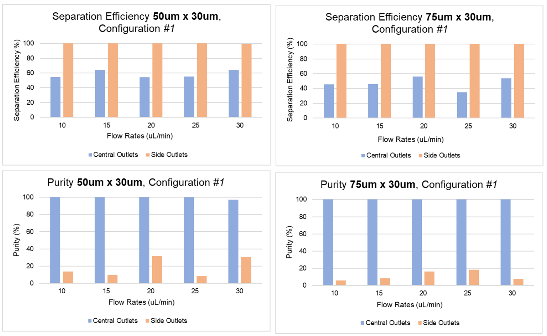

Figura 9 – Efficienza di separazione e valori di purezza calcolati per tutte le portate e per entrambi i canali con AR = 1,67 e AR = 2,5 nella configurazione #1.

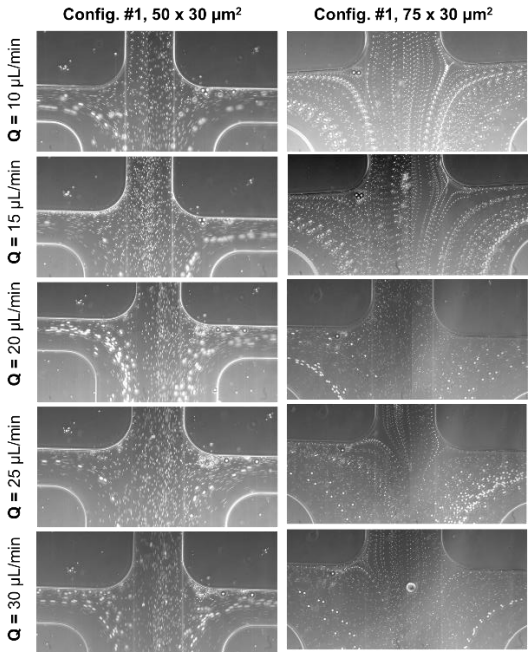

Figura 10 – Immagini in campo chiaro di spermatozoi e particelle da 15µm catturate all'espansione sia per i canali con AR = 1,67 che per AR = 2,5 nella configurazione #1.

La miscela di spermatozoi e RBCs è stata testata in entrambi i canali e con entrambe le configurazioni. All'inizio, non ci aspettavamo di ottenere una separazione perché, dagli esperimenti precedenti, era stato osservato che sia lo sperma che i globuli rossi si localizzavano nell'area centrale del canale. Ma, fortunatamente, quello che all'inizio consideravamo uno svantaggio, si è rivelato essere l'unica opzione possibile per ottenere la separazione. Infatti, come detto prima, mentre gli eritrociti erano strettamente focalizzati al centro del canale, gli spermatozoi erano distribuiti in modo più casuale in un'area centrale e alcuni di loro sfuggivano all'outlet

centrale e venivano raccolti da quelli laterali (figura 11). Questa situazione si è presentata solo con il canale con AR = 1.67 perché nel più grande si potevano vedere diverse posizioni di equilibrio dei globuli rossi e quindi questi potevano essere raccolti da tutte e tre gli outlets, rendendo quello specifico canale inadatto alla nostra applicazione finale. Le migliori condizioni sono state ottenute solo nel canale da 50µm x 30µm; nella configurazione #1 a 20µL/min l'efficienza di separazione degli eritrociti e la purezza degli spermatozoi raccolti erano del 100% e l'efficienza di separazione degli spermatozoi, quindi il numero di spermatozoi recuperati rispetto ai valori iniziali, era del 72%. Una situazione analoga si è verificata nella configurazione #2 a 30µL/min; l'unica differenza è l'efficienza di separazione per gli spermatozoi che hanno raggiunto il 70% (figura 12).

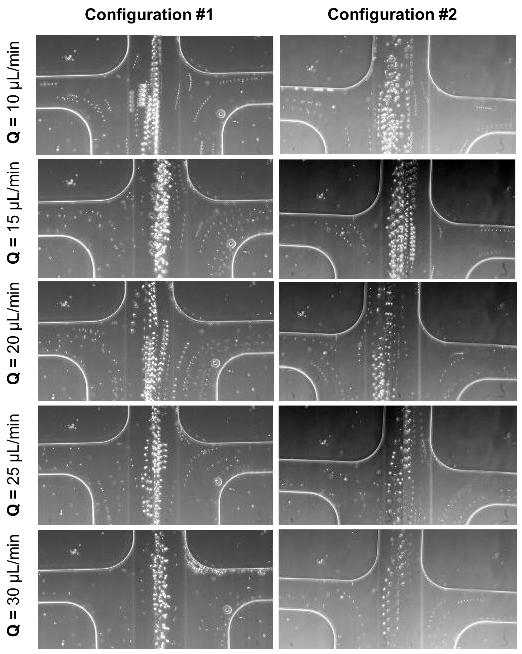

Figura 11 – Immagini in campo chiaro di spermatozoi ed eritrociti catturate all'espansione per il canale con AR = 1,67 in entrambe le configurazioni, #1 e #2.

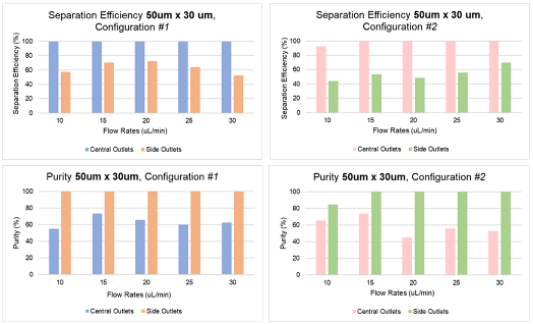

Figura 12 – Efficienza di separazione e valori di purezza calcolati per tutte le portate e per il canale con AR = 1,67 in entrambe le configurazioni, #1 e #2.

Conclusioni

Lo scopo principale di questo progetto di tesi era la creazione di un dispositivo microfluidico passivo in grado di eseguire la separazione tra spermatozoi e altre cellule, come leucociti ed eritrociti, che possono essere trovati nel liquido seminale di pazienti affetti da patologie urologiche. Con la nostra ricerca siamo stati in

grado di dimostrare il recupero di un campione puro di spermatozoi da utilizzare per le successive procedure di fecondazione in vitro, al fine di permettere anche a uomini che hanno una patologia che, in passato, precludeva la possibilità di avere bambini, di diventare padri. In particolare, poiché il numero di spermatozoi necessari nella procedura di fecondazione in vitro è compreso tra 100 000 e 10 000 per ovocita[14], e la nostra concentrazione iniziale di spermatozoi nelle soluzioni utilizzate è di circa 3 x 10^6 spermatozoi/mL, con i nostri valori di efficienza di separazione sempre tra il 60% e il 70%, saremmo in grado di ottenere il recupero di abbastanza spermatozoi puri in meno di 30 minuti per entrambe le soluzioni da noi testate, eliminando così con successo sia i leucociti che gli eritrociti dalla soluzione iniziale. Naturalmente, ci sono stati alcuni problemi incontrati durante questo percorso, tra i quali vale la pena citare la formazione di cluster e l'intasamento del dispositivo, che potrebbero essere risolti rivestendo il canale interno con una soluzione idrofobica prima dell'utilizzo e aggiungendo tensioattivi alle soluzioni; inoltre vi è la necessità di testare veri leucociti e veri campioni patologici o biopsie nel nostro canale così da poter convalidare una volta per tutte le prestazioni del nostro dispositivo; bisognerebbe anche procedere con il testare le configurazioni rimanenti per verificare se l'eventuale cambiamento di distanza dell'outlet centrale potrebbe fornire migliori valori di efficienza e purezza; infine, altri diversi fluidi viscoelastici potrebbero e dovrebbero essere presi in considerazione per questa applicazione perché il PEO ha mostrato effetti di shear-thinning che causano una diminuzione della focalizzazione ad alte portate, limitando il flusso massimo utilizzabile e quindi la velocità effettiva del dispositivo. Nel complesso, il nostro dispositivo è in grado di fornire un modo semplice, veloce, efficiente, conveniente e fattibile per eseguire la separazione degli spermatozoi da tutti i diversi tipi di cellule nocive e non volute, ed ha tutte le potenzialità per diventare un valido metodo alternativo a quelli oggigiorno utilizzati.

Bibliografia

1. Fathalla, M. F. Reproductive health: a global overview. Early Hum. Dev. 29, 35–42 (1992)
2. Cao, X. W., Lin, K., Li, C. Y. & Yuan, C. W. A review of WHO Laboratory Manual for the Examination and Processing of Human Semen (5th edition). *Zhonghua Nan Ke Xue* 17, 1059–1063 (2011)
3. Jung, J. H. et al. Treatment of Leukocytospermia in Male Infertility: A Systematic Review. World J. Mens. Health 34, 165 (2016).
4. De Bellabarba, G. A. et al. Non-sperm cells in human semen and their relationship with semen parameters. Arch. Androl. 45, 131–136 (2000)

5. Wosnitzer, M., Goldstein, M. & Hardy, M. P. Review of Azoospermia. Spermatogenesis 4, e28218 (2014).
6. Whitesides, G. M. The origins and the future of microfluidics. Nature 442, (2006).
7. Samuel, R. et al. Microfluidic-based sperm sorting & analysis for treatment of male infertility. Transl. Androl. Urol. 7, S336–S347 (2018)
8. Zhou, J. & Papautsky, I. Fundamentals of inertial focusing in microchannels. Lab Chip 1121–1132 (2013). doi:10.1039/c2lc41248a
9. Li, D., Lu, X. & Xuan, X. Viscoelastic separation of particles by size in straight rectangular microchannels: A parametric study for a refined understanding. Anal. Chem. 88, 12303–12309 (2016)
10. Fan, L. L. et al. Enhanced viscoelastic focusing of particle in microchannel. Electrophoresis 1–10 (2020). doi:10.1002/elps.201900397
11. Liu, C. et al. Size-Based Separation of Particles and Cells Utilizing Viscoelastic Effects in Straight Microchannels. Anal. Chem. (2015). doi:10.1021/acs.analchem.5b00516
12. Yuan, D. et al. Sheathless separation of microalgae from bacteria using a simple straight channel based on viscoelastic microfluidics. Lab Chip 19, (2019).
13. Lu, X., Zhu, L., Hua, R. mao & Xuan, X. Continuous sheath-free separation of particles by shape in viscoelastic fluids. Appl. Phys. Lett. 107, (2015)
14. Kim, Y. Y. et al. Use of the total motile sperm count to predict pregnancy outcomes in in vitro fertilization. Fertil. Steril. 100, S448 (2013)

CHAPTER 1

INTRODUCTION

1.1 Male Infertility

Infertility is defined as the inability to conceive after one year of regular sexual intercourse without the use of contraceptives[1–3], and it has been estimated to affect more than 70 million couples around the world[1,4–8] In particular, male infertility is recognized as the cause of more than half of the cases of global childness[3,4,6]. Even though may seem a non-urgent threat to physical health, it has been recognized to have a great impact on mental and social health[5]; moreover, it is always associated with health issues that must be taken into consideration. Indeed, the male-factor may occur due to several different reasons, such as varicocele, genetic alterations, low sperm production, abnormal sperm function, injuries, infectious processes in the genitourinary tract[2], poor lifestyle choices, and systemic diseases[3].

Among others, leukospermia, azoospermia, and hematospermia are serious pathologies with a similar effect, *i.e.* the presence in the semen of non-sperm cells such as white blood cells (WBCs) and/or red blood cells (RBCs) that could affect the fertilization ability of the spermatozoa and, in many cases, could be also correlated to sperm defects or can cause DNA fragmentation. The silver lining of these pathologies is the fact that science is coming in help of affected patients and, after removing the undesired cells and retrieving only spermatozoa, new technologies can be used to increase the chances for parenthood, such as assisted reproductive technologies (ART) or in-vitro fertilization (IVF) processes. Microfluidics is starting to become a powerful tool to solve some of the technical hitches that emerged from the standard clinical separation procedures; indeed, it is able to provide efficient cells sorting solutions without requiring external forces or cell labeling; it is also a low cost and no time-

consuming approach to recover not only motile sperm but also viable less-motile and non-motile sperm cells while at the same time reducing the concentration of unwanted cells and/or corpuscles[9].

1.1.1 Leukospermia

The threshold value of leukocytes present in physiological semen is considered by the WHO to be 1 x 10^6 white blood cells/mL[1]; above this value, the patient is considered to be affected by leukospermia[2,3,10–12], an inflammatory disease that could be present in both fertile and infertile men and with or without a genital tract infection[11]. Although there are some disagreements on whether there is a negative correlation between leukocytes presence and semen quality[12,13], most of the scientific community agrees on leukospermia being a cause of decreased male fertility[2,3,9–12,14–16]. The prevalence of leukospermia does not have a specific value but is variable depending on which particular study is quoted; nevertheless, the real incidence of this pathologic status is believed to range between 16.1% and 60.7%[11], while the mean value that has been frequently reported is between 20 and 32%[12,14,16]. Even though leukospermia is considered an inflammatory disease, 80% of leukocytospermic infertile males cannot be diagnosed with a microbial infection in their semen; there exist other conditions that are believed to lead to leukocytospermia such as viral infections, varicocele, smoking, or trauma (*e.g.* spinal cord injury)[9].

The main sperm dysfunctions are associated with the release of reactive oxygen species (ROS), which are defined as oxygen molecules with an unpaired electron[3], and they are mainly produced by the phagocytic leukocytes[11]; in particular, ROS production was closely correlated to the WBCs concentration[12,15]. A high amount of these species can cause oxidative stress by overpowering the body's antioxidant defense mechanisms and it can lead to the loss of the sperm functional integrity by disrupting multiple mechanisms such as a decreased mitochondrial activity, alterations in the sperm-egg binding, loss of DNA integrity[11], sperm tail defects, acrosomal damage, and high sperm deformity index[12]. Indeed, the high concentration of polyunsaturated fatty acids (PUFA)-methylene groups in the spermatozoa's plasma membrane between the double bonds in the carbon chain makes the sperm cells particularly vulnerable to oxidative stress, and the ROS species can easily extract the hydrogen

molecules and cause the lipid peroxidation that can ultimately result in mitochondrial activity loss and increased DNA fragmentation[3]. Besides, in order to preserve the electrolytic gradient between the inner and outer compartments, mitochondrial membranes must be selectively permeable but when ROS are present the membrane permeability is altered causing the inhibition of the oxidative phosphorylation, which at the same time causes the decreased ATP production[3]. Since ATP is essential for sperm metabolism, the spermatozoa motility results severely affected[11]. The third phenomenon that happens is DNA damage: it can occur with the binding to DNA of the produced lipid degradation by-products, through oxidation of DNA bases, especially guanosine, or by directly interacting with the DNA strand, resulting in non-specific single and double-strand breaks[3]. Finally, it has also been demonstrated that by altering cytokine levels, which, in turn, weaken Sertoli cell function, spermatogenesis can be impaired[9].

Regardless of these negative effects, two mainly positive outcomes have been documented. The first is the Haber–Weiss reaction which generates the hydroxyl radical by combining superoxide anion and hydrogen peroxide; this initiates the lipid peroxidation but if controlled amounts are produced, these will satisfy the physiologic role in fertilization[11]. Secondly, signs of sperm capacitation, hyperactivation, and acrosome reaction have been shown for limited ROS levels which are needed to have a physiological function in cell signaling[12].

Overall, it has been demonstrated that sperm deformities are progressively increasing with leukocyte counts and thus are concentration dependent[12] and that leukocytospermia impairs spermatogenesis and sperm maturation[9].

Since the majority of men suffering from leukocytospermia are infertile, assisted reproductive techniques (ART), such as IVF and intracytoplasmic sperm injection, are necessary to overcome the conceiving difficulties and make fatherhood possible. To achieve a successful IVF procedure, the removal of WBCs from semen represents a mandatory step; the main methods include the swim-up from a washed pellet, glass wool filtration, mechanical filtration using physical filters such as micropore filters, and density gradient centrifugation[9,17]. The advantages of the swim-up method, which is the

oldest one, are the retrieving of a very high percentage of motile sperm (90%)[3], a great proportion of morphologically regular sperm, and a small percentage of non-sperm cells such as WBCs or immature germ cells[9], which are round too and cannot be easily distinguished from the leukocytes[10,14]. But, this technique reduces the percentage of normally chromatin-condensed sperm and increases the sperm damage by ROS in patients with elevated ROS levels[9]. The glass wood filtration method is able to isolate the spermatozoa even from low concentration ejaculate and can diminish considerably the WBCs and ROS presence. However, it is very expensive, the filtrate is not clean, and traces of debris can be found[9]. Traditional mechanical filtration techniques are not suitable for this application because of the frequent clogging of the membranes used due to the high concentration of leukocytes and the presence of other possible tissues in the sample[9]. Finally, the density gradient centrifugation has been shown to be very efficient in removing leukocytes, cellular debris, and dead or immotile sperm[3] by exploiting the centrifugal force across one or more layers of silane-coated silica particles that become gradually concentrated[9]. But, on the negative side, this technique is time-consuming and more expensive than the other methods since it eliminates the antioxidant-rich seminal plasma and therefore it enhances ROS production and release, of both sperm and leukocytes[3]. The activation of leukocytes by centrifugation will result in a 100-fold increase in ROS production[15].

1.1.2 Azoospermia

The WHO defines azoospermia as the absence of spermatozoa in at least two different ejaculate samples that were centrifuged for 15 min at the maximum speed possible[1,18,19]. Indeed, the finding of small amounts of sperm in the centrifuged specimen rules out full ductal blocking and allows for rapid sperm cryopreservation for ICSI cycles[18]. Azoospermia is a pathological condition that can be identified in approximately 15-20% of all infertile men[18,20–25] and can be clinically classified as obstructive azoospermia (OA) and non-obstructive azoospermia (NOA)[19,21,25–27]. OA is less common and occurs only in 40% of the azoospermic cases; it is caused by a physical blockage in the male excurrent ductal system, and it can happen somewhere between the rete testis and the ejaculatory ducts. Many reasons may cause obstruction, including infection, surgery (*e.g.* vasectomies), or a missing vas deferens[26]. However, normal exocrine and endocrine activity, as well as normal spermatogenesis in the testis, are

preserved[21]. On the other hand, NOA is the prevalent one with an incidence percentage of 60%; it can be the consequences of either primary testicular failure, secondary testicular failure, or incomplete or ambiguous testicular failure, and the causes usually include toxic exposures or abnormal testicular development[21].

In obstructive azoospermia (OA), the etiology can be found in the obstruction of the epidermis as a result of elevated epididymal intratubular pressure caused by prolonged vasal obstruction or as a result of pelvic or scrotal trauma; in the iatrogenic epididymal obstruction post-hydrocelectomy, percutaneous epididymal sperm aspiration (PESA), microsurgical epididymal sperm aspiration (MESA), or inadvertent epididymal biopsy[21]; in the congenital unilateral absence of the vas deferens (CUAVD) or congenital bilateral absence of the vas deferens (CBAVD)[19], typically related to mutations of the cystic fibrosis transmembrane regulator (CFTR) protein, which result in absent vasa ad the partial or complete absence of the epididymis, or finally in the male excurrent ductal obstruction due to severe inflammation of the epididymis, prostate, seminal vesicles, or lower genitourinary tract infection[21]. Since OA is commonly treatable[18] and microfluidics would not be of help, it would not be discussed any further.

Non-obstructive azoospermia (NOA) is associated with the different testicular failures cited above and those can either cause reduced spermatogenesis, maturation arrest, or a complete failure of spermatogenesis noted with Sertoli-cell only syndrome[20]. In particular, the primary testicular failure is caused by autosomal and Y chromosomal genetic aberrations, as well as several, putative genetic anomalies affecting the complex process of spermatogenesis[22]; Klinefelter syndrome (47, XXY) is the most commonly identified karyotype abnormality, while Robertsonian translocations (fusion of long arms of two acrocentric chromosomes 13, 14, 15, 21, or 22) are a common structural abnormality[21]. Moreover, a rise in the number of X chromosomes is linked to a decline in spermatogenesis[21]. The secondary testicular failure is associated with congenital hypogonadotropic hypogonadism and other endocrine abnormalities[19,21]. Toxic exposures, such as chemotherapy or radiation, or a history of irregular growth, cryptorchidism, or large varicoceles may also lead to NOA[21,22]. Undescended testes, testicular torsion, mumps orchitis, gonadotoxic effects from antibiotics, genetic defects, and idiopathic causes are also possible triggers of direct testicular pathology[18,25].

An alternative classification for azoospermic patients is based on where anatomically and physiologically the primary problem occurs[22]. Accordingly, the three main groups are:

1. Pre-testicular azoospermia
2. Testicular azoospermia
3. Post-testicular azoospermia

The second one is also called non-obstructive azoospermia, while the first one and the third one are the obstructive azoospermia; thus, all the precedented enumerated causes are still valid for each of this group, they just have to be divided based on the physical location: pre-testicular azoospermia is due to a hypothalamic or pituitary abnormality, the testicular azoospermia is still associated with the reduced or absent spermatogenesis and maturation arrest, and finally the post-testicular azoospermia is caused by an obstruction or an ejaculatory dysfunction[20].

Given the fact that OA is easily resolved, I will discuss the only option available for the NOA patients who want to embark on the fatherhood journey. Indeed, there exist four techniques currently available to collect sperm for IVF: MESA (microsurgical epididymal sperm aspiration), PESA (percutaneous epididymal sperm aspiration), TESA (testicular sperm aspiration), and TESE (testicular sperm extraction)[26]. However, only the latter can successfully retrieve the few spermatozoa needed for the oocyte fertilization[28]. It is necessary to clarify that sperm does not need to pass through the epididymis to acquire the characteristics needed for successful assisted reproductive technology fertilization and this is why, even for non-obstructive patients[19], this procedure can be quite effective. The TESE procedure consists of a surgical intervention under mild sedation or local anesthesia in which a small area of the testis is exposed and the surgeon performs an incision on the scrotum where the seminiferous tubules are forcibly uncovered and a biopsy sample of the tubules can be collected[26]. Then, the challenging part begins: the sample has to be divided into small pieces using fine needles, then mechanical, enzymatic, or a combination of both detachment techniques must be applied[4] to the tissues retrieved to eliminate the mixture of other tissue cells, like a large number of RBCs that are introduced due to blood vessel damage[27], and cell debris. Finally, an embryologist checks the presence of

spermatozoa under a stereomicroscope. This treatment necessitates the incubation of testicular tissues with various enzymes, such as collagenase type IA or trypsin-DNAse, which may have detrimental consequences for spermatozoa, such as reduced motility or the development of intercellular bridges[4]; it is highly time-consuming (can take from 2-3 hours[26]), extremely difficult, and it is an operator-dependable process in which the expertise of the specialist is fundamental for a successful outcome, along with the degree of sperm production and the etiology of testicular failure.

1.1.3 Hematospermia

Hematospermia is defined by WHO as the presence of blood in the ejaculate[1]. The blood can sometimes be seen with the naked eye, but more often it is only detectable through specific instruments that can analyze microscopic quantities of blood in the seminal fluid. Hematospermia is found as a symptom in 1.0-1.5% of cases of all the urological referrals but this condition can occur as a single episode or be chronic or sporadic[29]; the current incidence of this condition is still unknown due to the lack of regular examinations of the semen by men. The male patients are generally between 30 and 40 years old, even though the pathology can affect elder men[9,29,30]. In recent years, the etiology of hematospermia has been examined and several factors were identified and here are reported in order of occurrence[29]:

1. Iatrogenic causes, such as prostate biopsy and other urological interventions
2. Trauma
3. Infection
4. Tumor
5. Systemic disease
6. Anomalies
7. Deviant sexual practices

Although several pathophysiological mechanisms are reported for hematospermia, about 30–70% of cases are idiopathic[9].

The iatrogenic trauma is the most common known cause for hematospermia[9,29,30], and it is the one of interest for our research; indeed, after surgeries such as transrectal ultrasound-guided prostate biopsy, brachytherapy, cystoscopy, etc. the presence of RBCs in seminal fluid is quite common, for the surgical sperm retrieval from the testis or epididymis of infertile men (*e.g.* TESE) the contamination with RBCs is inevitable and could impair procedures such as IVF.

Erythrocytes have been found in the ejaculate of 13.4% of infertile men[9]. The main concerns lie in the potential effects of RBCs in the semen. Toxic substances released by erythrocytes may affect the fertilization potential of spermatozoa, especially if cryopreservation of these samples is required[9]; this is particularly due to the presence of high amounts of hemoglobin originating from RBC hemolysis. Furthermore, it has been demonstrated that RBCs in the semen can impair the spermatozoa mobility, ruin the sperm membrane integrity, and damage acrosomal status in the thawed specimens[9,29].

The laboratory methods to separate the erythrocytes from spermatozoa include swim-up and gradient centrifugation; this latter has reported a higher quality when compared to the first one[9]. But both these techniques are time-consuming and involve the use of reagents and media to obtain the separation.

1.1.4 A Promising Solution

For all of these pathological conditions, which are recognized as the main causes of male infertility, there exist several methods used to obtain the separation of spermatozoa from all the other cells, such as RBCs and/or WBCs; those were listed in the paragraphs above and for each of them microfluidics could solve many disadvantages and, thus, could represent the promising solution sought after.

Specifically, the techniques used to separate leukocytes from sperm cells are various, and along with the fact that they could only retrieve motile sperm cells and could require complicated equipment, they also need elevated time to perform, have an extremely high cost, but most of all they could increase the spermatozoa damage by eliminating the antioxidant factors that prevent and exaggerated the ROS production; this latter is the major issue when we realize that the damage caused by WBCs in semen is done by elevated ROS levels. This is where microfluidics takes over and it can potentially overcome all

the enumerated drawbacks: it has the potential to separate sperm cells from others by just implementing a sorting by shape and size, it does not require a labeling system or external forces, it would not eliminate the antioxidant factors, it can also recover less motile and non-motile sperm cells, and last but not least, it would be a cheaper and less time-consuming procedure.

In the case of azoospermic patients, the retrieval of the few spermatozoa present requires the TESE procedure, which was explained in paragraph 1.1.2 and can cause the introduction of non-sperm cells such as RBCs or cells debris into the biopsy sample. But the final part of the procedure has a long list of difficulties that could be potentially overcome by microfluidics; indeed, microfluidics can offer an easy, fast, efficient, cost-effective, operator-independent, and clinically feasible way to separate sperm cells from all the other cells present in the retrieved biopsy. Furthermore, the microfluidic channel that we propose can exploit the viscoelastic fluid to dilute and avoid the clogging of the device while assuring a comparable environment for the cells and eliminating the need for the mechanic or enzymatic additions to ensure a high-performance separation.

Lastly, both some of the techniques used to eliminate WBCs from semen and the TESE procedure could be used to remove RBCs from the semen of hematospermic patients; thus, once again, microfluidics could be advantageous because would allow the label-free separation independently from the sperm-mobility but also it would perform the entire separation in way less time, maybe in few minutes; since time is a critical factor in IVF or ICSI procedure, microfluidics could represent the solution of many existing problems and improve the performances of this fertilization techniques.

1.2 Microfluidics

Microfluidics is defined as the science and technology of precise manipulation of small amount of fluids (10^{-9} – 10^{-18} liters)[31] in microchannel systems with dimensions of about 100 nm to 100 µm [32]. It is the science and engineering of systems in which fluid behavior differs from conventional flow theory primarily due to the small length scale of the system[33].

The origin of microfluidics could be traced back combining four different contributions from as many different fields: firstly, microanalytical methods (*e.g.* gas-phase chromatography (GPC), high-pressure

liquid chromatography (HPLC), and capillary electrophoresis (CE)), were the first to achieve high sensitivity and high resolution using very small amounts of sample and thus, making understandable the needs to develop new, more compact and versatile setups for performing these operations while looking for other applications of microscale methods in chemistry and biochemistry[31]; secondly, the explosion of genomics in the 1980s, and the advent of high-throughput DNA sequencing, for instance, required analytical methods with much greater throughput, and higher sensitivity and resolution than had previously been used in biology; microfluidics was the appropriate technology that offered advantageous solutions to overcome these problems[31]. Thirdly, after the end of the cold war, chemical and biological weapons became major military and terrorist threats and the Defense Advanced Research Projects Agency (DARPA) of the US Department of Defense supported a series of programs in the 1990s aimed at developing field-deployable microfluidic systems designed to serve as detectors for these threats[31]. Fourthly and finally, the success of photolithography in silicon microelectronics and microelectromechanical systems (MEMS) gave birth to the concrete opportunity to manufacture microfluidics devices[33–35].

Only recently, Microfluidics has become a mainstream enabling technology for life science and diagnostic, due to the undeniable progress with manufacturing methods but most of all due to plenty of proven advantages: the faster reaction time, simpler kinematics[36], its inherently demand of small volumes of samples, the precise control on flow conditions[37], the manipulation of cells and/or particles with higher sensitivity and accuracy than their macroscale counterpart[38], the potential integration with other unit operations such as separation processes[39], the lower cost and fast processing and analysis[40], and the possibility to exploit the typical micro-level properties such as fluid laminarity, capillarity, surface tension and predominance of diffusion as the type of mixing. Other advantageous facts that must be taken into consideration are first of all that this microtechnology has a wide range of detection methods that could be leveraged, such as optical (*e.g.* Fluorescence, Spectroscopy, Si-Photonics, etc.) or non-optical (*e.g.* Electrochemical or Si-based sensors) that makes microfluidics a strategic tool for so many different fields, and second that all these advantages combined can change crucially the diagnosis technologies; the most flagrant example is the latest use of paper-based Later Flow Assays

(LFA) for Covid-19 diagnosis tests, such as rapid buffers or rapid serologic test that were the turning point for fast, affordable and accurate screening. Undeniably, this could be the starting point to redeem the importance of microfluidics as the major technology for the analysis, synthesis, manipulation of molecules and biological samples.

The main classification for microfluidics devices consists of the differentiation between active or passive devices: the former bases the manipulation technologies on external forces induced by external fields like electric, magnetic, acoustic, and optical[40]; the latter takes advantage of geometrical effects[41], hydrodynamic forces to manipulate particles towards equilibrium positions, of size, filtration, and sedimentation[42]. Passive methods are more convenient because they have a lower power consumption since no external forces are required, they can exploit simpler structures to manipulate corpuscles[43], they are easy to fabricate[44] and easier to operate due to the significant reduction of complexity[45] while still achieving the high throughput needed for clinical applications[46]. Typically, passive microfluidics devices are used for focusing, manipulation, separation, and trapping methods[40].

The fluid used for passive manipulation techniques assumes fundamental importance for the final application and outcome since the hydrodynamic forces generated have the leading role in the manipulation and focusing of particles and/or cells. The fluids can be Newtonian or non-Newtonian, based on the fact that they follow or not Newton's law of viscosity; Newtonian fluids were the first to be investigated in microfluidics due to their easier behavior's prediction and calculation but also availability and low cost: water and its different typologies are the most common fluids used in microfluidics. Nevertheless, in recent years viscoelastic fluids have gained much more attention because not only non-Newtonian fluids are the only true representation of bodily fluids such as blood, cytoplasm, saliva, semen fluid, but also has been demonstrated a better capability of manipulation of smaller particles at higher throughput than inertial fluids[47,48], superior performances in simpler channel design[41] (*e.g.* straight channels), it allows to study cell deformability and damage[39], and these fluids can enable 3D particles focusing in a microchannel by just tuning the rheological properties of the suspending medium.

For all these reasons our passive microfluidic device, with a straight geometry and a square cross-section that exploits the nonlinear elastic forces arising from the viscoelastic medium, appeared the most appropriate and optimal choice.

1.2.1 Viscoelastic Microfluidics

A fluid can be defined as "a substance that deforms continuously under the application of shear (tangential) stress, no matter how small that stress may be[33]". If the shear stress is directly proportional to the rate of strain within the fluid, the fluid is said to be Newtonian[49]; indeed, Newton's law of viscosity is defined as:

$$\tau = -\mu\,\gamma \tag{1}$$

where τ is the shear stress defined as force per unit area, μ is the proportionality constant or viscosity and γ is the shear rate (∂u/∂y). Many fluids exist for which this Newtonian formulation is inaccurate: those are called non-Newtonian fluids and their stress-strain rate relation is not linear[50]. Their viscosity is dependent on the shear rate and shear stress ratio of the fluid and so another model, which is able to describe and predict their behavior, was developed[49]; these viscoelastic fluids are characterized by the Power Law:

$$\tau = -K\,\gamma^{n} \tag{2}$$

where K is the consistency index and the other variables were already defined above; when n = 1 the fluid type is Newtonian; n > 1 corresponds to shear-thickening fluids; and n < 1 corresponds to shear-thinning fluids which possessed μ_{app}, the apparent viscosity, that is not a thermophysical property of the fluid, but it depends on the characteristic of the flow. Shear-thickening fluids are much less common and have effective viscosities that increase as the strain rate increases; Shear-thinning fluids have an opposite behavior: their apparent viscosity decreases as the strain rate increases. This latter behavior is typical of fluids made of long polymeric molecules, which align when they are sheared and slide along one another more easily at a high strain rate[50].

In microfluidics, the most used non-Newtonian fluids in biological experiments were:

- Polyethylene oxide (PEO)
- Polyvinylpyrrolidone (PVP)
- Polyacrylamide (PAA)
- Hyaluronic acid (HA)
- Diluted λ-DNA solution
- Xanthan gum (XG)

And all of them exhibited viscoelastic behaviors[42]. The choice of PEO in our project lies in the large availability, lower cost, simpler preparation, and consistency with the previous research of Barilla L. for the asymmetric cells' separation. Besides, PEO solution has a medium elasticity and a weak shear-thinning effect which involves a less decrease of focusing of particles or cells at higher flow rates. It was also demonstrated that this viscoelastic fluid enhanced the size and shape-dependent lateral position focusing[48]. Since the shear viscosity can be approximated to be constant due to the weak shear-thinning effect, the PEO can be also modeled with the Oldroyd-B model or the Giesekus equation. In particular, when the mobility factor in the Giesekus constitutive law (eq. 3) is equal to zero, that equation can be reduced to the Oldroyd-B equation.

$$\tau + \lambda \left(\frac{\delta \tau}{\delta t} + u \cdot \nabla \tau - \nabla u^T \cdot \tau - \tau \cdot \nabla u + \frac{\alpha}{\eta_p} (\tau \cdot \tau) \right) = \eta_p (\nabla u + \nabla u^T) \quad (3)$$

where τ is the shear-stress, α is the mobility factor, ηp is the polymeric viscosity, and λ is the relaxation time. Both models were demonstrated to be used for shear-thinning fluids[51]; usually, particles in Oldroyd-B fluids focus at the center of the channel while in Giesekus fluid particles are speculated to reach their equilibrium positions away from the center[52].

In viscoelastic fluids, has been demonstrated that both inertial and elastic effects affect the particles focusing and migration[37,39,41–43,48,53–56].

In the inertial particle focusing, neutrally buoyant corpuscles experience the inertial lift force, which can be divided into three different components: wall-induced lift force (F_w), shear-induced force (F_s), and the rotational-induced lift force (F_Ω). The wall-induced lift force drives the particles towards the

center of the channel, the shear-induced force does the opposite, so it pushes the particles towards the wall[43,53], and the rotational-induced lift force acts up the velocity gradient near the channel walls and directs particle migration to the face-centered equilibrium positions[57]; hence, particles near the channel wall would further migrate to the center of the wall[46]. This latter force allows to create a more complex model for inertia migration which can be described as a two-stage migration: during the first stage, in rectangular microchannels particles first moves towards the equilibrium positions near the walls, then, in the second stage, they are pushed towards the wall-centered equilibrium positions[46] (figure 2). In the end, when the net force is considered and all the forces are balanced, the equilibrium positions can be found between the centerline and the channel walls in rectangular microchannels[58] (figure 1).

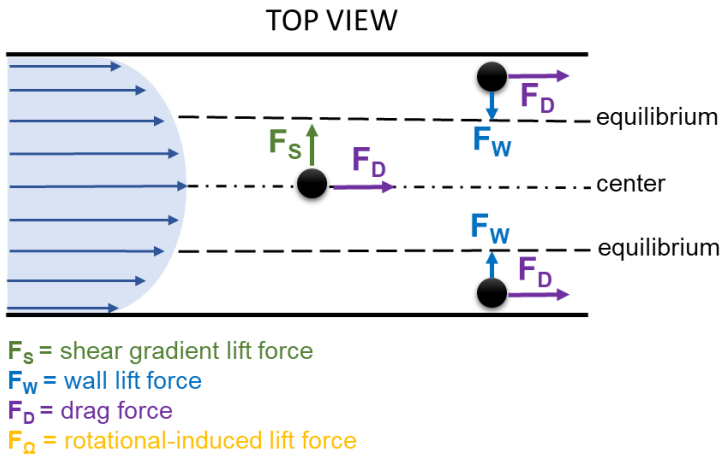

Figure 1 *– Top view of the different components of the inertia lift force acting on particles in a straight-rectangular cross-section channel. As in the legend, F_S represents the shear gradient lift force, F_W the wall-lift force, F_D the drag force and the blue arrows on the left side of the image represent the velocity vectors. When these forces are sum up together, the equilibrium positions between the channel centerline and the side walls can be reached*[46].

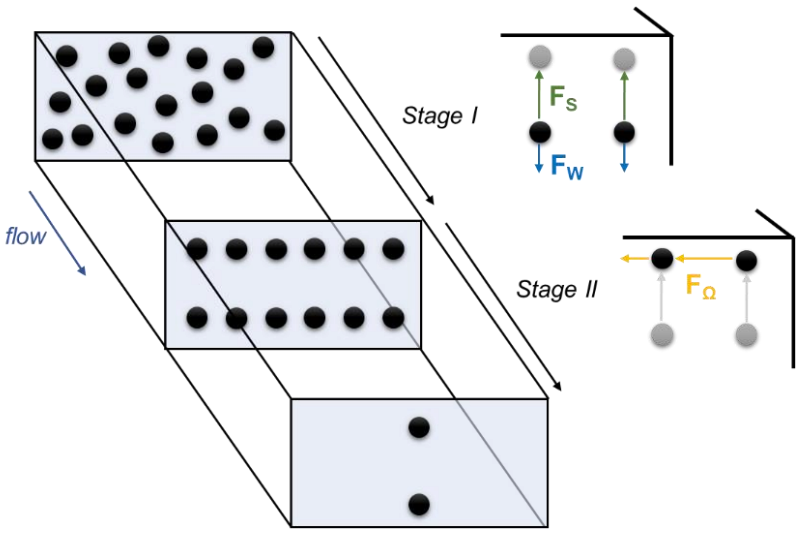

Figure 2 *– Two-stages migration of particles inside a low aspect ratio microchannel with a rectangular cross-section and at moderate Re. In the first stage, particles are pushed toward the equilibrium positions near walls thanks to the action of Fs shear gradient lift force and Fw wall-lift force, then in the second stage, particles move towards the wall-centered equilibrium positions under the effect of the rotation-induced lift force FΩ*[46]*.*

The net lift force acting on a neutrally buoyant particle flowing in a Poiseuille flow can be estimated as[58]:

$$F_L = \rho\, C_L\, \gamma^2\, a_p^4 \tag{4}$$

where ρ is the fluid density, γ is the shear rate of the fluid, a_p is the particle diameter, and C_L is lift coefficient which is a function of the particle position across the channel cross-section. The coefficient C_L at Re < 100 remains relatively constant[59] at a value of ~ 0.5 [57]; its sign indicates the direction of the particles migration: when $C_L > 0$ the particles are pushed away from the walls of the channel towards the center of the channel; when $C_L < 0$ the migration happens on the opposite direction so from the centerline towards the channel walls[58]. Both the positive and the negative lift coefficients are dependent on particle size and also the C_L^+ exhibits dependence on H^2 (height of the channel) while the C_L^- shows dependence on W^2 (width of the channel) in the case W>>H[46]. One consequence of equation 4 is the faster and more precise focusing of larger particles in the channel which also requires a shorter length for focusing. On the other hand, decreasing the particles' size does not mean increasing the focusing length, rather it acts more linearly concerning the reciprocal of particles' size[46]. Furthermore, the focusing length and focusing precision could be improved by exploiting the viscoelastic properties of the fluid, if used.

In viscoelastic fluids, particles' behavior is affected by the elastic force. In particular, this force is induced by a non-uniform normal stress difference in the channel[43], where the first normal stress difference ($N_1 = \tau_{xx} - \tau_{yy}$) creates an extra tension along the streamlines and the second normal stress difference ($N_2 = \tau_{yy} - \tau_{zz}$) produces a secondary flow over the channel cross-section[48]; τ_{xx}, τ_{yy}, and τ_{zz} are the normal stresses in the translational, velocity gradient and the rotational directions, respectively. Considering diluted PEO solutions, like our case, the magnitude of N_2 is at least 30 times smaller than that of N_1, thus the second normal stress difference can be neglected[41,43,48] and the elastic force (F_e) can be expressed as:

$$F_e = C_e\, a_p^3\, \nabla N_1 = -2\, C_e\, a_p^3\, \eta\, \lambda\, \nabla \gamma^2 \quad (5)$$

where C_e is the non-dimensional elastic lift coefficient, a_p is the particle's diameter, η is the polymeric contribution to the solution viscosity, λ is the relaxation time of the fluid, and γ is the local shear rate. Suspended particles migrate towards the low normal stress regions, where the shear rate tends to zero; in square or rectangular microchannel these regions are usually the center and the four corners of the cross-section[60] (figure 3).

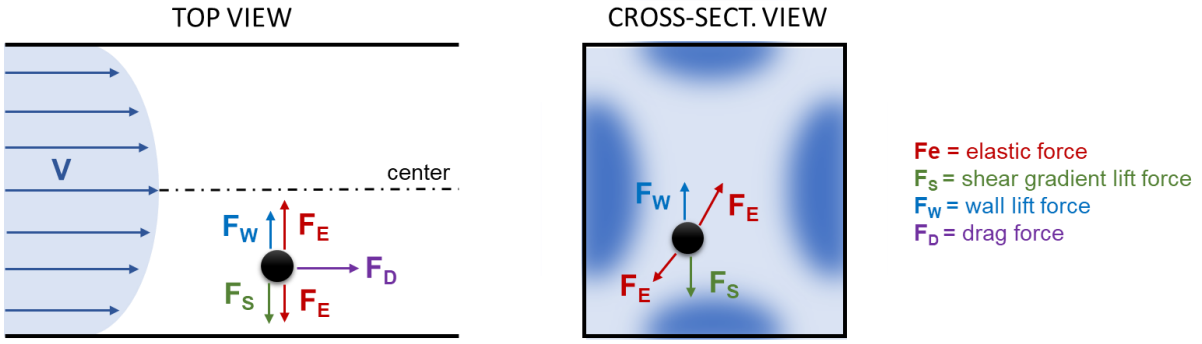

Figure 3 *- Top and cross-section views of the forces acting on particles in a viscoelastic fluid: in the top view, the Fw wall-induced lift force is pushing the particle towards the center of the channel while Fs shear-gradient induced lift force is responsible for the movement of the particle towards the walls; the F elastic force pushes the particles both towards the centerline and the equilibrium positions near the side walls while at the same time the F_D drag force is dragging the particles from the inlet to the outlet of the channel. In the cross-sectional view Fw and Fs has the same behavior as described before while here it is clearer how the elastic force F_E is pushing the particles towards the lower normal-stress difference regions, which are the four corners and the center of the channel (the darker the color, the higher is shear rate)*[48].

When inertial and elastic effects act together, the focusing is called "elasto-inertial focusing" and inertia pushes the particles away from both the walls and the center while the elasticity pushes the particles towards the centerline[53]. So, in flow with $0 < Re < O(1)$ particles are focused at the channel center due to the synergic combination of elastic force and wall-induced lift force; when $Re > O(1)$ the shear-gradient lift force becomes more relevant and drives the particles away from the centerline into equilibrium positions between the sidewalls and the channel's center[38]. Considering the equations of both inertial and elastic force we can speculate that larger components will be focused near the sidewalls, since the inertial lift has a stronger scaling than the elastic force[38], while the smaller particles will be focused on the centerline of the channel. We also have to take into consideration that in elasto-

inertial flow the equilibrium positions caused by the elasticity at the corners would be more quickly destructed by the inertial while the equilibrium positions in the middle of the channel would still be retained by the elastic force[53]. Indeed, the wall-lift force induced by inertia can impair the corner attraction effect of elasticity, so equilibrium positions at the corners become unstable and particles are focused only at the channel centerline[40]; to do so the flow rate can be increased and the importance of inertial and elastic effects can be regulated. It is important to notice that this separation by size is possible only in elasto-inertial fluids, indeed in Newtonian fluids, the particles cannot be separated decently by the pure effect of inertial forces[41]. As footnote is worth considering that the focusing of submicrometer particles with a diameter around or less than 1 μm may degrade due to the diffusive effect of Brownian motion[38], but since this is not the case of our research we would not speculate further about it.

There exist other two important forces that act on the particles and affect their migrations inside the microchannel: the Stokes drag force (F_D) and the Saffman lift force (F_{Saff}). The Stokes drag force is exerted on the corpuscles in the lateral direction because of the velocity difference between the particles and the fluid element[40] and it can be calculated as:

$$F_D = 3\,\pi\,\mu\,a_p\,(v_f - v_p) \tag{6}$$

where μ is the dynamic viscosity of the fluid, a_p is always the particle's diameter, v_f is the velocity of the fluid, and v_p is the velocity of the particle.

The Saffman lift force is exerted on the particle when the particle leads or lags behind the fluid; this involves the movement of the corpuscle towards the wall when the particles lead the fluid and towards the center when it lags behind the fluid[43]. It can be expressed as:

$$F_{Saff} = 6.46\,a_p\,\mu\,R_G(r)^{1/2}\,U_s \tag{7}$$

where $R_G(r)$ is the particle-scale Reynolds number based on the local shear rate, r is the radial coordinate, and U_S is the relative velocity between the particle and the fluid in the lateral direction.

As the magnitude of the driving force highly depends on the particles size, as shown from equation 4 to 6, we can speculate that large particles will be better focused than small ones; in particular, the bigger particles will be more tightly focused near the side walls while the smaller one will be found distributed at the center of the channel.

The last case to consider in viscoelastic fluids is the viscoelasticity-dominant flow situation that happens when the inertia is negligible. A separatrix (figure 4) divides the particles' migration according to their initial positions: if particles are found inside the separatrix, they migrate towards the centerline of the channel, if particles are found outside the separatrix, they migrate oppositely, so towards the walls[40]. The separatrix is the locus where the migration velocity of the particles is equal to zero; its location depends on the rheological properties of the suspending fluid. The lower is the shear-thinning effect, the closer it moves to the channel walls; the higher is the Wi number, the closer to the channel centerline it moves, thus increasing the area of the corner-attractive region[40].

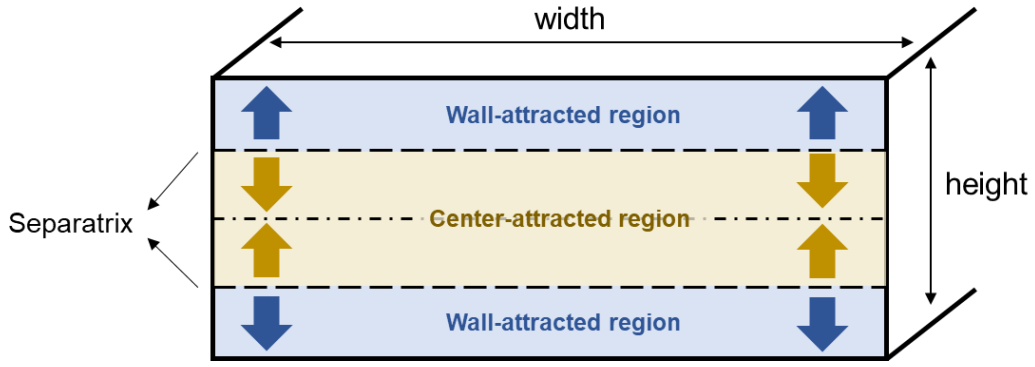

Figure 4 *- Separatrix in straight microchannels with a wide slit, W/H >> 1, and in a viscoelastic-dominant flow. The separatrix is represented by the dashed lines and it is a non-tangible line that divides the regions of the channel into wall-attracted regions where the particles are reported to move towards the sidewalls and the center-attracted region where the particles found in it move towards the center equilibrium position*[40].

1.2.2 Microfabrication Techniques

The main techniques used worldwide to produce microfluidic devices are photolithography and soft lithography. In particular, photolithography is the process that was first intended for the fabrication of microelectronic devices[61] and it consists of projecting a pattern onto a substrate after a selected exposure of a photoresist to UV light. Unfortunately, it is an intrinsically expensive technique because it required high-cost and high-maintenance equipment, like a cleanroom. Other disadvantages of this process are

the limited set of materials where the photolithography can be applied, the time and the cost involved in the fabrication of the mask, and the fact that it has no control over the surface chemistry and cannot be used for curved or non-planar substrates[61]. Soft lithography, on the other hand, solve some of these issues, and it is more suitable for microfluidics applications. Indeed, this technique is also defined as a suite of nonphotolithographic methods for replicating a pattern[62] and can be used for both microscale and nano-scale structures, for planar, curved, and flexible devices, and soft substrates, all with rapid and inexpensive prototyping[61]. Furthermore, soft lithography offers access to a broader choice of materials, as well as experimental simplicity and flexibility in forming certain types of test patterns[61]. But this technique still relies on the photolithography process to create the master.

For biomedical applications, poly(dimethylsiloxane) (PDMS) is usually chosen as material in the soft lithography process for its unique and attractive features: (i) a tunable shear modulus and Young's modulus by balancing the amount of pre-polymer in respect to the curing agent, (ii) an affordable cost (~$80/kg), (iii) compatibility with biological materials and non-toxicity, (iv) hydrophobic surface that, however, can be modified to become hydrophilic, and (v) capability to adhere to substrates in both reversibly and irreversibly ways, depending on its oxidation.

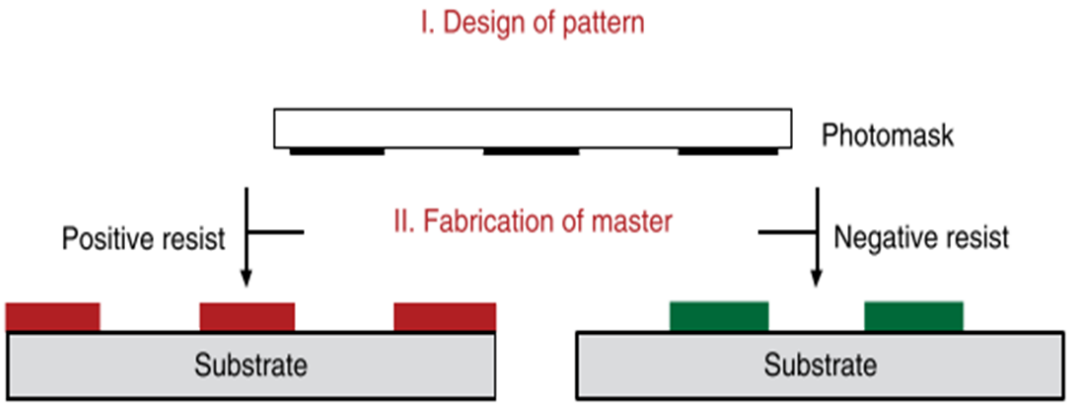

Figure 5 *- Photolithography technique with Positive or Negative photoresist. With a positive resist the areas exposed to light are removed in the development while with a negative resist the exposed areas are the remaining ones. Image is taken from Qin D, Xia Y, Whitesides GM. Soft lithography for micro-and nanoscale patterning. Nat Protoc. 2010;5(3):491–502.*

The microfabrication procedure starts with the pattern design on a computer-aided design (CAD) software program; for quick design of a pattern with feature sizes down to 1 μm two vector-based drawing programs can be used, instead, if higher precision and higher drawing speed are required,

computer-aided design (CAD) software programs are more suitable[61]. Then, the chosen layout has to be transferred to the silica mask. Before performing this step, the wafer surface must be dehydrated on a hotplate, cleaned, and treated with adhesion promoters to allow a solid bond between it and the photoresist polymer. Thereafter the chosen photoresist, that could be a positive photoresist (e.g., AZ) or a negative photoresist (e.g., SU-8) based on which areas has to be removed during the development (figure 5), is poured on the surface, and homogenously distributed with a spin coater. The desired thickness could be obtained by modulating the spin coater's parameters as rotational speed (rpm), acceleration (rpm/s), and time (s) that can be found in a specific table of the used photoresist. Before the exposure, the wafer with the photoresist film needs to be pre-baked to remove any remaining solvent and stabilize the film[63]; the time is dependent on the thickness. Then the transfer of the specific pattern takes place; there exist two different methods to perform this step: (i) by using a photomask that, thanks to the transparent and opaque layout, can cross-link the photoresist with the desired pattern, (ii) by exposing the wafer to a laser light which cross-links the negative photoresist following the design created with the specific software and uploaded into the laser source file. This latter procedure is easier to perform since it does not require the interposition of the mask and its alignment. Finally, the post-exposure bake (PEB) is required to continue the polymerization process. The final step consists of the film development: the wafer is placed on a SU-8 developer bath for a few minutes to allow the elimination of the unpolymerized photoresist, then the template is blow-dried. To prevent the PDMS from sticking to the features and ruining the wafer, Silanization is required. This process is performed carefully in a designated place and equipment to avoid any contamination due to its high toxicity and cancerogenic characteristic. It has to be noted that after this process, the first PDMS casting has to be tossed away to avoid any adverse reaction with the biological material used for the experiments.

Once the wafer with the desired features is created, the soft lithography process (figure 6) allows the production of microfluidics devices. This technique begins with the preparation of the PDMS by mixing monomer and curing agent, then the polymer is cast over the replica mold, degassed in a vacuum chamber, and cured in an oven to obtain the right consistency and level of cross-linkage of the polymer's chains. Once the PDMS is reticulated, the replica is peeled off the mold, and inlets and outlets can be

punched. To ensure the closure of the microfluidics device, which contains three of the four walls necessary for enclosed channels, the polymer has to be sealed with another surface, like a glass slide; for different application, different sealings are possible: the reversible one can be obtained by just pushing the two surfaces in contact by applying pressure while the irreversible sealing can be achieved by treating the involved surfaces with plasm oxygen, for instance.

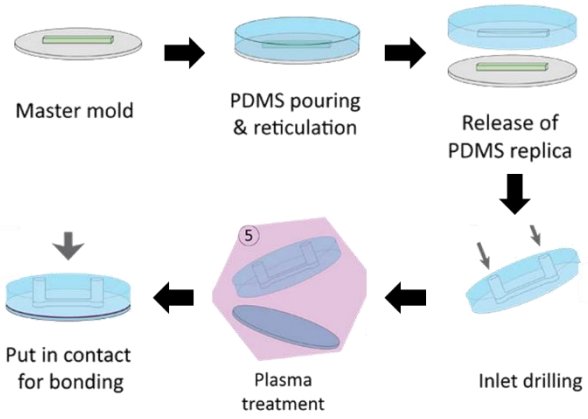

Figure 6 *- Soft lithography procedure: from the master mold to the final devices.*

1.3 Microfluidics Devices for Corpuscles Separation

In literature, from the extent of my knowledge, it does not exist a simple microfluidic device that operates with viscoelastic fluids and it is able to perform spermatozoa sorting from other cells and debris with the scope of improving and supporting the efforts of surgeons in obtaining pure sperm cells to use in IVF procedures. Indeed, only two publications exist that studied a microfluidic device designed to separate spermatozoa from leukocytes or red blood cells; both these studies were conducted by the group of Jiyoung Son et al[64,65] from the University of Utah and exploited inertial microfluidics in a spiral channel to perform the separation of spermatozoa from the red blood cells (in 2015), and the sorting of spermatozoa from leukocytes (in 2017). Overall, the results obtained from the first work were better than those from the second one, probably because inertia microfluidics is not the most suitable choice for cell separation by size, as discussed in paragraph 1.2. Below, in figure 7, are reported the main achievements for the optimal flow conditions from these studies; as we can observe, they were not able to perfectly separate the cells and a great amount of them was overlapped thus making their

device still in need of improvements to answer the real requirement of pure spermatozoa samples at the outlets.

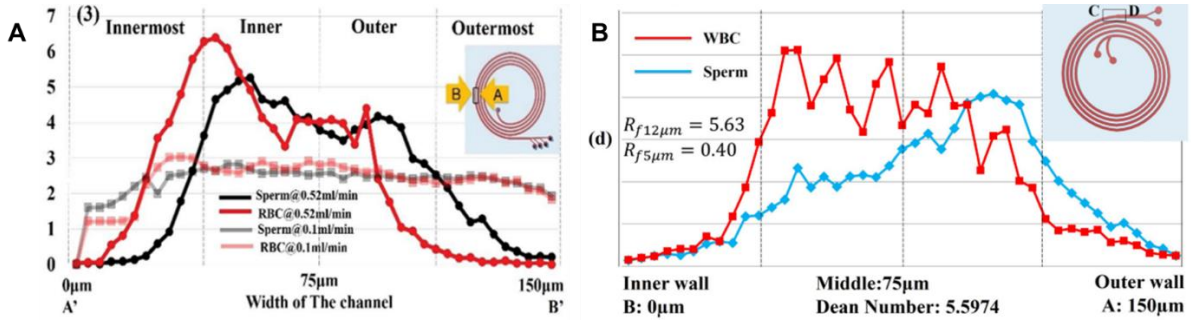

Figure 7 *- Stained cell population intensity analysis throughout the width of the channels taken from the papers of Jiyoung Son et al:* ***A)*** *Non-motile sperm cell separation using a spiral channel. Anal Methods. 2015; http://dx.doi.org/10.1039/C5AY02205C - analysis of RBCs-sperm separation at the outlet;* ***B)*** *Separation of sperm cells from samples containing high concentrations of white blood cells using a spiral channel. Biomicrofluidics. 2017; http://dx.doi.org/10.1063/1.4994548 - analysis of the WBCs-sperm separation at the outlet.*

The main issues encountered during these studies were the lack of achievement of a net separation between the different types of cells, and the poor spermatozoa focusing due to an incomplete understanding of how sperm cells behave in the inertial microfluidic channel[64]. This may happen because spermatozoa are not used to swim into inertial fluids, but they rather naturally swim into viscoelastic fluids; indeed, there exist only computational studies about the movement of sperm cells in their natural environment, so in non-Newtonian fluids, but there are no investigations available about the movements of spermatozoa in inertial fluids. Finally, it is worth noticing that the use of a spiral channel intrinsically required long channels and thus, it creates high-pressure drop issues.

For these reasons, and all the others mentioned in paragraph 1.2, I reviewed the main studies about viscoelastic microfluidics carried out in both spiral and straight channels:

In spiral channels, the few papers published did not use any biological samples but simply studied the behavior of synthetic particles. Almost all of the papers used the PEO[66–69] as viscoelastic fluid, while only the group of Xiang Nan et al. also studied the behavior of particles into PVP fluid[70]. The diameters of the particles employed ranged between 1 and 10 µm in all the studies except for Chao Liu et al.[68] group that decided to test also nanoparticles (results for particles with a diameter of 100 and 200 nm were reported). This latest group only reported the focusing efficiency for the particles, which was in

the order of 80%, but did not test the purity and efficiency of separation; their results were in agreement with the viscoelastic theory which expects smaller particles to focus on the center of the channel while larger ones to focus near its sidewalls. The major drawback of this study is the extremely low flow rate: 0.023 µL/min which is not suitable for applications outside the academic world. Higher flow rates were investigated by Doo Jin Lee et al.[67] and Haidong Feng et al.[69]. In particular, the work of Doo Jin Lee et al.[67] used a range of 1 – 12.5µL/min while the group of Haidong Feng et al.[69] tested the flow rates between 5 – 100µL/min, considering the optimal flow rate between 10 – 50µL/min. Neither of these studies calculates the sorting parameters, but instead only measured the focusing efficiency and were able to obtain the predicted equilibrium positions: in the middle of the channel for the smaller particles (diameter < 5 µm) and near the sidewalls the larger ones. Slightly higher flow rate values were achieved by the group of Xiang Nan et. al[66,70], between 60 – 120µL/min because the PVP allowed reaching a greater throughput. However, it must be noted that these two latter projects did the experiments with just one size of particles at the time and so they were only able to study the behavior of corpuscles inside the curved microchannel without taking into consideration the interaction between particle types and the ability of their device to sort particles. Summarizing, the ability of spiral channels to separate cells is yet to be demonstrated and the contribution of the Dean force to all other effects acting on the corpuscles in a viscoelastic fluid makes the prediction of the results still unclear. Furthermore, the complexity of the channel design, the pressure drops, and the final throughput did not make this choice of design worth our final aim. Indeed, similar flow rates have been used in straight microfluidics channels for different applications and better results not only of focusing but also of sorting were demonstrated.

Three major groups can be identified, based on the different viscoelastic fluids used: hyaluronic acid (HA), polyethylene oxide (PEO), and other less common fluids such as polyvinylpyrrolidone (PVP), Xanthan Gum and λ-DNA segments. This distinction has been made to group similar particle or cell migrations, and parameters needed due to the different rheological properties of each fluid.

The papers that mentioned the use of HA as viscoelastic fluid are similar in the choice of particles tested, with diameters ranging between 2 – 10µm and all of them tested WBCs inside their straight

channels. Only the group of Hyunjung Lim et al[55] tested particles with a diameter ranging from 6 to 27μm. The studies of Hyunjung Lim et al[55] and Jeonghun Nam[71] are similar in the design since they both used microchannel with a rectangular cross-section with an aspect ratio of about 2. The first one tried to separate the CTCs from WBCs and was able to achieve their separation at 500μL/min; the CTCs were recovered from the side walls while the WBCs were tightly focused on the center of the channel. The second one tested only the WBCs instead and studied their equilibrium positions in respect to the variation of the flow rates, which ranged between 10 – 300μL/min; the optimal flow rate of 100μL/min was discovered for the central focusing of the WBCs. The scientific paper of Jeonghun Nam and Woong Sik Jang et al.[72] decided to use a smaller microfluidic device with 50 μm x 25 μm dimensions and was able to perform the separation between Candida cells and RBCs at around 100μL/min; as expected the smaller cells were focused at the centerline of the channel while the WBCs were focused into two streamlines near the sidewalls. Eugene J. Lim et al.[73] exploited a channel with a square cross-section instead and only tested the WBCs behavior inside it. Lastly, Jeonghun Nam and Yong Shin et al.[74] tried to implement a two-stages separation for parasite malaria and WBCs sorting; they were able to obtain at 400μL/min a 94% recovery rate and 99% purity for this separation. Unfortunately, all these examples using HA as viscoelastic fluid operated with an Elasticity value lower than 0.3; this means that their devices were working in elasto-inertial conditions with a predominance of inertial effects. Thus, the main concern about these works is that, even though the throughput of the microchannel using HA can be high, the parameters used are more in line with an inertial approach[75].

About the groups that used non-conventional viscoelastic fluids, the works of Di Li et al[42], Bookun Kim et al.[39], and Jeonghun Nama,1, Bumseok Namgung et al.[44] are worth to be mentioned. In particular, the group of Di Li et al[42] chose to use a fluid with a strong shear-thinning effect and low elasticity, xanthan gum, which permitted the achievement of the typical viscoelastic focusing positions while keeping a high throughput similar to the one in inertial works, around 100μL/min. The major issue is that this fluid is not compatible with biological samples and so cannot be used for our application. Bookun Kim et al.[39] obtained a remarkable Elasticity number, equal to 140, by using just a small amount of λ-DNA fragments but their very low flow rate, between 0.3 and 3μL/min, is a problem for practical channels

needed for our application. Furthermore, they were only able to demonstrate the focusing of RBCs at the center of the channel while we would need them to be focused near the sidewalls for an efficient separation from spermatozoa. Lastly, Jeonghun Nama,1, Bumseok Namgung et al.[44] tried to exploit the PVP rheological properties to achieve a two-stage separation of blood cells. Unfortunately, their work was able to utilize only low flow rates, representing a strong limitation in clinical applications. Thereby, also these unconventional viscoelastic fluids are not suitable for our aims.

In the following, I will present the five major studies that used the PEO as viscoelastic fluid and separating channel dimensions compatible with my application: Liang-Liang Fan et al[43], Dan Yuan et al[41], Chao Liu et al[38], Xinyu Lu et al[76], Jeonghun Nam, Hyunjung Lim et al.[60], and Seungyoung Yang et al.[53]. In particular, the principal characteristic to consider was the Elasticity number, which was around 18, thus falling in the elasto-inertial focusing theory where corpuscles can be separated by size. Besides, the geometrical dimensions used were around 30 – 50μm for the width and 10 – 50μm for the height. These values were chosen based on the particles and cells used for the experiments: the smaller the particles, the smaller the channel. Since the cells that were employed for their experiments were microalgae, bacteria, CTCs, and blood cells, the particles used to simulate their behavior were in the order of tens of microns. The rheological properties of the PEO added to the geometrical requirements of the channel allowed flow rates in the range of 1 – 20μL/min. These values are promising for our research when compared to my previous Master Thesis work of Barilla L.[75] , where I demonstrated how the flow rate could be improved till 30 – 40μL/min while still obtaining good results in terms of focusing. In all these mentioned research studies the quantitative parameters to define the sorting were calculated and the overall efficiency and purity were always between 85% and 95%, which is higher as compared to the inertial counterparts. Among the previously cited works, one is worth mentioning separately because the authors separated particles based on their shape rather than their dimension. Xinyu Lu et al[76] used both spherical microbeads and peanut-shaped beads suspended into a 1000ppm PEO solution and investigated their sorting by just exploiting the action of the different forces on the different shapes. They were able to successfully separate the two types of particles by using a 2.5μL/min flow rate and by tuning the elasticity at a value to 18.8. This project is particularly relevant for our study

because the peanut-shaped particles are very similar to the head of the sperm cells and thus we do expect them to behave in a very similar way, so by focusing within a bandwidth at the center of the channel, along the flux.

The state of the art just considered has established the starting point of my thesis research and it has set the issues to overcome; I understood that the best choice of fluid is a viscoelastic fluid, which is more similar to the natural environment of the biological sample we have to separate, and it is more suitable for achieving the size and shape-based separation of cell thanks to the elasto-inertial effect. Furthermore, I chose to use a straight microchannel because the synergistic action of the Dean force with all the other effects makes too unpredictable the behavior of spermatozoa inside the channel and, besides, the flow rates and throughput achieved were comparable with the one achieved in straight channels. Plus, in this last type of device, there are fewer concerns about pressure drops and the purity of the extracted sample. Finally, the literature examples of devices using PEO have provided hints on the choice of design parameters such as geometrical dimensions, the concentration of viscoelastic fluids, and thus the rheological parameters needed to achieve our goals. To conclude, the path of continuing using straight microfluidics channels with viscoelastic fluids was the optimal one since it allows to offer the best performances in terms of cost, user-friendliness, throughput improvement, cell separation purity, and similarity of cells natural environment was taken. This was also pondered with my previous thesis research[75] in which the feasibility of asymmetric cell separation was demonstrated and its improvement and change of application seemed the right continuation.

1.4 Aims of the thesis

The scope of this project is to create a passive microfluidic device consisting of a straight channel with a rectangular cross-section that is able to perform the separation between spermatozoa and other cells that can be found in the semen or the biopsy fluid of a male testicle by exploiting the viscoelastic effect of the medium.

In particular, the thesis has three main objectives: at first, to find the optimal conditions for sorting microparticles (with a size similar to target cells) based on their dimensions; secondly, to separate

spermatozoa from leukocytes in order to obtain a pure sample of sperm cells for their subsequent use in IVF procedures; lastly, to achieve the optimal separation of spermatozoa from all the cells that could be found in the supernatant, so in the biopsy's tissues collected, such as red blood cells, leukocytes, cells debris, etc. This latter is needed to obtain a valuable device that supports clinicians after different procedures, such as TESE or just from samples of leukocytospermic patients, and permits pure spermatozoa extraction for optimized ART procedures.

To accomplish these aims we started by studying previous works and by trying to improve my previous own results reported in my master thesis completed at the University of Illinois at Chicago (UIC) under the guidance of Dr. Papautsky. That investigation helped me to start from an established strategy of asymmetric cells sorting by exploiting the viscoelastic effect of the fluid, which was demonstrated to represent an optimal choice in terms of straightforwardness of channel design, low cost, and feasibility of the final clinical demand. Afterward, the improvement of the geometrical dimensions was made in order to accomplish a different cell sorting: bigger and different shapes of cells were used in our project and little adjustments were required; these changes were made by taking into consideration quantitative data such as dimensionless numbers, pressure drops, concentrations values, and other parameters calculations. When the optimal conditions of particle separation were found, experiments with human cells were performed first starting with the testing of a single type of cells alone then by adding all of them together. The ultimate objective was to test the supernatant liquid obtained by the testicle's biopsy to investigate the feasibility of the direct cells sorting with our device. Some issues were reported, and improvements are still needed; indeed, it must be noted that not all the proper and planned experiments were brought to a conclusion due to the delays and complications encountered during the current pandemic situation. Nevertheless, promising results were found, and improvements to the current device were proposed.

CHAPTER 2

MATERIALS AND METHODS

2.1 Microfluidic Channel

Two different straight microfluidic channels with a rectangular cross-section (figure 8) were produced using classic soft-lithography techniques. The straight design was chosen instead of the curved one because we wanted to avoid the issue of the high-pressure drop required if compared to the long channel, especially when using viscoelastic fluids[38], but also because, as said in the previous chapter, the unpredictability of the synergic action of the Dean force summed with all the other forces would make too uncertain our research project. The choice of this particular shape for the cross-sections is not only dictated by the simpler production process, but also by the fact that this type of channel is the most common and easiest to implement in most lab-on-a-chip applications[40].

Both channels have a height of 30 µm, a length of the main straight body of 3cm, and 3 different branches of 1.5cm before the outlets. The difference between the two channels is the width which is 50µm and 75µm for the first and the second channel, respectively. The aspect ratio (AR) of the channels is 1.67 for the 50µm x 30µm and 2.5 for the 75µm x 30µm channel. The dimensions have been calculated considering the notorious blockage ratio ($a_p/Dh > 0.07$) condition[57,77] needed to obtain the focusing of microspheres in a microchannel. In the equation, a_p is the particle diameter and Dh is the hydraulic diameter defined as $Dh = 2WH/(W+H)$, where W is the width and H is the height of the microchannel cross-section. The length of the main channel was decided after the evaluation of previous studies and, in particular, of Barilla L. Master Thesis[75] in which an optimal length of 3 cm for the sorting of both spherical and asymmetric cells was demonstrated.

As we can observe from figure 8, the inlet and outlet sections are made of a larger area in which two rows of pillars operate as filters: everything larger than 25µm cannot go through. These structures are needed to avoid the clogging of the channel and are created by taking into consideration the biological cells that are intended to be separated: human red blood cells that have a mean diameter of 8µm, human leukocytes that have a mean diameter of 15µm and spermatozoa that have 10, 4 and 2µm as main head dimensions. The expansion after 3cm is needed to obtain the enhancement of the particles' separation and the improvement of the corpuscular sorting.

The reason for this specific configuration, called open outlets configuration, with different ramifications after the main body and its expansion lies in the necessity of controlling and adjusting the sorting cutoff, the fluid resistance, and resistance ratio; indeed, the different marks on the different branches are positioned at different length values so that, after specific calculations, the purity and separation efficiency can be changed and regulated by just changing the position of the punched outlets without having to redesign and refabricate the entire device.

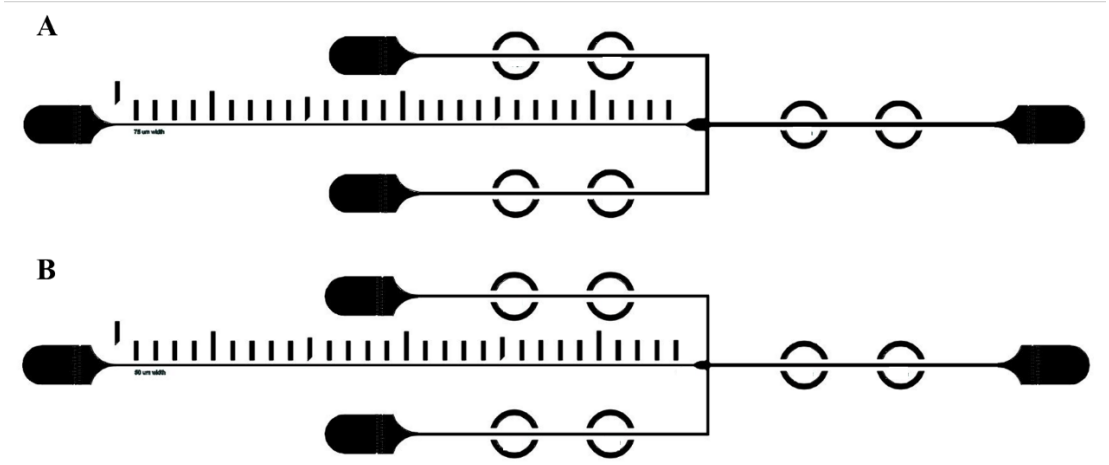

Figure 8 *- Two different straight microfluidics channels with a rectangular cross-section. A) 75 µm x 30 µm channel, B) 50 µm x 30 µm channel.*

2.2 Microfabrication Process

The microfabrication process started with the creation of the microfluidic channels on computer-aided design (CAD) software programs (AutoCAD, Autodesk Inc.), then the chosen pattern was transferred to the Layout Editor software where the drawings were adapted and uploaded into the laser source file.

To create the master a 4 inches Si wafer was used; before covering it with the photoresist and obtaining a good adherence it was necessary to clean the wafer surface, then to improve the resist adhesion on the wafer so Ti Prime was used; it was poured on the surfaced and spin-coated with a two-step spinning functions: 1) 500 rpm for 10 seconds with an acceleration of 100 rpm/second and 2) 6000 rpm for 40 seconds with an acceleration of 300 rpm/second); in the end, it was baked at 120°C for 2 min. After this, a layer thick 30 µm of photoresist was spin-coated over the wafer surface. The negative photoresist used was the SU-8 (2035) (MicroChem, USA) and to obtain the right thickness, a spin-coater machine (POLOS SPIN150i) was used with a two-step spinning function: 1) 500 rpm for 10 seconds with an acceleration of 100 rpm/second and 2) 4300 rpm for 30 seconds with an acceleration of 300 rpm/second), following the guidelines of figure 9. Then, the master was subjected to the pre-exposure bake (PEB) on a hotplate firstly for 1 min at 65°C and secondly for 5 min at 90°C to remove any remaining solvent and stabilize the film while eliminating the sticking effect.

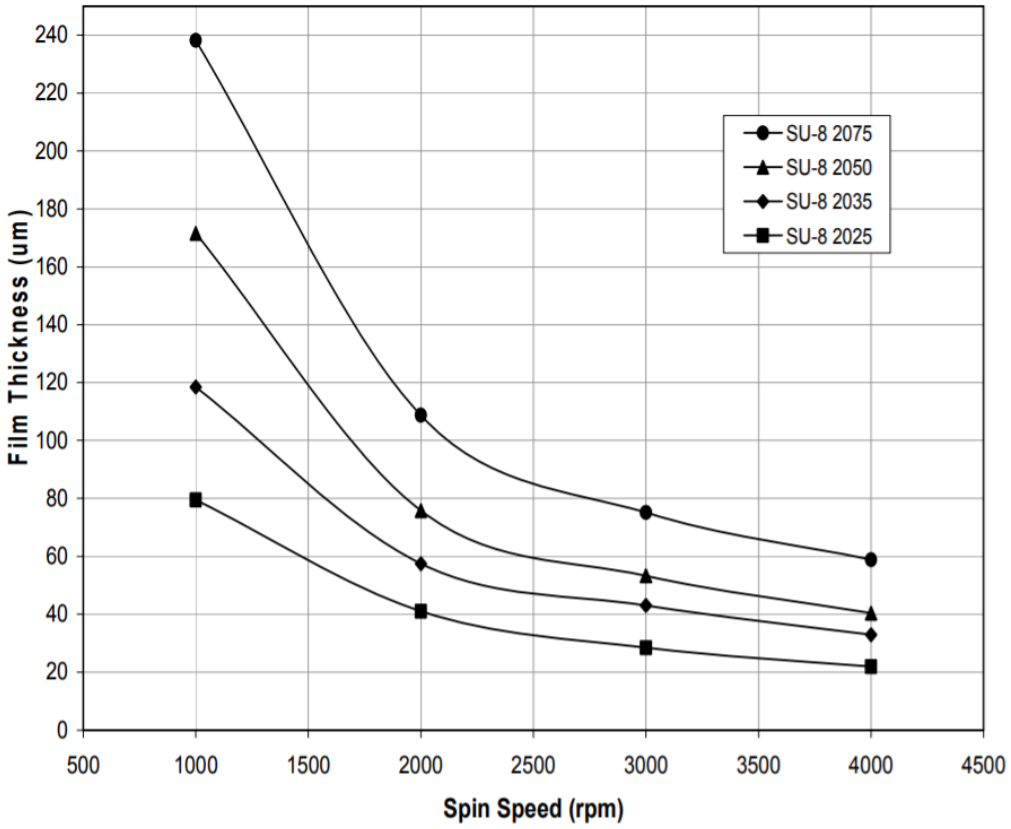

Figure 9 *- Spinning curve for different types of SU-8 taken from www.microchem.com and used for our experiment set-up.*

The desired design was recreated on the 4" Si wafer in a cleanroom environment (Polifab, Politecnico di Milano) by exposing it to a laser light (Maskless aligner (Heidelberg MLA100) exposure) with 650mJ/cm^2 dose and -2 defocus, which cross-linked the negative photoresist following our features. To continue the polymerization process, the master was post-exposure baked always on a hotplate firstly at 65°C for 1 min, secondly at 90°C for 5 min, and lastly at 65°C for 1 min. Finally, the film of photoresist on the wafer was developed into the developer, ethylene glycol monomethyl ether acetate, bath for 3 minutes. The final master was then rinsed and blow-dried. In conclusion, the silanization process was performed by adding few drops of xylene onto the features' side of the wafer, then leaving it to ventilate for 20 min, and the reticulation was finished at room temperature for 24h (or by baking it at 65°C for 2h).

The soft-lithography technique was used to create the PDMS devices but since the increasing of the production rate was necessary, before proceeding with the production copies of the master were made with epoxy resin (10 10 CFS, C-system). To begin, the first PDMS master mold obtain from the wafer was placed into a petri dish; component A and component B of the cited resin were mixed at a 2:1 ratio respectively for at least 30 seconds. Then the mixture was de-bubbled with a vacuum pump for 1 min and let it rest for a few second, twice. The resin was poured into the petri dish starting from the borders and finishing on the PDMS master; finally, everything was degassed again for 1 min, twice. To allow a flawless reticulation, the petri dish with the master covered in resins was left on a flat surface overnight at room temperature. The following day the PDMS master was peeled off and stored accurately while the epoxy mold was treated with xylene for 20 min to ensure the resistance of the features. The device production consisted of mixing PDMS monomer and curing agent with a ratio of 10:1 (Sylgard 184, Dow Corning Midland, MI, USA); the mixture was then poured over the replica mold, degassed in a vacuum chamber for at least 20 min and finally baked at 65°C for 2h or left at room temperature on a flat surface for 24h; in this latter case, curing in the oven at 65°C for 1h is recommended to eliminate the sticking effect on the surface. After this, PDMS replicas were peeled off from the mold, and the inlets and outlets were created with a puncher. Finally, as described in chapter 1 section 1.2.2, the device

was bonded to a glass slide by treating the surfaces with plasma oxygen (Harrick Plasma, Basic Plasma Cleaner, Ithaca, USA). To ensure the bonding, the device was baked once again at 65°C for 1 h.

2.3 Sample Preparation

The viscoelastic fluid chosen for our research was Poly(ethylene oxide) (PEO) (MW = 2 x 10^6 Da) (Sigma-Aldrich, USA); it was diluted in phosphate-buffered saline (PBS) (Dulbecco's Phosphanate Buffered Saline 1X, Microgem, Napoli, Italy) to create a viscoelastic solution of 1000ppm that could match the osmolarity required by cells (290 mOsm/kg). The choice of the PEO, among the other long-chain polymers that allows creating a non-Newton fluid, was based not only on the larger availability, lower cost, and simpler preparation[42] but also because our research project wants to establish a continuance with my previous Master Thesis project and demonstrate the ability to exploit viscoelasticity in straight microfluidics channels for various biological samples and to improve the separation ability while creating a tangible and functioning device to use in hospital environments. There was no need of adding Tween 20 to the solution in order to prevent particle aggregation because it was already included in the microbeads solutions purchased from Bangs Laboratories Inc.

2.3.1 Microbeads

To replicate the cells' behavior polystyrene microbeads are needed; they are utterly important to predict the biological sample movement and to find the optimal parameters for achieving the separation of the cells. This step is then crucial to understand the expected behavior and eventually adjust the procedure and the device before starting with the samples experiments and consequently wasting biological material.

For our test, we decided to use three different dimensions, 4μm (~4.19μm), 7μm (~7.32μm), and 15μm (~15.25μm), of fluorescent polystyrene particles (Bangs Laboratories Inc., Indiana, USA) that were then diluted in our viscoelastic fluid to obtain a specific concentration that wanted to mimic the biological one. Those dimensions were chosen because we wanted to mimic as much as possible the real biological samples that we would have used. It is knowledge of all that the RBCs have a discoid shape with a mean diameter of 7-8μm[78], the leukocytes are more spherical and have a mean diameter

of 15µm[79] while the spermatozoa have a much more complicated shape; their tiny tail could be as long as 50µm, instead, their head has a flat ellipsoid shape of about 4µm x 3µm[80]. Since the more relevant dimensions are the radius for the RBCs and WBCs and the length for the spermatozoa, we decided to purchase PS particles that could simulate them, even though the spherical shape could be very far from the reality in the specific case of sperm cells. All the concentration values of the microbeads used in the experiments are reported in Table 1 below.

particles diameter (µm)	concentration (particles/mL)
4	1.00 x 10^6
7	1.01 x 10^6
15	9.96 x 10^5

Table 1 *- Table of the particles' concentrations of our used solutions*

To calculate the exact values, the concentration formula and the dilution formula were used; the concentration formula takes into consideration the space occupied by each bead and its size and it is the following:

$$\frac{particles}{mL} = \frac{6\,W\,10^{12}}{\rho\,\pi\,d^3} \tag{8}$$

where e W is the weight of particles in g per mL in the solution (0.010 g/mL for Bangs Laboratories microbeads), ρ is the density of polymer (1.06 g/mL) and d is the mean diameter of the particles in microns (4.19 µm, 7.32 µm, and 15.25 µm).

The dilution formula is the renowned C_1 x V_1 = C_2 x V_2, where C is the concentration expressed in particles/mL, V is the volume expressed in mL and 1 and 2 refers to the initial and final step, respectively.

2.3.2 Biological Samples

For our experiments human cells were used; in particular, seminal fluid, spermatozoa, red blood cells, and leukocytes were obtained from the waste of samples collected from healthy subjects that underwent a periodical check-up at Centro Scienze della Natalità of San Raffaele Hospital. Routine exams of both

seminal fluid and whole blood were performed to ensure the physiological conditions of the biological samples.

The spermatozoa were obtained by centrifuging (Heraeus Multifuge 3SR Plus, Thermo Scientific, US) without brakes 100µL of human seminal fluid diluted in 10 mL of 1000ppm PEO in PBS for 10 min at 3000 rpm; to get rid of all the cellular debris, the sample was then washed twice in the PEO in PBS solution and resuspended in 3mL of the 1000ppm PEO in PBS solution to obtain the final concentration of about 3.7 x 10^6 cells/mL. The overall motility of the sperm cells was always between 70 and 80% for all the samples used; the morphology was in the optimal ranges, and the presence of round cells, specifically of leukocytes was always between 1-2%. Thus, the samples were classified as normospermic.

To separate the whole blood and obtain the RBCs and WBCs separately, the density gradient centrifugation method was used: in a 15mL falcon tube 1 part of 1X PBS (Dulbecco's Phosphate Buffered Saline, Biowest, USA) and Percoll (Merck Millipore, USA) solutions with a matching osmolarity, 1 part of HBSS (Hanks' Balanced Salts Solution 10X, Biowest, USA) solution, and 1 part of whole blood were added together carefully in this particular order to avoid their mixing; the entire solution was then centrifuged (Heraeus Multifuge 3SR Plus, Thermo Scientific, US) for 40 min at 1500g with the brakes. Right after, the five different phases formed were withdrawn with a pipette; in particular, the plasma, the PBMC (peripheral blood mononuclear cells), and the medium were eliminated while the granulocytes and the RBCs were retrieved. Unfortunately, the leukocytes could not be fully retrieved due to the massive presence of the RBCs and thus could not be used in the experiments. The recovered erythrocytes were diluted 1:1000 with the 1000ppm PEO in PBS solution and the concentration was calculated by using a hemocytometer; the final concentration of the solution used was about 4.5 x 10^6 cells/mL.

For the experiments with the entire seminal fluid, it was diluted without further treatments in the 1000ppm PEO in PBS solution to test the ability of our device to retrieve the spermatozoa from the non-treated sample; the concentration used was about 3.5 x 10^6 cells/mL. Finally, the solutions of

spermatozoa mixed with RBCs or with the 15µm particles were created by following the specific procedure already explained in the previous paragraphs and were just added together to obtain a concentration of about 3 x 10^6 cells/mL for the spermatozoa, 6 x 10^6 cells/mL for the erythrocytes and 2.5 x 10^6 particles/mL for the 15µm beads. A high concentration of RBCs was required because the first solution with a match concentration with the sperm cells was not suitable since it did not allow us to see and count the erythrocytes present. While the concentration of the microbeads was dictated by the particles' solution availability; indeed, only 1mL of the solution was bought and it did not allow higher concentrations due to the consistent number of experiments that had to be carried out.

2.4 Experimental Procedure

The setting of the experiments is reported in figure 10, where both the general set with all the instrumentation used and the details of the microfluidic device could be seen.

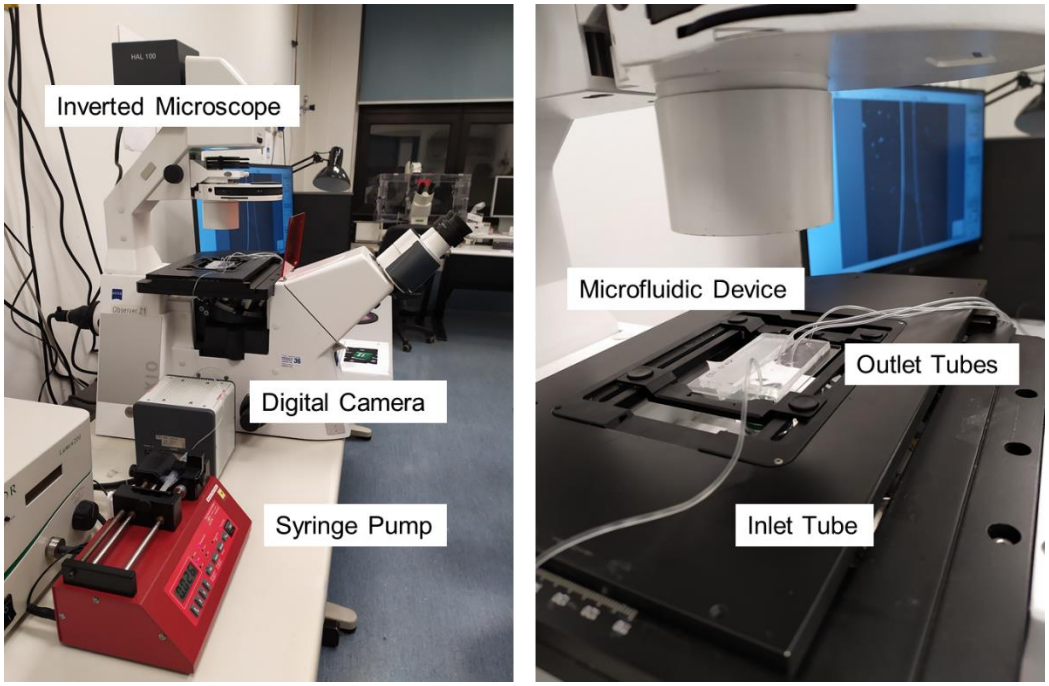

Figure 10 *- Images of the setting for the experiments of this research; in the first image the inverted microscope, along with the digital camera and the syringe pump used could be seen, while in the second one the microfluidic device setting, and the inlet and outlets tubes are reported.*

2.4.1 Microbeads

Polystyrene microparticles of 4 µm, 7 µm, and 15 µm (Bangs Laboratories, Inc., Indiana, USA) were used to simulate the spermatozoa, red blood cells, and leukocytes, respectively. The sample solution created by adding the microbeads to the viscoelastic fluid was pumped into the microfluidic device using a 2.5 mL syringe (Pic Solution, Italy) connected to a Tygon tube; the flow conditions were controlled by a syringe pump (Aladdin Syringe Pump, WPI, Florida, USA). An Inverted Phase Contrast Fluorescence Microscope (Zeiss Axio Observer Z1, Zeiss, Germany) fitted with a digital EMCCD camera (Hamamatzu, EM-CCD C9100, Japan) was used to capture fluorescent images. The exposure time used was 100ms, the specific setting was binning 2 and 111 gain; the fluorescence channel was tuned on the different fluorescence of the different particles tested, and a 20X objective was used.

2.4.2 Biological Samples

Biological samples used were spermatozoa, RBCs, WBCs, and seminal fluids from healthy human patients of San Raffaele Hospital. The biological solution was created by adding the cell species to the 1000ppm PEO in PBS solution, then it was pumped into the microfluidic device using a 2.5 mL syringe (Pic Solution, Italy) connected to a Tygon tube; the flow conditions were always controlled by a syringe pump (Aladdin Syringe Pump, WPI, Florida, USA). An Inverted Phase Contrast Fluorescence Microscope (Zeiss Axio Observer Z1, Zeiss, Germany) fitted with a digital EMCCD camera (Hamamatzu, EM-CCD C9100, Japan) was used to capture bright-field images. The setting was: exposure time = 1ms, binning 2, and 500 frames; all the pictures were captured with a phase-contrast and the objective used was 20X for the straight channel and 10X for the expansion before the outlets.

2.5 Data Analysis

The analysis of data was possible thanks to different software: Volocity was to capture the images from the Zeiss Axio Observer Z1 Microscope; ImageJ, Excel, Origin Lab, R, and MatLab were used to perform the post-process analysis and to convert what we could observe qualitatively in quantitative data that could be analyzed.

Before starting with the experiments, the values of the important parameters needed for the behavior prediction and experiment set-up were calculated. In particular, dimensionless numbers, pressure drop,

blockage ratio, hydraulic diameter, particles, and cell concentrations were determined by implementing a sheet code in MatLab. During the experiments, fluorescence images were acquired with 20X and 10X objectives; for 4 μm, 7 μm, and 15 μm particles 300 images were then stacked together with the "stacks", "Z project" and "standard deviation" tool in ImageJ; for the BF images, 500 frames were summed together and "stacks", "Z project" and "max intensity" setting were used. For the fluorescence pictures, ImageJ also allowed us to measure the dimensions of the channel, the streamlines, and their relative position with respect to the width. Then, all these data were analyzed with Excel and plotted using Origin Lab; Excel was used to create the database and to normalize all the quantitative data obtained from the fluorescent images, then Origin Lab allowed us to calculate important parameters such as the full width half maximum (FWHM), peak positions, underlying areas, baselines, and to recreate the Gray Values-Positions graphs.

With all these quantitative data, we were able to calculate the focusing efficiency and purity of the single particles or cells as reported below[48]:

$$focusing\ efficiency = \frac{mean\ diameter\ of\ the\ corpuscles}{FWHM\ of\ the\ streamline}\ x\ 100 \tag{9}$$

$$separation\ efficiency = \frac{total\ target\ entities\ in\ the\ outlet}{total\ target\ entities}\ x\ 100 \tag{10}$$

$$purity = \frac{total\ target\ entities\ in\ the\ outlet}{total\ entities\ in\ the\ outlet}\ x\ 100 \tag{11}$$

The focusing efficiency graphs were created by plotting the calculated values with R, while the graphs about the separation efficiency and purity were designed with Excel.

CHAPTER 3

RESULTS

3.1 Characterization

The characterization of the wafers created, and the verification of the right heights and lengths of the features is a crucial step: a variation in the measurements from the original CAD project to the final realization could undermine the whole process. To verify the correct dimensions, the first PDMS casting onto the wafers was cut longitudinally in thin slices exactly where the most important features were located. Then, these pieces were placed onto a glass slide and observed with an Optical Microscope (AmScope, US). In figure 11 and 12 are reported the main cross-section measurements of our channels, while in table 2 below it is possible to observe the mean and standard deviation errors values of respectively the 50µm x 30µm and 75µm x 30µm channels.

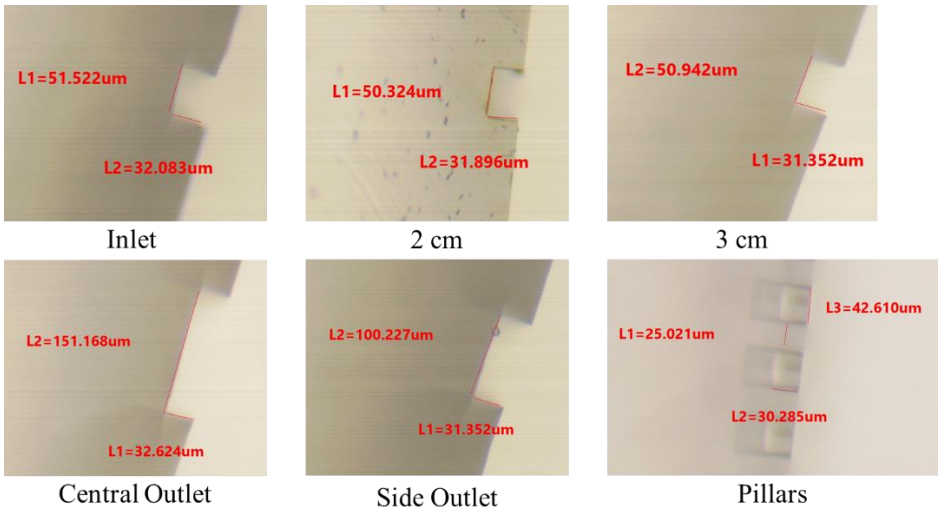

Figure 11 *- Bright-field major pictures of wafer cross-sections of 50 µm x 25 µm channel; from top left to bottom right: inlet, at 2 cm, at 3 cm, central outlet, side outlet, pillars.*

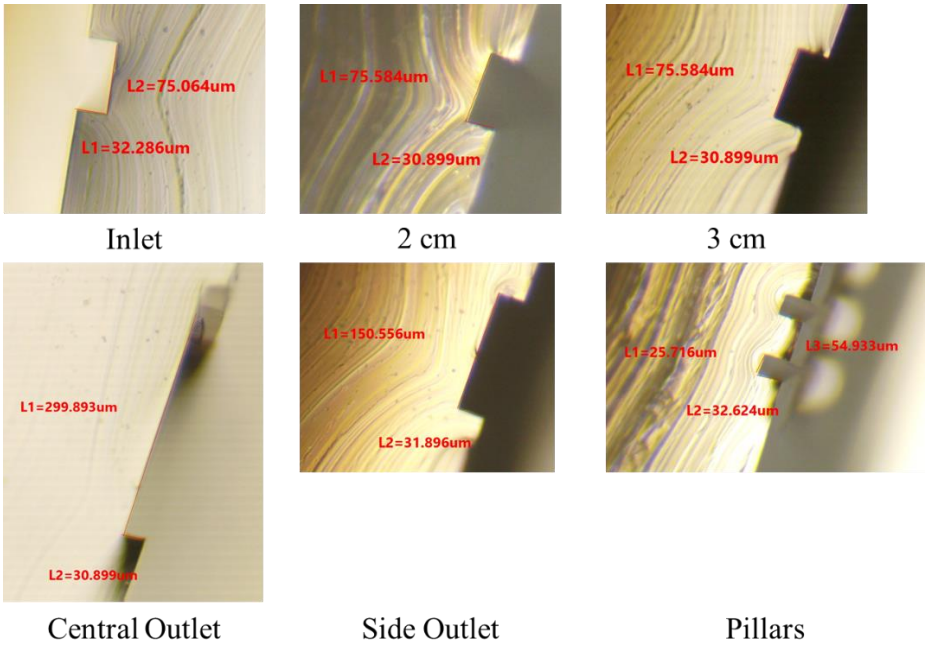

Figure 12 *- Bright-field major pictures of wafer cross-sections of 75 μm x 25 μm channel; from top left to bottom right: inlet, at 2 cm, at 3 cm, central outlet, side outlet, pillars.*

50 μm x 30 μm		75 μm x 30 μm	
Width	Heigth	Width	Heigth
50.9 ± 0.3	31.6 ± 0.3	75.4 ± 0.2	31.6 ± 0.3

Table 2 *- Means plus standard deviation errors of widths and heights of the 50 μm x 30 μm and 75 μm x 30 μm channels.*

3.2 Dimensionless Parameters

To understand the physics of fluids on miniaturized devices it is necessary to take into consideration the different forces that affect the behavior at such scales[36]; to do so dimensionless parameters compare the dynamics of the different forces and allow us to comprehend, analyze and predict the performances in our microchannels.

Reynolds number (*Re*) is defined as the ratio of the inertial force to the viscous force[33]:

$$Re = \frac{\rho\, Vm\, Dh}{\eta_0} = \frac{2\,\rho\, Q}{\eta_0 (w + h)} \tag{12}$$

where ρ is the solution density, *Vm* is the mean velocity of the channel, *Dh* is the hydraulic diameter, η_0 is the zero-shear fluid viscosity of the solution, *Q* is the flow rate and *w* and *h* are, respectively, the width and height of the rectangular cross-section microchannel[48,53].

Weissenberg number (*Wi*) is the ratio between two different time constants:

$$Wi = \frac{\lambda}{T_c} = \frac{2\,\lambda_e\,Q}{w^2\,h} \tag{13}$$

where λ is the relaxation time of the fluid and T_C is the characteristic time of the channel flow. The characteristic time is approximately equal to the inverse of the average (characteristic) shear rate[48]. λe is the effective relaxation time and *Q*, *w* and *h* were already defined above[41,53].

Elasticity number (*El*), which measures the relative importance of elasticity to inertia[53,54], can be written as:

$$El = \frac{Wi}{Re} = \frac{\lambda_e\,\eta_0\,(w+h)}{\rho\,w^2\,h} \tag{14}$$

In table 3 are reported the rheological properties of the PEO solution used to calculate all the dimensionless numbers used to predict and better understand the behavior of our corpuscles in our device.

PEO concentration (ppm)	1000
Density ρ (kg/m^3)	1000
Zero-shear viscosity η0 (mPa*s)	2.3
Relaxation time λe (ms)	6.8

Table 3 *- PEO rheological properties found in literature.*

In table 4, instead, all the values of the dimensionless numbers calculated for the flow rates tested in our experiments can be found.

		50 x 30	75 x 30
Q uL/min		**1000ppm**	**1000ppm**
5	*Re*	0.906	0.690
	Wi	15.111	6.716
	El	16.683	9.732
10	*Re*	1.812	1.380
	Wi	30.222	13.432
	El	16.683	9.732
15	*Re*	2.717	2.070
	Wi	45.333	20.148
	El	16.683	9.732
20	*Re*	3.623	2.761
	Wi	60.444	26.864
	El	16.683	9.732
25	*Re*	4.529	3.451
	Wi	75.556	33.580
	El	16.683	9.732
30	*Re*	5.435	4.141
	Wi	90.667	40.296
	El	16.683	9.732
40	*Re*	7.246	5.521
	Wi	120.889	53.728
	El	16.683	9.732
50	*Re*	9.058	6.901
	Wi	151.111	67.161
	El	16.683	9.732

Table 4 *- Dimensionless numbers calculated for every flow rate tested for both microchannels. The number calculated were Reynolds number, Weissenberg number, and Elasticity number in both 50 µm x 30 µm and 75 µm x 30 µm.*

The blockage ratio ($\beta = \frac{a}{H}$) is defined as the ratio between *a*, the particle diameter, and *H*, the channel height; this dimensionless number is important to predict how corpuscles behave inside a microchannel. In reality, this number is highly capable of forecasting the focusing of spherical particles inside a microfluidic channel, but it can only give an approximate idea for corpuscles with an asymmetric shape. Nevertheless, it is very useful to consider before designing the device because it helps us select the right dimensions to accomplish our research purposes. When β has a high value, the elastic force drives the cells towards the channel walls since the compressive normal stress is enhanced at the near-center side of particles[38], when β has a lower value, the elastic force drives the small cells towards the channel center instead. In particular, when β > 0.25 the side wall-bound elastic lift force acts on particles due to

the elasticity and pushes them towards the walls while when $\beta < 0.25$ the particles tend to focus on the channel centerline[55,74,75]. In table 5, all the blockage ratio values calculated for all the particles in the different channels are reported.

Particles Diameter	Blockage Ratio
4 μm	0.1397
7 μm	0.2440
15 μm	0.5083

Table 5 *- Blockage ratio values calculated for each microbead used in our experiments.*

Another important number to consider when evaluating the corpuscles migration in a viscoelastic fluid is the aspect ratio (AR) of the channel. This can be calculated as AR = W / H, where W represents the width and H the height of the channel. This because it has been proven that with the increasing of the width of the channel, the velocity distribution along the width becomes progressively flat[74] because the shear rate is not strong enough to induce the normal stress difference that pushes the particles towards the sidewalls[75]. Hence, to design a microfluidic channel for specific cells or particles' separation, it is important to consider not only the renowned dimensionless parameters but also the AR and the blockage ratio.

Finally, before proceeding with the experiments, we decided to calculate the pressure drop values (table 6) for each flow rate that we would have tested to predict and avoid the burst of our channels; all the flow rates reported are not problematic and do not have adverse behaviors.

ΔP	1000ppm	
Q µL/min	**50 x 30**	**75 x 30**
5	17.182	10.072
10	34.365	20.144
15	51.547	30.216
20	68.730	40.288
25	85.912	50.360
30	103.094	60.432
40	137.459	80.576
50	171.824	100.720

Table 6 *- Pressure drop values calculated in both 50 x 30 and 75 x 30 channels for each flow rate used. All the values of pressure drop were calculated in psi (pound-force per square inch).*

3.3 Microbeads Experiments

3.3.1 Particles inside 50 µm x 30 µm channel

The different sizes of polystyrene microbeads were firstly tested one at a time in the 50µm x 30µm channel; in particular, the behavior of the particles was investigated at different flow rates, from 5µL/min to 50µL/min and the relative images acquired were then analyzed to obtain quantitative data of the intensity values and the focusing efficiencies.

In figure 13, the fluorescence images of the 4µm particles at both the inlet and the outlet are reported along with the intensity values graphs. It is observable how at the inlet the particles were homogeneously distributed along the width of the channel while at the outlet, so after 3 cm, the 4µm beads were focused on the center of the channel for all the flow rates tested. From figure 14 we can notice how the focusing efficiency increases from 5µL/min to 25µL/min, where it reaches the peak value of about 98%, then from 25µL/min till 50µL/min it decreases. Overall, we can say that the equilibrium position of the 4µm PS microbeads in AR = 1.67 channel is achieved at the centerline for all flow rates, even though the width of the streamline can vary based on the flow rate and thus, on the different contribution of the forces acting.

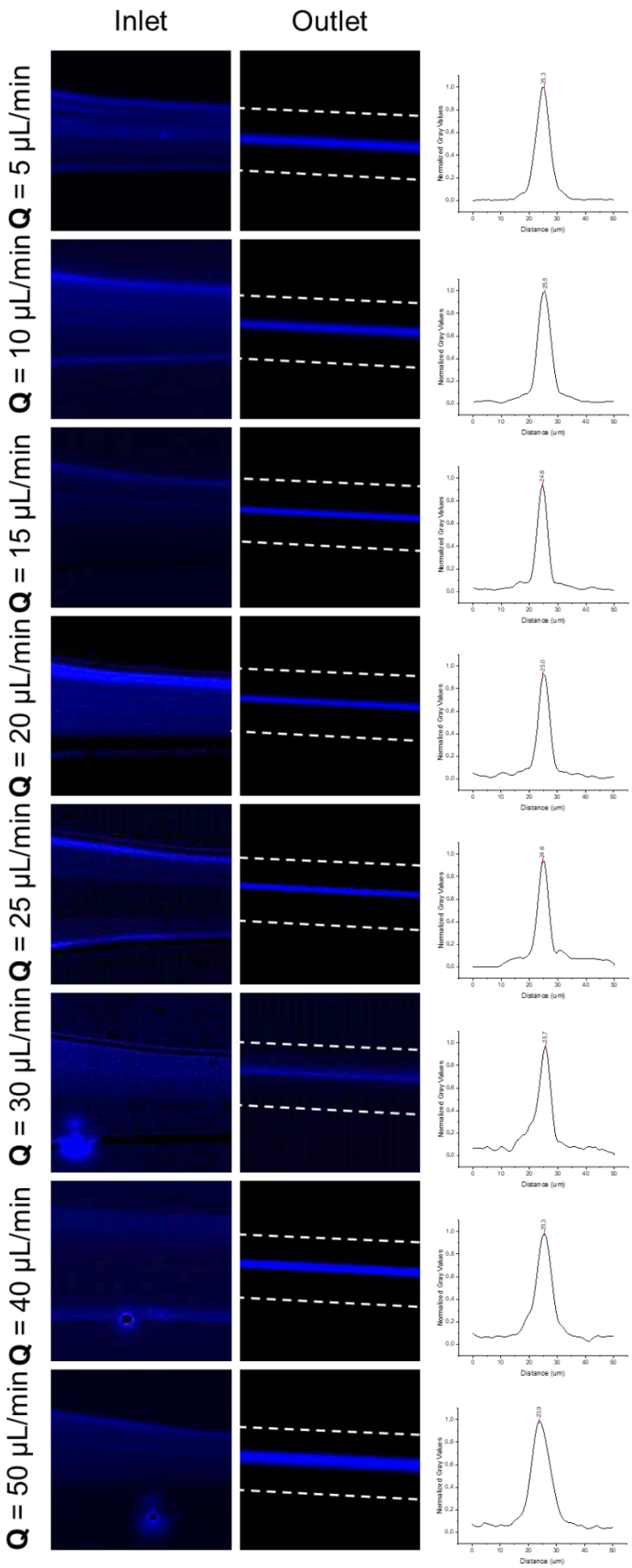

Figure 13 *– Fluorescence images of 4 µm PS particles in 1000ppm PEO in PBS solution in 50 µm x 30 µm channel at different flow rates along with the intensities values profiles for each flow rate tested.*

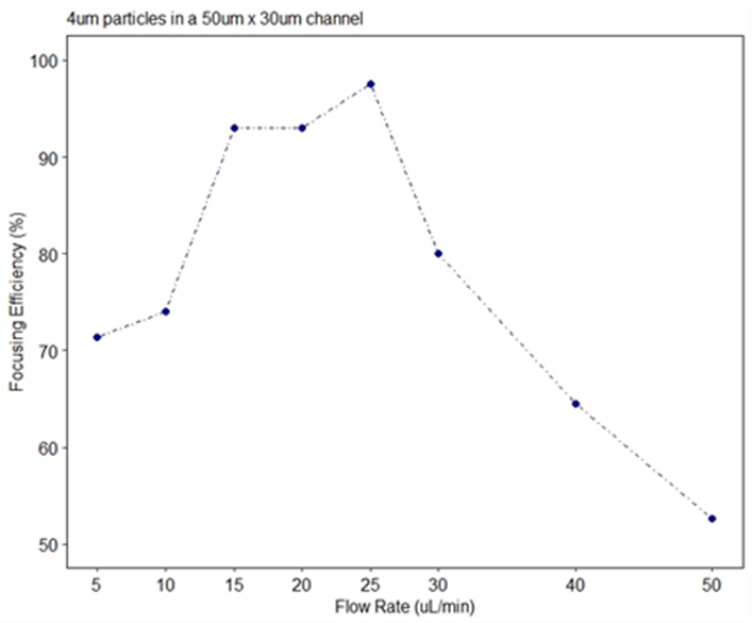

Figure 14 *- Focusing Efficiency values of 4μm particles in 50μm x 30μm channel at each flow rate tested. The points represent the focusing efficiency values of the single streamline detected in the fluorescence image.*

In figure 15, the fluorescence images of the 7μm particles at both the inlet and the outlet are reported along with the intensity values graphs. As happened before, at the inlet the particles are evenly distributed while at the outlet the different focusing is appreciable. We can notice that, like the 4μm particles, also the 7μm microbeads tend to focus on the center of the channel for every flow rate. In contrast with the previous focusing efficiency graph, for this different size of particles, the focusing efficiency pattern is not that much dependent on the flow rates but it rather shows performances of efficiency higher than 93% for every flow rate > 5μL/min, as illustrated in figure 16.

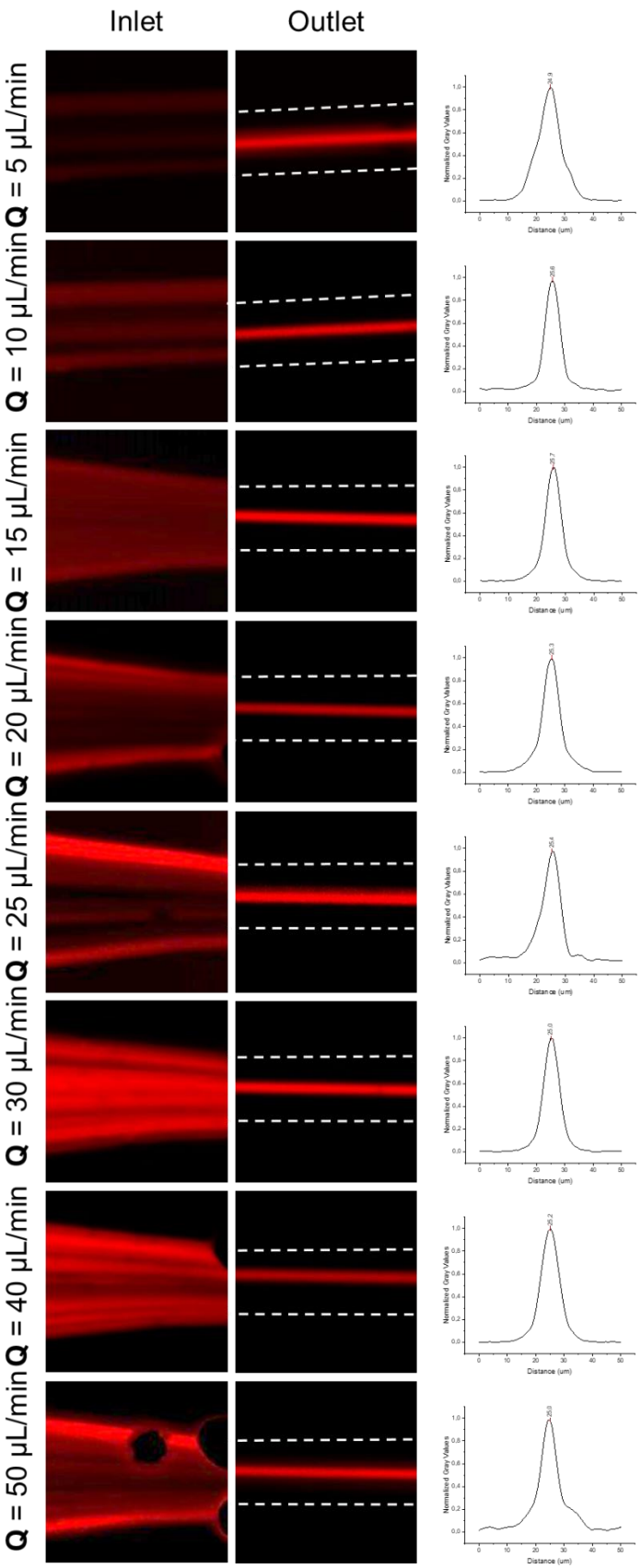

Figure 15 *- Fluorescence images of 7 µm PS particles in 1000ppm PEO in PBS solution in 50 µm x 30 µm channel at different flow rates along with the intensities values profiles for each flow rate tested.*

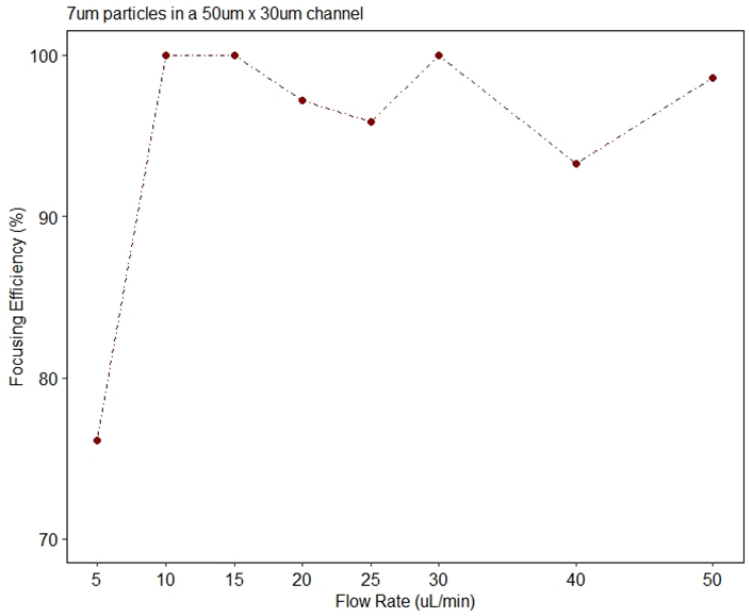

Figure 16 *- Focusing Efficiency values of 7μm particles in 50μm x 30μm channel at each flow rate tested. The points represent the focusing efficiency values of the single streamline detected in the fluorescence image.*

In figure 17, the fluorescence images of the 15μm particles at both the inlet and the outlet are reported along with the intensity values graphs. Once again, at the inlet, all the microbeads are uniformly distributed along the whole width of the channel while, as we move towards the end of the channel till the outlet, the equilibrium positions are reached. In particular, a different number of streamlines can appear based on the different flow rate tested; until 30μL/min we can observe two different streamlines located near the sidewalls of the channel, with the only exception of the 10μL/min where only a single streamline was detected. The single equilibrium position was achieved again at 40μL/min; instead, at the maximum flow rate tested, 50μL/min, three different streamlines can be seen. From figure 18, it is clear how the focusing efficiency attained with the 15μm microbeads was almost perfect: the only value under 100% of focusing efficiency is obtained at 10μL/min but it is still around 97%.

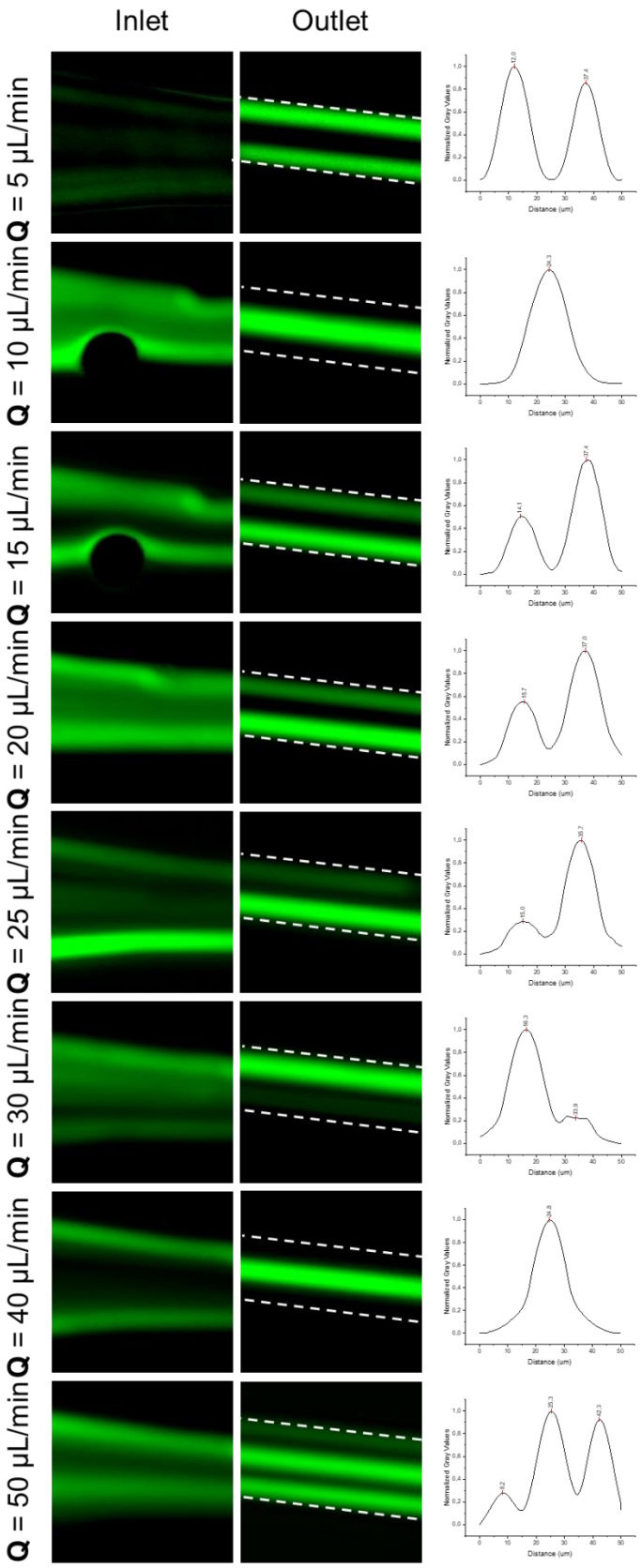

Figure 17 *- Fluorescence images of 15 µm PS particles in 1000ppm PEO in PBS solution in 50 µm x 30 µm channel at different flow rates along with the intensities values profiles for each flow rate tested.*

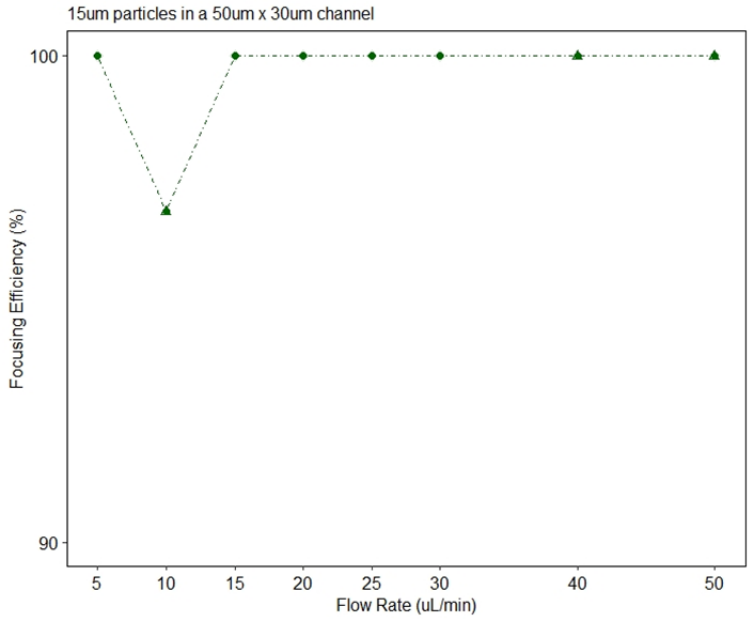

Figure 18 *- Focusing Efficiency values of 15μm particles in 50μm x 30μm channel at each flow rate tested. The points represent the mean value of the focusing efficiency calculated for each flow rate; the values of the focusing efficiency of the single streamline in each flow rate are reported with the different symbols at the corresponding flow rate.*

3.3.2 Particles inside 75 μm x 30 μm channel

After testing the different sizes of polystyrene microbeads in the 50μm x 30μm channel, analogous experiments were performed in the 75μm x 30μm channel; so, again all the flow rates between 5μL/min and 50μL/min were investigated and the relative fluorescence images acquired were then analyzed to obtain quantitative data of the intensity values and the focusing efficiencies.

In figure 19, the fluorescence images of the 4μm particles at both the inlet and the outlet are reported along with the intensity values graphs. At the inlet, the microbeads were as always equally distributed along the width of the channel, while at the outlet the different focusing could be noticed. Specifically, at 5μL/min the distribution of the 4μm particles was still almost random throughout the width of the channel, but some separated streamlines along the central area could be seen; from 10μL/min to 25μL/min the focusing of the particles becomes tighter and only a few streamlines at the center of the channel could be observed; at 30μL/min the space between the three streamlines start to broaden a bit even though their position is still at the center; at 40μL/min we can observe a similar situation to what happened at 5μL/min, so a random distribution along the whole width of the channel; finally, at 50μL/min a central focusing once again could be noticed. By looking at figure 20, we can observe how

the focusing efficiency of the single streamlines is more complicated to calculate and understand; even though there are only from five to two streamlines visible and detectable in the intensity values graphs (figure 19) the real streamlines can be much more: indeed, the 4μm particles are superimposed to one another and this could be understood when the FWHM obtained is analyzed and the focusing efficiency calculated. For instance, at 5μL/min the first three streamlines visible are in reality all double streamlines superimposed and their final focusing efficiency goes from about 70% to 100%. Likewise, the streamlines seen from 10μL/min to 20μL/min and from 40μL/min to 50μL/min are all double. Overall, the mean values of the focusing efficiency increases from 5μL/min to about 89% at 20μL/min where it reaches the peak; but the important data to observe is the position of the streamlines which can be found in the 30μm of the central area of the channel from 10μL/min to 25μL/min (figure 20).

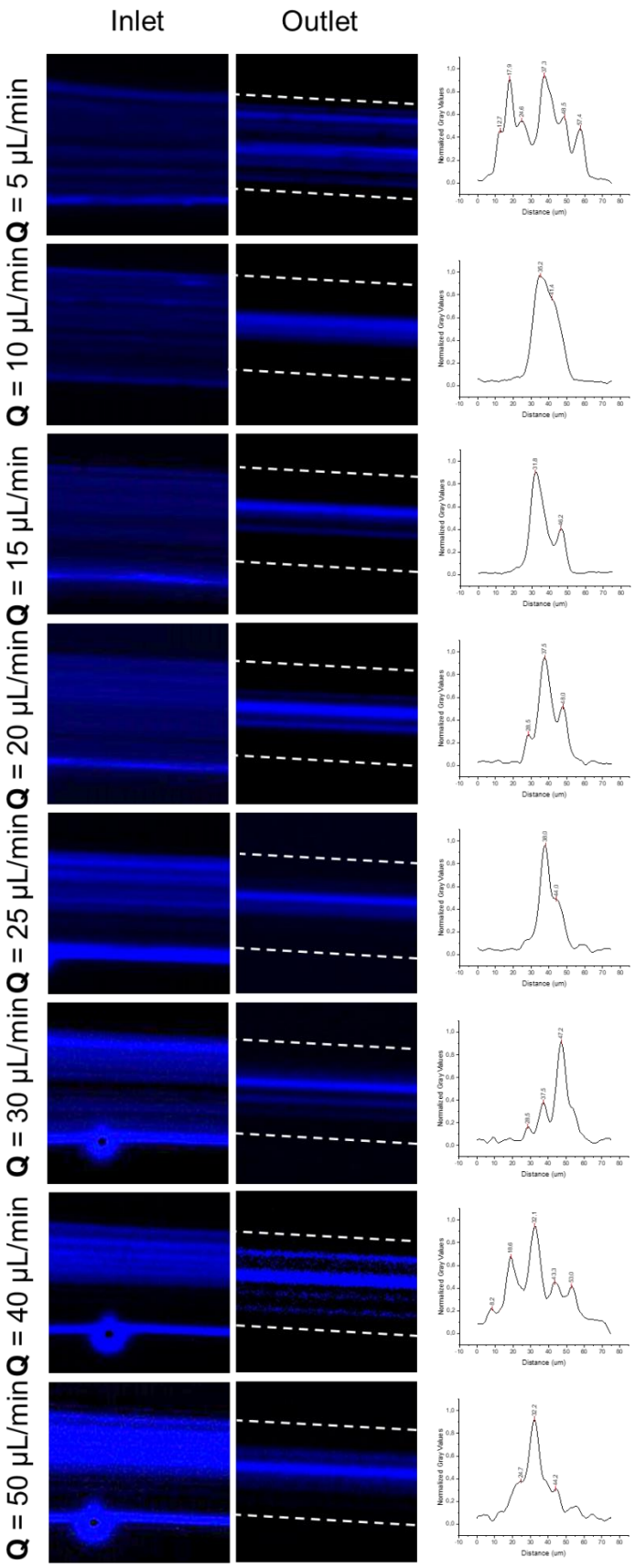

Figure 19 *- Fluorescence images of 4 µm PS particles in 1000ppm PEO in PBS solution in 75 µm x 30 µm channel at different flow rates along with the intensities values profiles for each flow rate tested.*

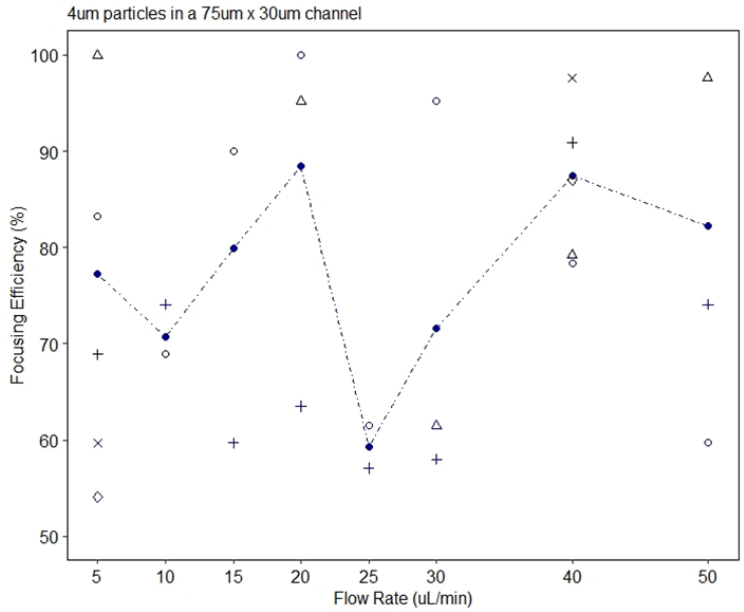

Figure 20 *- Focusing Efficiency values of 4μm particles in 75μm x 30μm channel at each flow rate tested. The points represent the mean value of the focusing efficiency calculated for each flow rate; the values of the focusing efficiency of the single streamline in each flow rate are reported with the different symbols at the corresponding flow rate. When a black symbol is present, it represents the superimposition of two different streamlines, which were detected as a single one in the intensity value graph.*

In figure 21, the fluorescence images of the 7μm particles at both the inlet and the outlet are reported along with the intensity values graphs. Once again, at the inlet, there is a uniform distribution of the microbeads along the width of the channel, while after 3cm the focusing of the particles happens. In particular, at 5μL/min three streamlines are visible but in reality, there are four focusing positions because the last one is made of two different streamlines superimposed, as I deduced from the FWHM values which was almost double the particle diameter. At 10μL/min two streamlines in the central area of the channel could be detected; at 15μL/min four different equilibrium positions are reached but they can be coupled two by two to obtain two-focusing equilibrium positions in the central area; at both 20μL/min and 25μL/min the 7μm microbeads are focused in about 40μm of the central area of the channel with streamlines superimposed; at 30μL/min and 50μL/min a similar behavior can be observed: two focusing positions near the center of the channel are achieved. Finally, at 40μL/min only three streamlines can be observed, one at the exact center of our device and the other two near it. By looking at figure 22, we can see how the focusing efficiency is always higher than 70% in all the flow rates tested but it increases till 25μL/min where it reached 100% after which the efficiency value decreases. Overall, the focusing of the 7μm particles remains in about 40μm of the central area of the AR = 2.5

channel and the streamlines formed are usually 2 or 4 and symmetrically distributed with respect to the channel center.

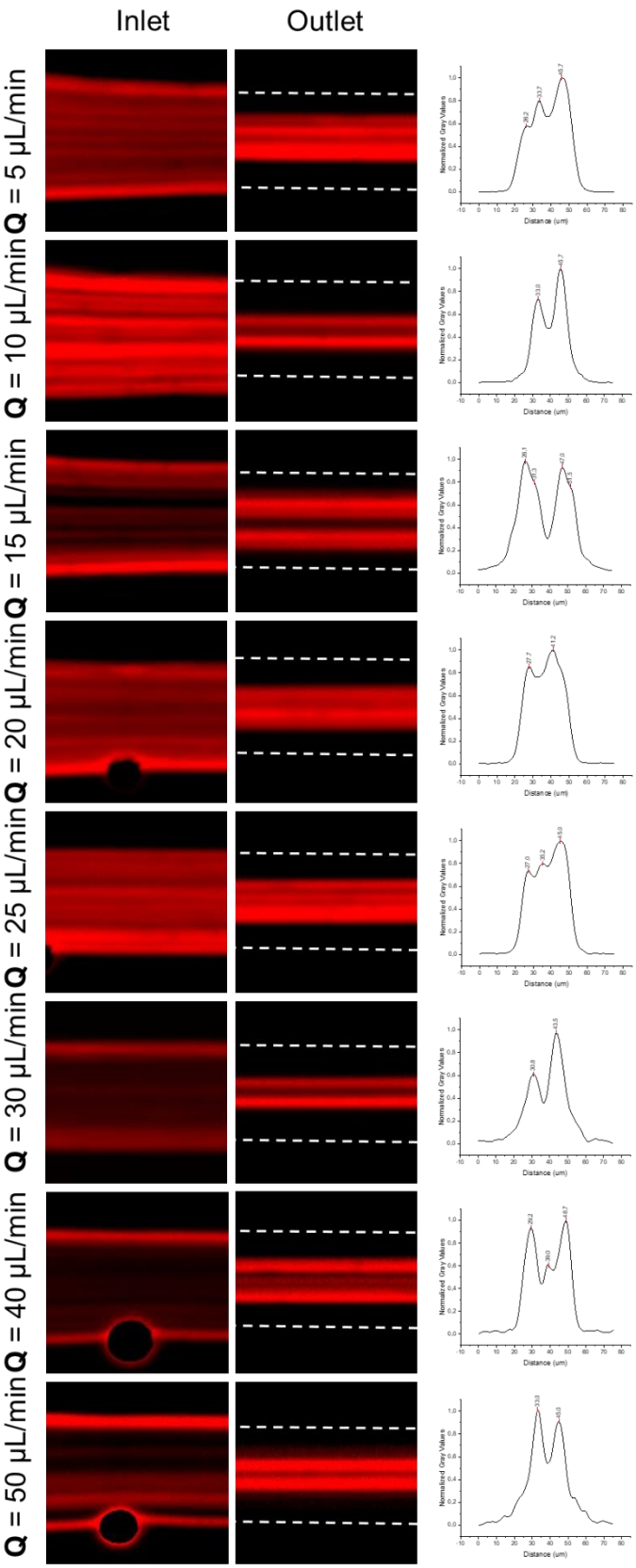

Figure 21 - *Fluorescence images of 7 µm PS particles in 1000ppm PEO in PBS solution in 75 µm x 30 µm channel at different flow rates along with the intensities values profiles for each flow rate tested.*

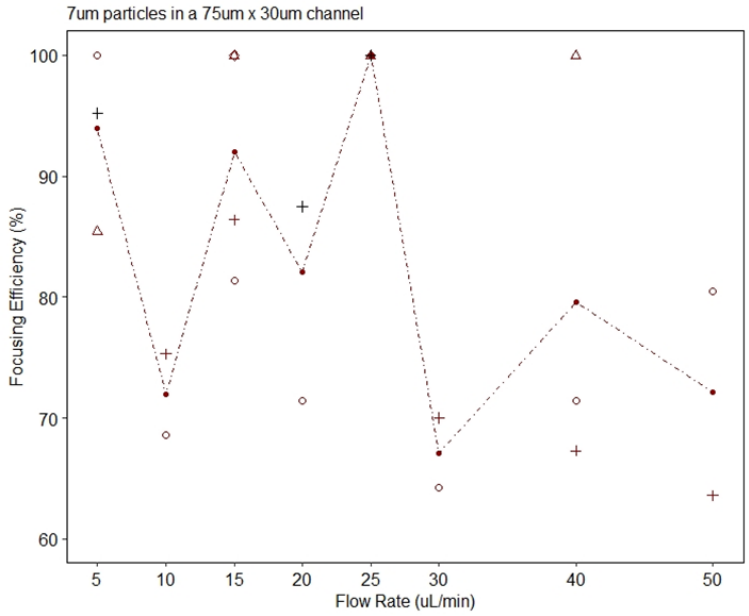

Figure 22 *- Focusing Efficiency values of 7μm particles in 75μm x 30μm channel at each flow rate tested. The points represent the mean value of the focusing efficiency calculated for each flow rate; the values of the focusing efficiency of the single streamline in each flow rate are reported with the different symbols at the corresponding flow rate. When a black symbol is present, it represents the superimposition of two different streamlines, which were detected as a single one in the intensity value graph.*

In figure 23, the fluorescence images of the 15μm particles at both the inlet and the outlet are reported along with the intensity values graphs. Even in this last experiment of a single type of particle the microbeads were evenly distributed at the inlet while reached their focusing position near the outlets. By observing the fluorescence images, it possible to say that the 15μm particles have two or three equilibrium positions based on the flow rate tested: from 5 μL/min to 30μL/min two main streamlines are visible, with the only exception of 20μL/min where three streamlines could be seen. Similarly, three equilibrium positions can be found at 40μL/min and 50μL/min. The tightest focusing is achieved at 5μL/min and 15μL/min when also the distance between the streamlines is the widest (more than 20μm). When the focusing efficiency is considered (figure 24), the 5μL/min, 15μL/min, 40μL/min, and 50μL/min have the best performances, 100%; and overall, the efficiency values are approximately all above 80%.

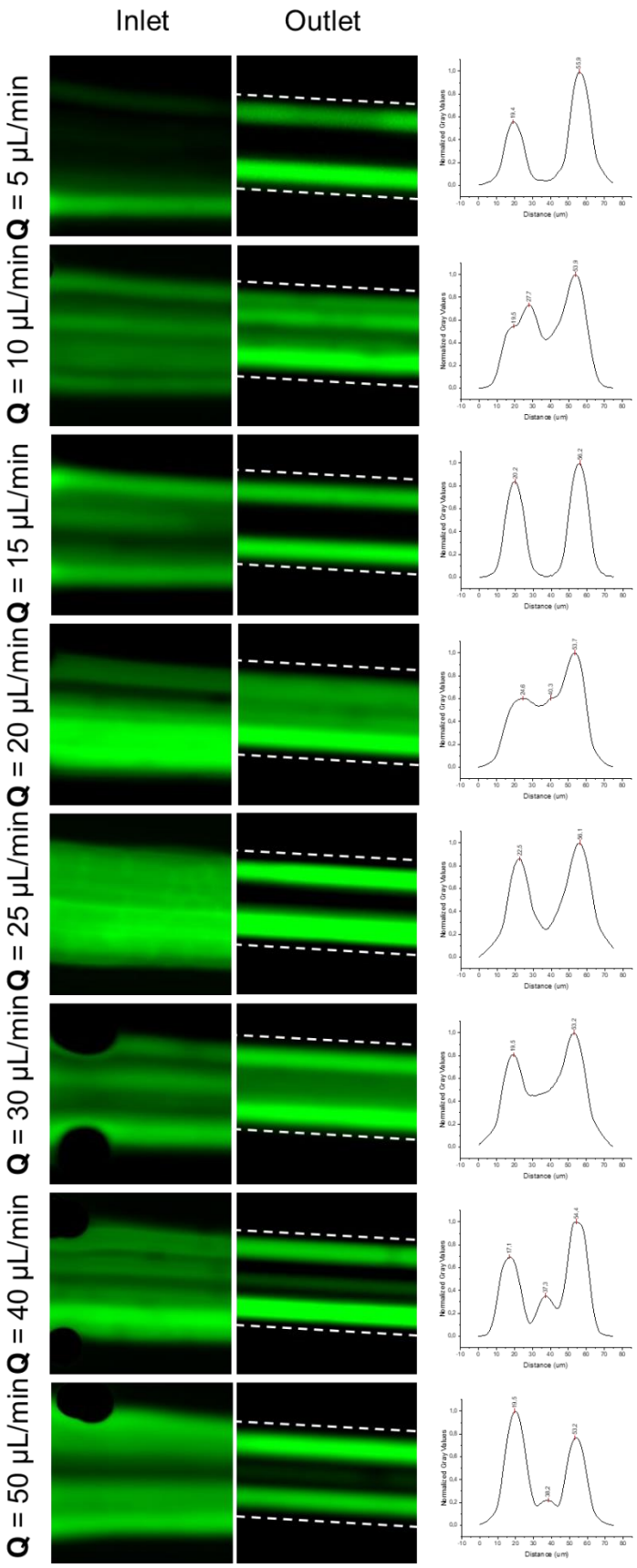

Figure 23 *-Fluorescence images of 15 µm PS particles in 1000ppm PEO in PBS solution in 75 µm x 30 µm channel at different flow rates along with the intensities values profiles for each flow rate tested.*

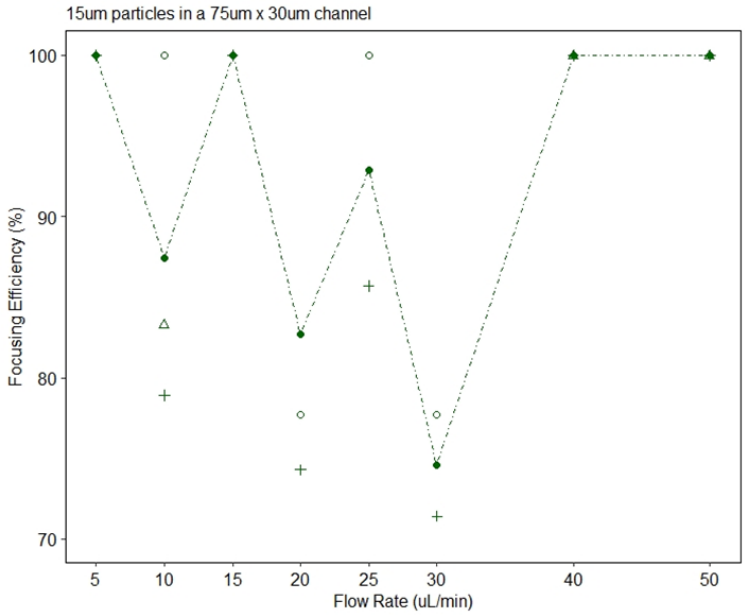

Figure 24 *- Focusing Efficiency values of 15µm particles in 75µm x 30µm channel at each flow rate tested. The points represent the mean value of the focusing efficiency calculated for each flow rate; the values of the focusing efficiency of the single streamline in each flow rate are reported with the different symbols at the corresponding flow rate. When a black symbol is present, it represents the superimposition of two different streamlines, which were detected as a single one in the intensity value graph.*

3.3.3 Comparisons between particles behaviors

Since the final aim of the project is sorting the different types of cells, I compared the different behavior of the different particles in the same channel at the same flow rate. Figures 25 and 26 show the fluorescence images along with the superimposed intensity values graphs; this allows a better understanding of the simultaneous equilibrium positions and thus, the visualization of the potential sorting. In the 50µm x 30µm channel (figure 25), from 5µL/min till 30µL/min, with the only exception of 10µL/min, the sorting of 4µm and 7µm particles from the 15µm particles could be feasible due to the different performances: the smaller particles are tightly focused on the center of the channel while the bigger ones can be found near the side walls. At 10µL/min and 40µL/min the separation is not possible due to the fact that all the particles used have a single-centered-streamline. At 50µL/min, instead, the separation would be possible but with a low efficiency because the 15µm particles present three different streamlines, one of which has the same location of the 4µm and 7µm equilibrium position.

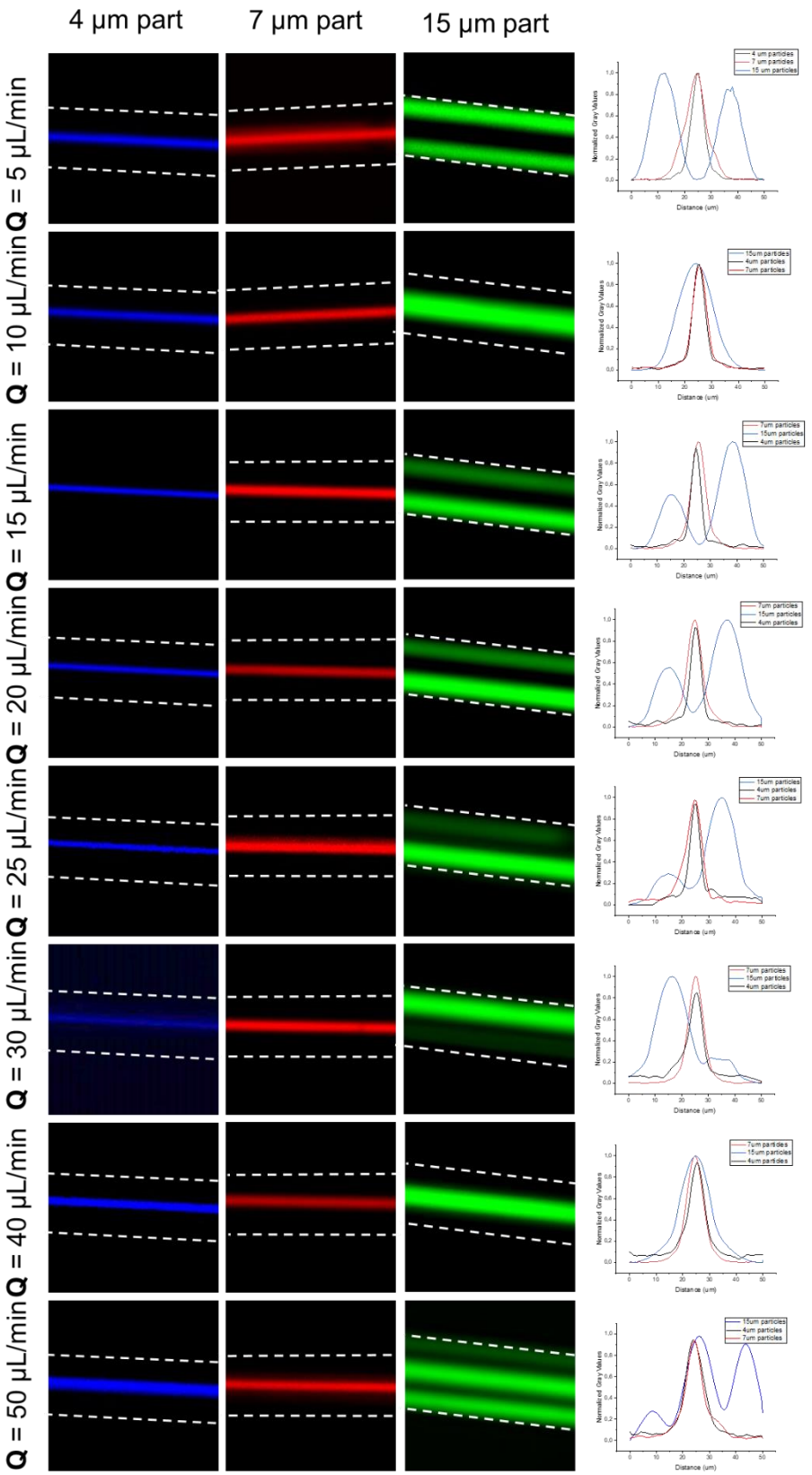

Figure 25 *- Fluorescence images of 4 µm (blue), 7 µm (red), and 15 µm (green) PS particles in 1000ppm PEO in PBS solution in 50 µm x 30 µm channel at different flow rates along with their superimposed intensities values profiles for each flow rate tested.*

In the 75µm x 30µm channel the streamlines and thus the equilibrium positions of the different particles are less defined, and more distributed along a certain area of the channel. Nevertheless, the particles' separation could be still reached from 10µL/min to 30µL/min because, as reported in the intensity values graphs of figure 26, the 4µm and 7µm particles streamlines can be usually found in the space between the two different equilibrium positions of the 15µm particles. The exceptions are at 5µL/min and 40µL/min where the 4µm beads behavior is not well defined, and at 40µL/min and 50µL/min where a third centered streamline is achieved by the 15µm particles, overlapping the equilibrium positions of the other microbeads.

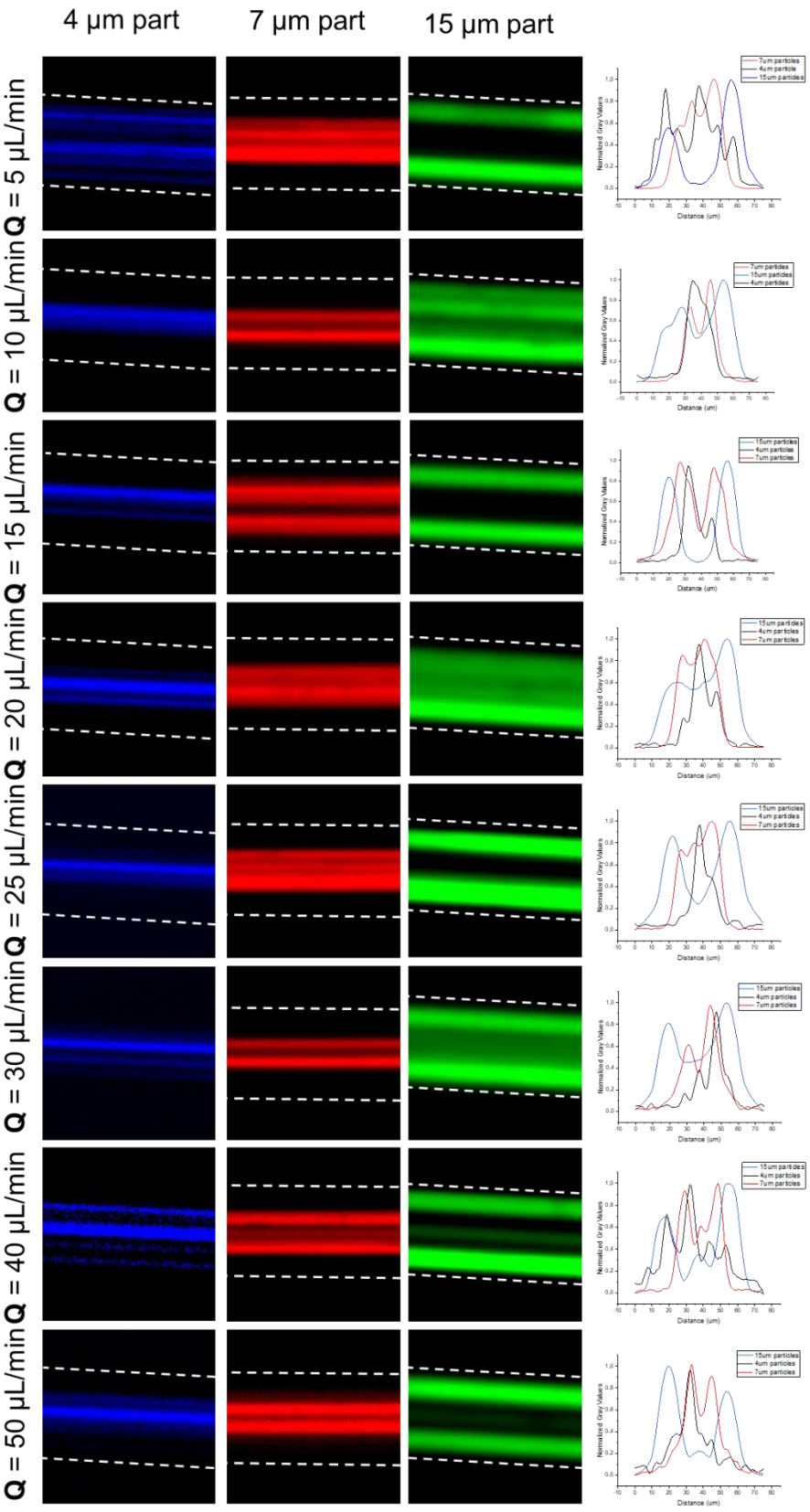

Figure 26 *- Fluorescence images of 4 µm (blue), 7 µm (red), and 15 µm (green) PS particles in 1000ppm PEO in PBS solution in 75 µm x 30 µm channel at different flow rates along with their superimposed intensities values profiles for each flow rate tested.*

3.3.4 Comparisons between the behaviors in different AR channels

An important aspect to take into consideration is the difference of behavior between the same particle size in the 50µm x 30µm when compared to the 75µm x 30 µm channel. In figure 27, it is possible to observe how the streamlines widen and can increase in number. In particular, the 4µm particles are tightly focused on the center of the channel when tested inside the 50µm x 30µm, but they become less focused in the wider channel; indeed, we can observe that the number of streamlines has increased, and it went from one single at the center to three or more in the center area of the channel. For the 7µm particles a similar situation happens: in the AR = 1.67 a single equilibrium position at the center of the channel is detected while in the AR = 2.5 an even number of streamlines is always present, it can go from two to four and the focusing positions are always between the center and the sidewalls, but majorly located in the central area. Lastly, for the 15µm particles, the behavior is similar between the different channels: two streamlines can be found near the side walls in both designs but the wider space between them in the 75µm x 30µm can cause the formation of a third streamline at the center of the channel.

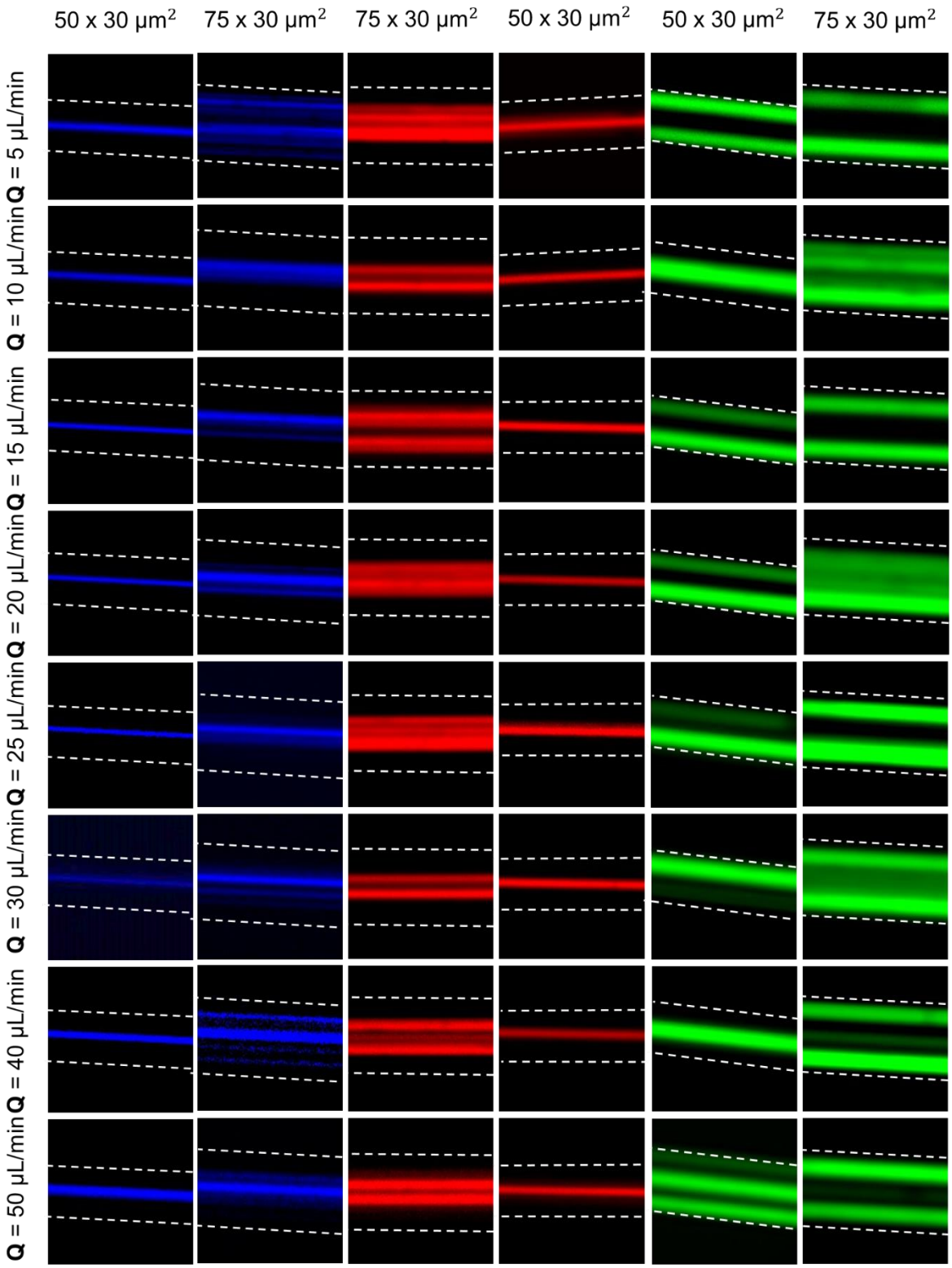

Figure 27 *– Comparison of fluorescence images of 4 µm (blue), 7 µm (red), and 15 µm (green) PS particles in 1000ppm PEO in PBS solution at different flow rates for the different AR channels (50 µm x 30 µm and 75 µm x 30 µm).*

3.3.5 Comparisons between different outlets configurations

Experiments with a mixture of 4µm and 15µm particles were performed to understand the real behavior of different microbeads in the same solution and to find the optimal configuration of outlets to achieve the best separation possible. Indeed, the expansion after 3cm was created to enhance the differences between the focusing positions but to achieve an optimal separation is important to also regulate the outlets' retrieval; to perform such thing our channel design included different positions at different distances for punching the outlets; this allowed to control and adjust the sorting cutoff and tune the fluid resistance, and the resistance ratio in order to obtain the optimal values of purity and separation efficiency.

The first configuration, which will be called #1 from now on, was created by punching at 1.5cm the central outlet and at 0.5cm the two side outlets. As reported in figure 28, the different flow rates tested previously were tested again with the microbeads mixture in both of the channels, 50µm x 30µm and 75µm x 30µm.

At 10µL/min in both microchannels, the 15µm particles were all retrieved in the side outlets while the majority of 4µm beads were collected in the central outlet. Only a few of the smaller particles go into the side outlets, meaning that sorting with high purity and high separation efficiency can be achieved. At 15µL/min in the AR = 1.67 channel all the 15µm particles are recovered in the side outlets and, once again, most of the 4µm beads go into the central outlet except for just a few of them. The situation is a bit different in the AR = 2.5 channel at the same flow rate: a considerable part of 4µm particles can be also collected in the side outlets, resulting in a reduction of purity of the sample retrieved in the side outlets and loss of some of the particles from the central one. Although, the purity of the central outlets remains perfect. At 20µL/min the situation in the 75µm x 30 µm channel remains unchanged but the performance in the 50µm x 30µm channel varies a little: some of the 15µm particles are lost in the central outlet meaning that the purity of the 4µm particles from the center is compromised. As the flow rate increases from 25µL/min till 50µL/min in the smaller channel the founding of 15µm particles in the central outlet increases, thus making the purity lower and not allowing the particles' sorting. On the

other hand, in the 75µm x 30 µm channel the 15µm beads are always totally collected by the side outlets, making the sorting efficiency the optimal one but, as the flow rate increase, also the number of 4µm particles retrieved by the side outlets increases. This would affect the efficiency of the smaller particles' retrieval.

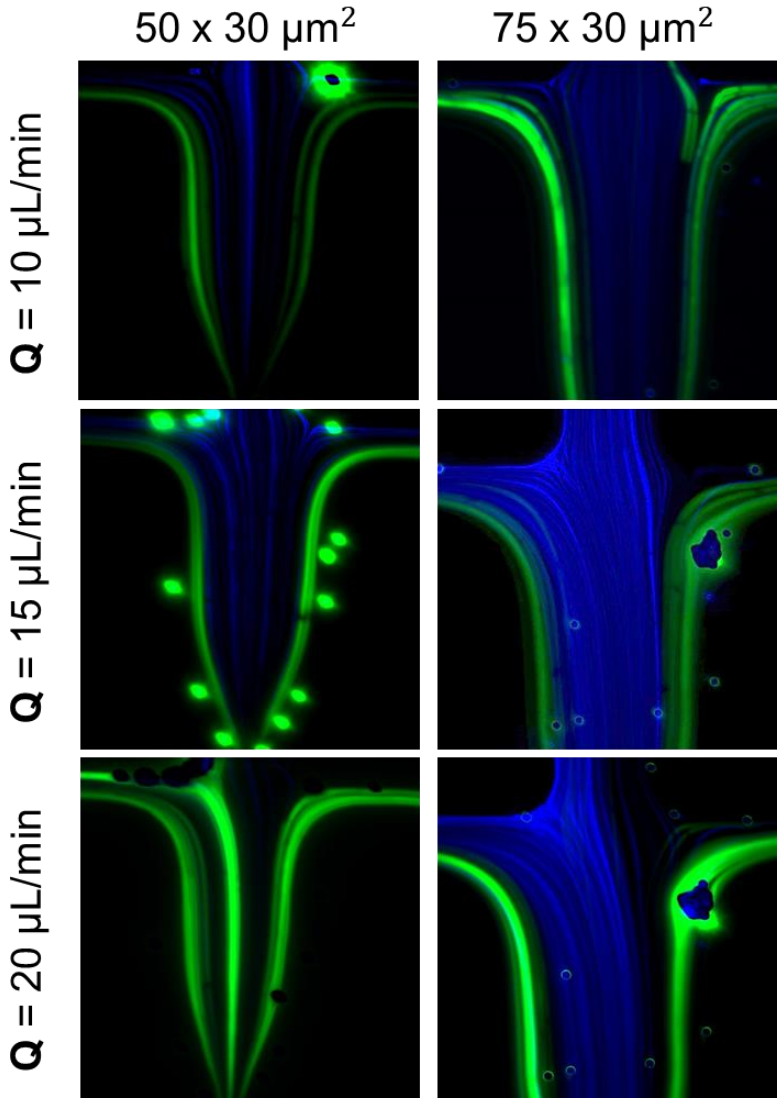

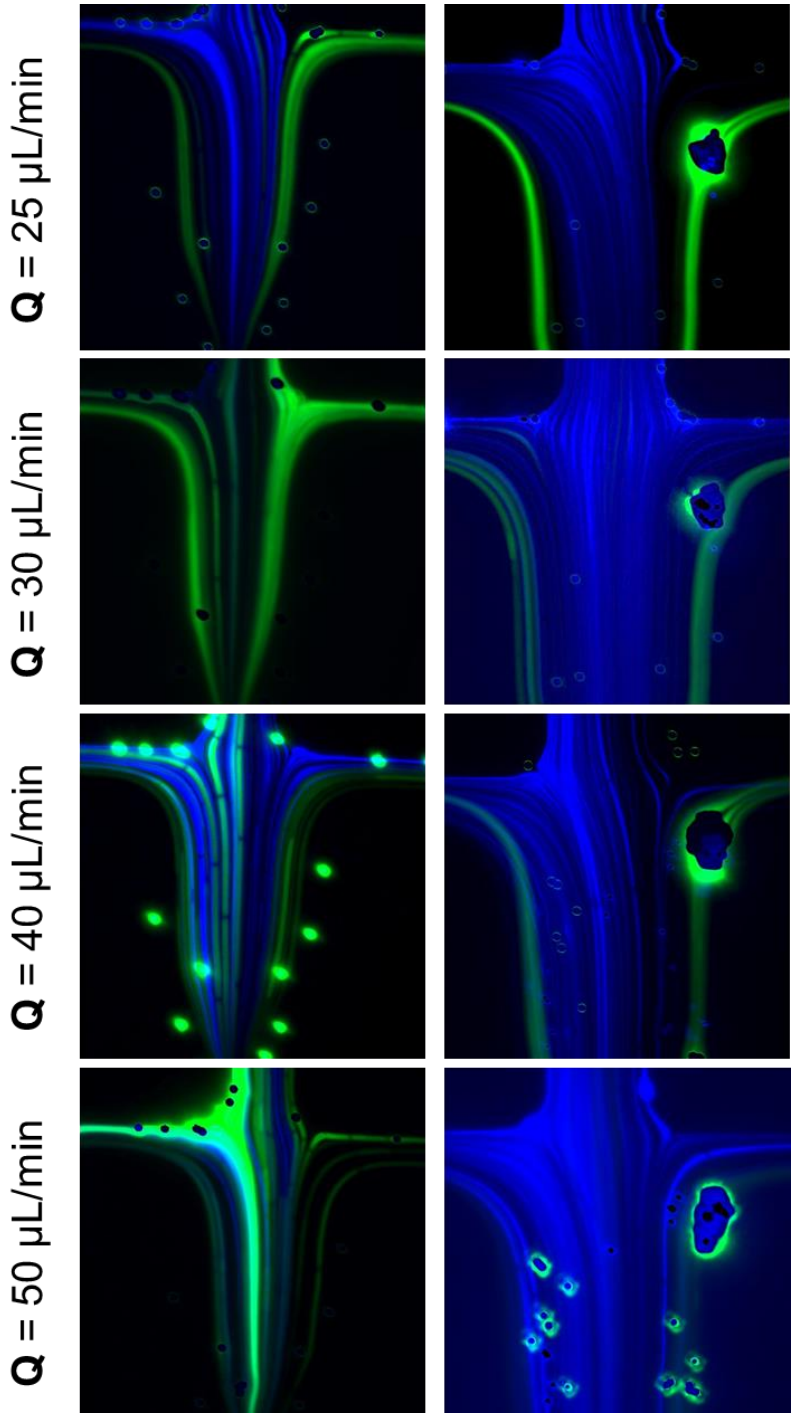

Figure 28 *– Fluorescence images of the 4 µm and 15µm mixture in 1000ppm PEO in PBS solution captured at the expansion of both different AR channels (50 µm x 30 µm and 75 µm x 30 µm) at different flow rates. The outlet configuration is #1, meaning the central outlet punched at 1.5 cm and the side outlets at 0.5 cm.*

The second configuration, which will be called #2, was created by punching at 1.5cm the central outlet and at 1cm the two side outlets. As reported in figure 29, the different flow rates tested previously were tested again with the microbeads mixture in both of the channels, 50µm x 30µm and 75µm x 30µm.

As we can observe from the images, all the flow rates tested in the AR = 1.67 channel showed the collection of both type of particles in the center outlet; even though the 4µm particles were tightly focused on the center of the channel till 25µL/min, a consistent part of the 15µm particles finished there as well. Furthermore, between 30µL/min and 50µL/min some of the 4µm beads were also collected in the side outlets. Thus, making the sorting of this mixture not possible in this type of channel in this configuration. On the other hand, the sorting of the mixture was more efficient in the AR = 2.5 channel; indeed, in all the flow rates tested all the 15µm particles were retrieved by the side outlets while the majority of 4µm beads were collected on the center outlet. Particularly, for 10µL/min hardly any of the smaller particles finished in the side outlets, making this specific setting the optimal one. From 15µL/min till 50µL/min, some of the 4µm particles could be also found in the side outlets, decreasing the efficiency of separation but still preserving the perfect purity of the central sample recovered. I must specify that at 40µL/min the presence of some clogged particles is visible on the left side and this could have caused the little deviation of the 15µm particles that could be observed at 50µL/min, making, therefore, that specific result a bit inaccurate.

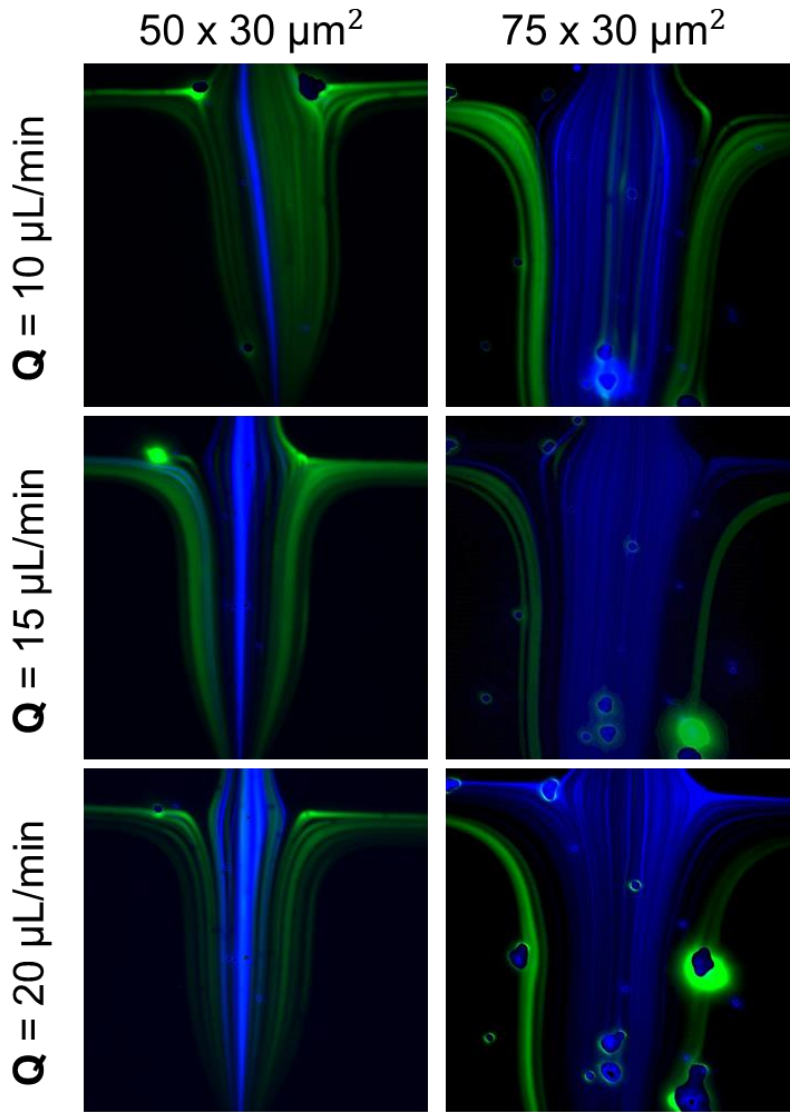
50 x 30 µm²
75 x 30 µm²
Q = 10 µL/min
Q = 15 µL/min
Q = 20 µL/min

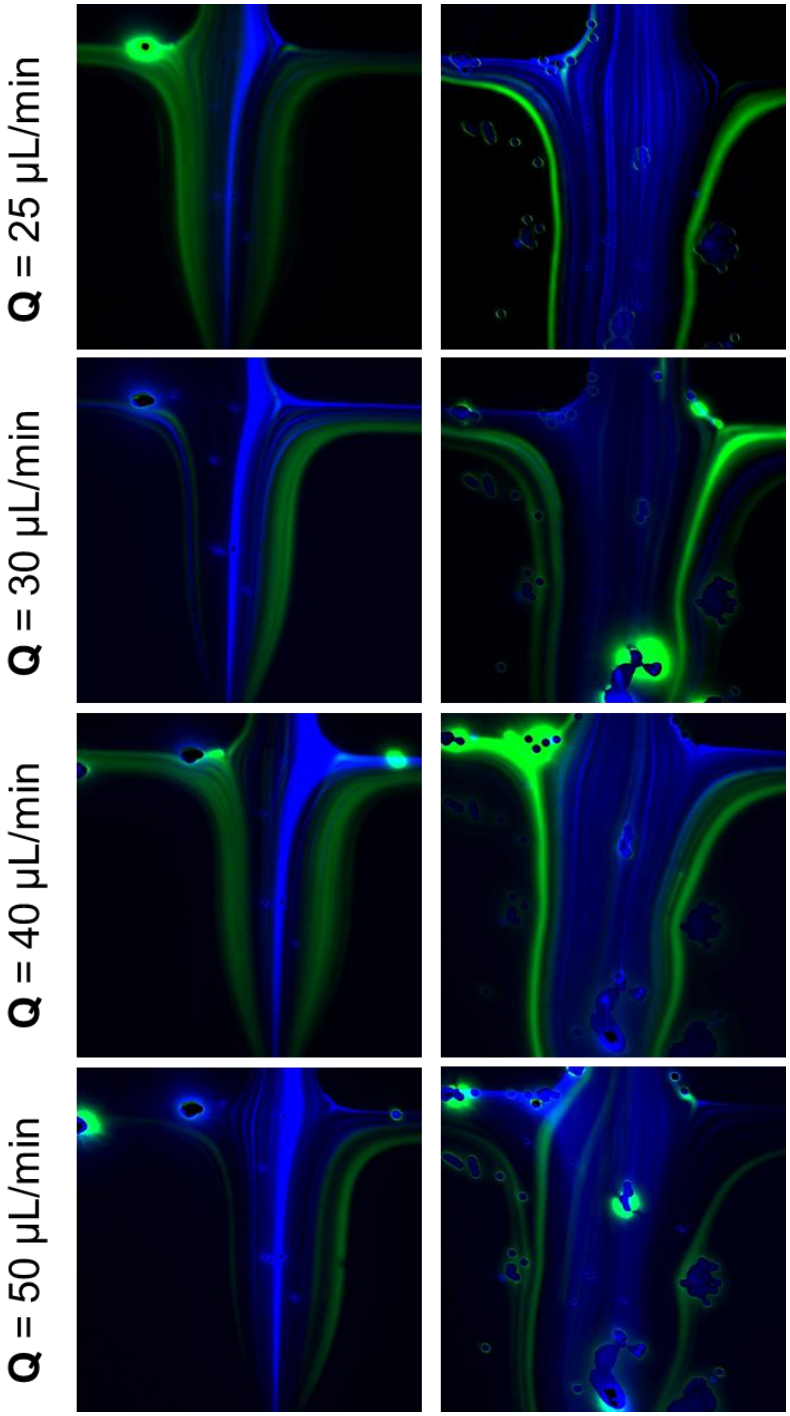

Figure 29 *- Fluorescence images of the 4 µm and 15µm mixture in 1000ppm PEO in PBS solution captured at the expansion of both different AR channels (50 µm x 30 µm and 75 µm x 30 µm) at different flow rates. The outlet configuration is #2, meaning the central outlet punched at 1.5 cm and side outlets at 1 cm.*

The last but not least configuration will be called #3, and it was created by punching at 1.5cm the central outlet and at 1.5cm the two side outlets. As reported in figure 30, the different flow rates tested in the previous configurations were tested again with the 4µm and 15µm particles mixture in both of the channels, 50µm x 30µm and 75µm x 30µm.

Once again, the 50µm x 30 µm channel was not able to separate the two different particles in the different outlets: for all the flow rates, from 10µL/min to 50µL/min, all the 4µm beads could actually be collected only on the center outlet due to their very tight center focusing but along with a portion of 15µm particles. In this particular configuration, the 75µm x 30µm channel was not a suitable sorting option neither. As we can observe, at 10µL/min and 15µL/min the 4µm beads were retrieved mainly by the central outlet and the left side outlet, while the 15µm particles were collected in both the side outlet and the center one. Inexplicably, from 20µL/min up the behavior of cells was very different from all we have seen before: at 20µL/min the 4µm beads were collected only from the left side outlet while the 15µm particles were retrieved from all the outlets; at 25µL/min both types of particles were withdrawn by the left side outlets, with the exception of a little portion of 15µm beads which were also found in the central one. Since this behavior seemed suspicious, the device tested was changed and the remaining flow rates were tested in a new channel. Regardless, a similar behavior was observable from 30µL/min to 50µL/min with the difference that the outlets which were withdrawing the majority of the particles were the right one. Indeed, at 30µL/min, 40µL/min and 50µL/min the 15µm beads could be collected at all the outlets while the 4µm particles were only retrieved by the right side one.

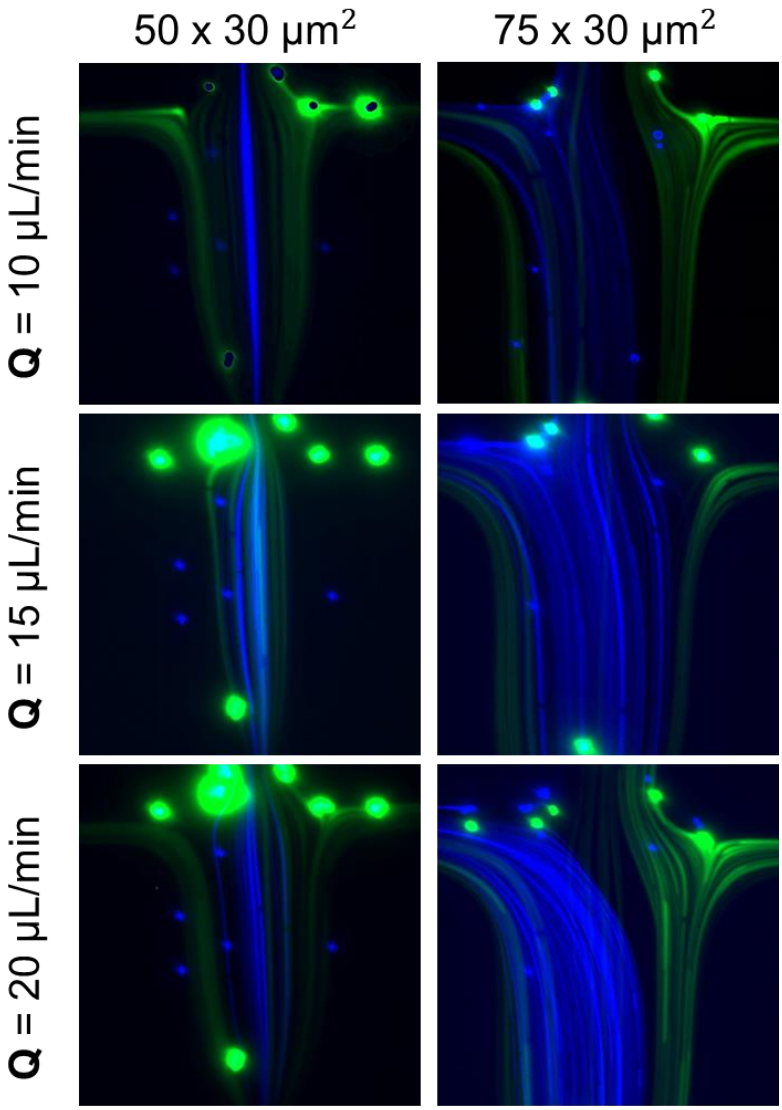
50 x 30 µm²
75 x 30 µm²
Q = 10 µL/min
Q = 15 µL/min
Q = 20 µL/min

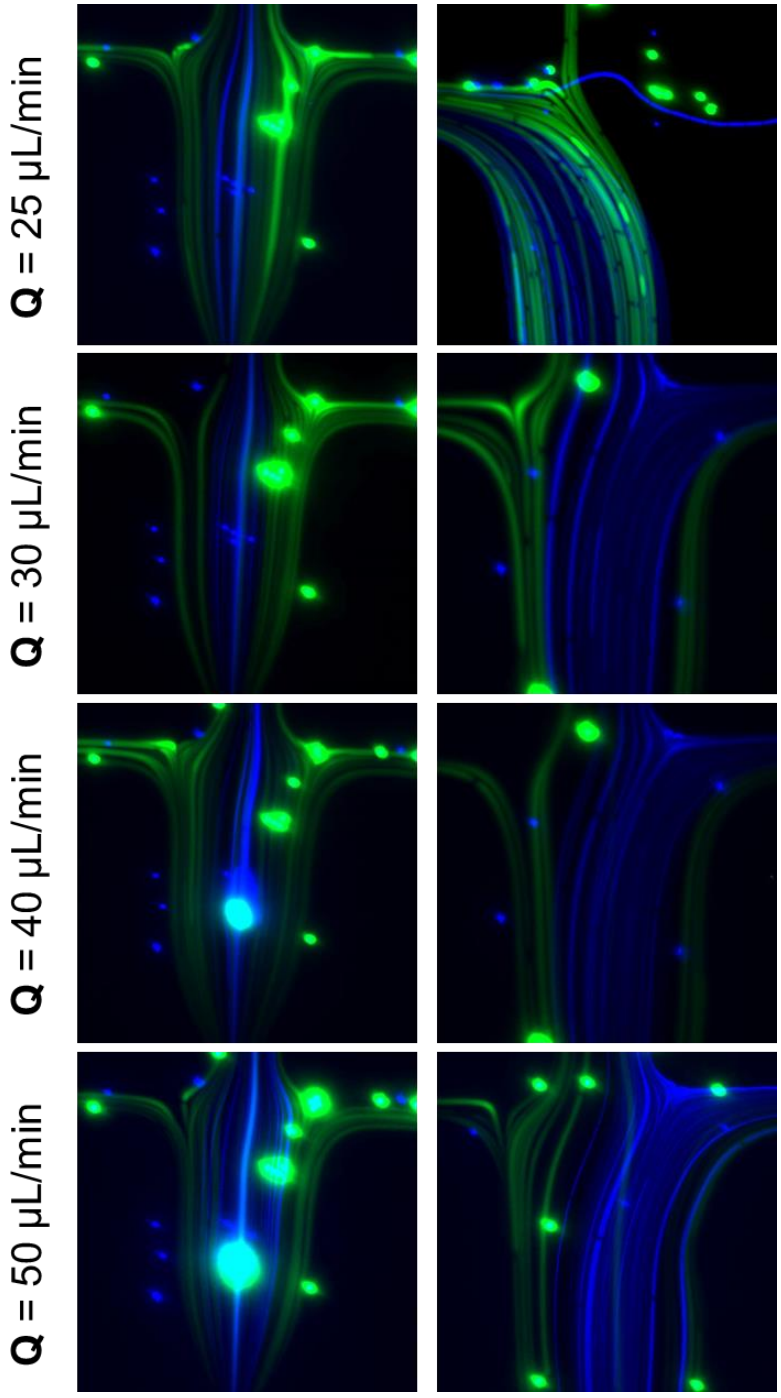

Figure 30 *- Fluorescence images of the 4 µm and 15µm mixture in 1000ppm PEO in PBS solution captured at the expansion of both different AR channels (50 µm x 30 µm and 75 µm x 30 µm) at different flow rates. The outlet configuration is #3, meaning the central outlet punched at 1.5 cm and side outlets at 1.5 cm.*

3.4 Biological Samples Experiments

After testing the polystyrene microbeads, establishing the possibility of corpuscles separation, and finding the optimal conditions and configurations, biological experiments were carried out. Firstly, we started by testing the single type of cells in our device, then we proceeded by testing a mixture of

different corpuscles together. The cellular type tested were spermatozoa obtained by centrifuged seminal fluid, erythrocytes obtain with the gradient centrifugation method, and the seminal fluid simply diluted. This latter was also tested because in the seminal fluid the presence of other cell types was established by urological routine exams and even though the round cells, specifically the leukocytes, were always lower than 2%, it would have been of interest to study the behavior of the whole fluid and to validate the separation with the direct sample collected without using further treatments. Finally, we tested two different mixtures of corpuscles: spermatozoa with 15µm particles, and spermatozoa with erythrocytes. The 15µm beads were used instead of the leukocytes because it was not possible to extract them from the blood samples that were provided without contaminating the sample with RBCs, which were predominant even in the isolated sample. But since the WBCs are perfectly round and of about 15µm in diameter, the results can still be considered valid and representative of the real samples.

3.4.1 Experiments with Centrifuged Sperm Cells

In figure 31 are reported the bright-field images of the spermatozoa acquired with phase-contrast for each flow rate in the 50µm x 30µm channel at both inlet and after 3cm after it, near the expansion; from now on it will be called outlet. We were able to measure the width of the distribution of the cells along the width of the channel and, since it was not possible to define a precise equilibrium position, some images of the expansion were captured to show how the different flow rates can have a very different allocation in this area. It is possible to observe how all the inlet images show a homogeneous distribution of the cells in the channel width, which guarantees a lack of bias in the further distribution. Another appreciable detail is the change of shape and sharpness of the cells as the flow rate increases: the lower is the flux, the clearer is the spermatozoa shape, the higher is the flux, the blurrier is the cell. At the expansion, this different behavior is not notable due to the lowering of velocity as a result of the increase of space.

In particular, from 5µL/min to 10µL/min the sperm have a very tight placement in the middle of the channel in an area of about 20µm, and for this reason, in the expansion, it is possible to observe how basically all the cells can be collected from the central outlet. From 15µL/min to 20µL/min the

distribution zone of the cells enlarges to around 25µm, but the majority of spermatozoa can be still found in the central outlet. Increasing the flow rate, between 25µL/min and 30µL/min the positioning of the bulk cells is around 32µm of the central area of the channel; at those flow rates, an important part of sperm cells is lost in the side outlets. Ultimately, from 40µL/min to 50µL/min we cannot say that the cells can be gathered in a specific area, indeed we can find them in about 35µm of the channel, which leaves about 7µm from each side as untouched space for the cells' collocation.

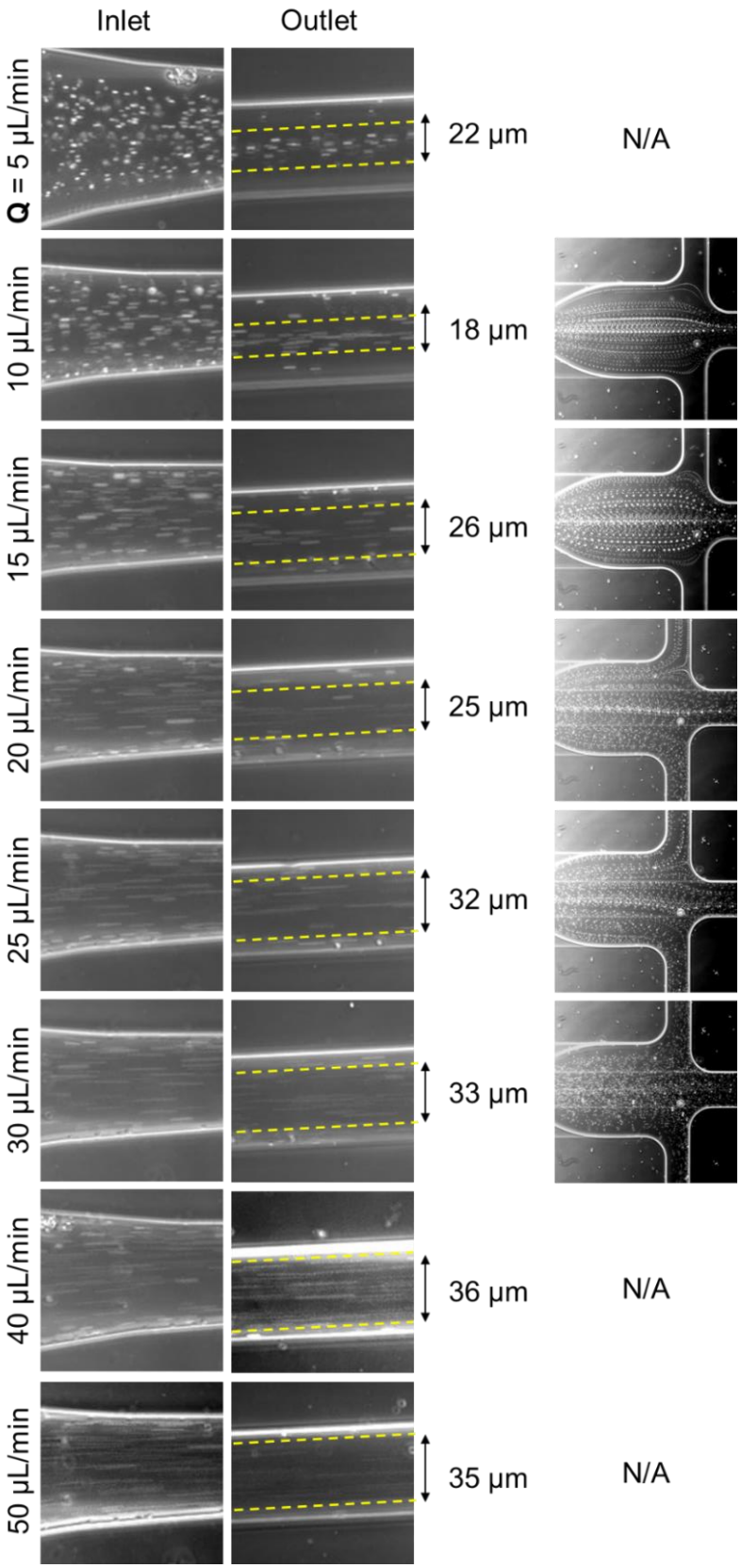

Figure 31 *– Bright-field images in phase contrast of spermatozoa in 1000ppm PEO in PBS solution in 50 µm x 30 µm channel at the different flow rates tested; the width of the equilibrium bandwidth is reported along with some of the bright-field in phase contrast expansion images.*

In figure 32 are reported the bright-field images of the spermatozoa acquired with phase-contrast for each flow rate in the 75µm x 30µm channel at both inlet and outlet. We were able to measure the width of the distribution of the cells along the width of the channel and, since it was not possible to define a precise equilibrium position, some images of the expansion were captured to show how the different flow rates can have a very different allocation in this area. Once again, all the inlet images show a homogeneous distribution of the cells in the channel width and the change of shape and sharpness of cells as the flow rate increases is appreciable.

At 5µL/min the distribution of the spermatozoa is tightly collocated in the central 34µm area of width. As the flow rate increases, from 10µL/min to 30µL/min the spermatozoa can be found in the 44µm central zone of the channel. Even though for all these flow rates the cells' distribution in the straight channel is pretty similar, a different collection of sperm can happen at the expansion: from 10µL/min to 20µL/min the majority of cells is gathered in the central outlet while from 25µL/min to 30µL/min an important part of spermatozoa can be also found in the side outlets. At 40µL/min the bulk of cells is located in the 46µm central zone but some of them can be also found moving slower near the channel walls. Ultimately, at 50µL/min a prevailing distribution is not visible and the cells can be found spread in 53µm of the 75µm width.

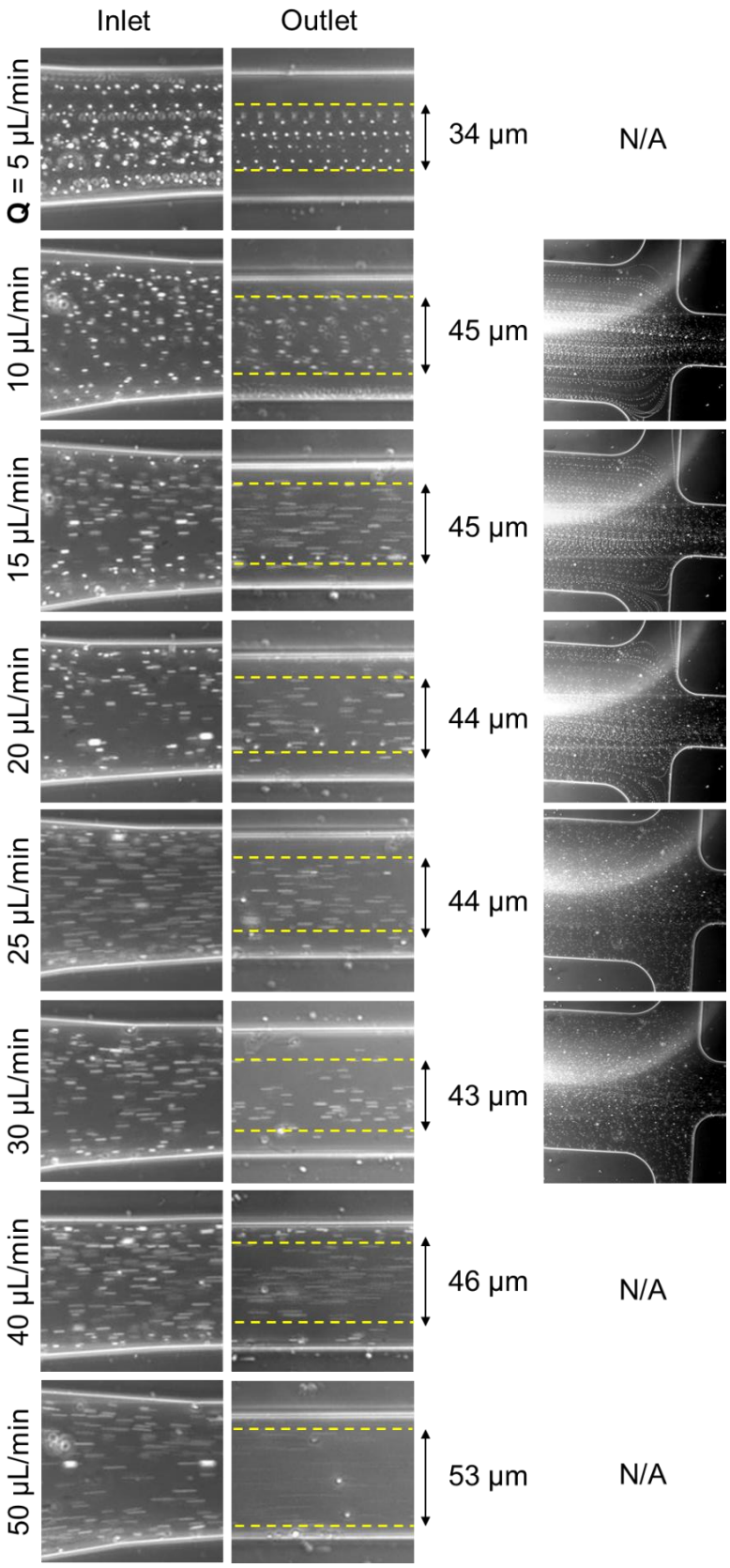

Figure 32 *- Bright-field images in phase contrast of spermatozoa in 1000ppm PEO in PBS solution in 75 µm x 30 µm channel at the different flow rates tested; the width of the equilibrium bandwidth is reported along with some of the bright-field in phase contrast expansion images.*

3.4.2 Experiments with Non-Treated Seminal Fluid

In figure 33 are reported the bright-field images of the non-treated seminal fluid diluted in the viscoelastic solution; all the pictures were acquired with phase-contrast for each flow rate in the 50µm x 30µm channel at both inlet and outlet. We were able to measure the width of the cells' distribution along the width of the channel and, since it was not possible to define a precise equilibrium position once again, all the expansion images were captured too to study how the different flow rates can cause a very different allocation in this area. Once more, all the inlet images show a homogeneous distribution of the cells in the channel width and the change of shape and sharpness of cells as the flow rate increases is appreciable.

At 5µL/min the cells are perfectly visible but not really focused in a specific area of the channel, even though we can say that they are mainly located in the 27µm of the central area. From the expansion image, it is possible to notice how the spermatozoa can be collected from all the outlets, although the majority of them can be pulled through the central one. At 10µL/min and 15µL/min a tighter distribution of cells is visible, and they can be found in the central 23µm. The main collection of spermatozoa is clearly observable in the central outlet, but an interesting part is also lost in the side outlets. From 20µL/min to 40µL/min, the cells have a similar behavior: the allocation of spermatozoa is in about 25µm of the central zone of the channel, and the final collection at the expansion is divided in about two-thirds of the cells in the central outlets and the remaining third in the side ones. Ultimately, at 50µL/min a central collection is still possible; indeed, the concentration of spermatozoa in the 27µm area of the central channel is visible and at the expansion, the collection of the majority of sperm cells in the central outlet can be achieved. It must be said that for all the flow rates tested, some of the spermatozoa got lost in the side outlets no matter what.

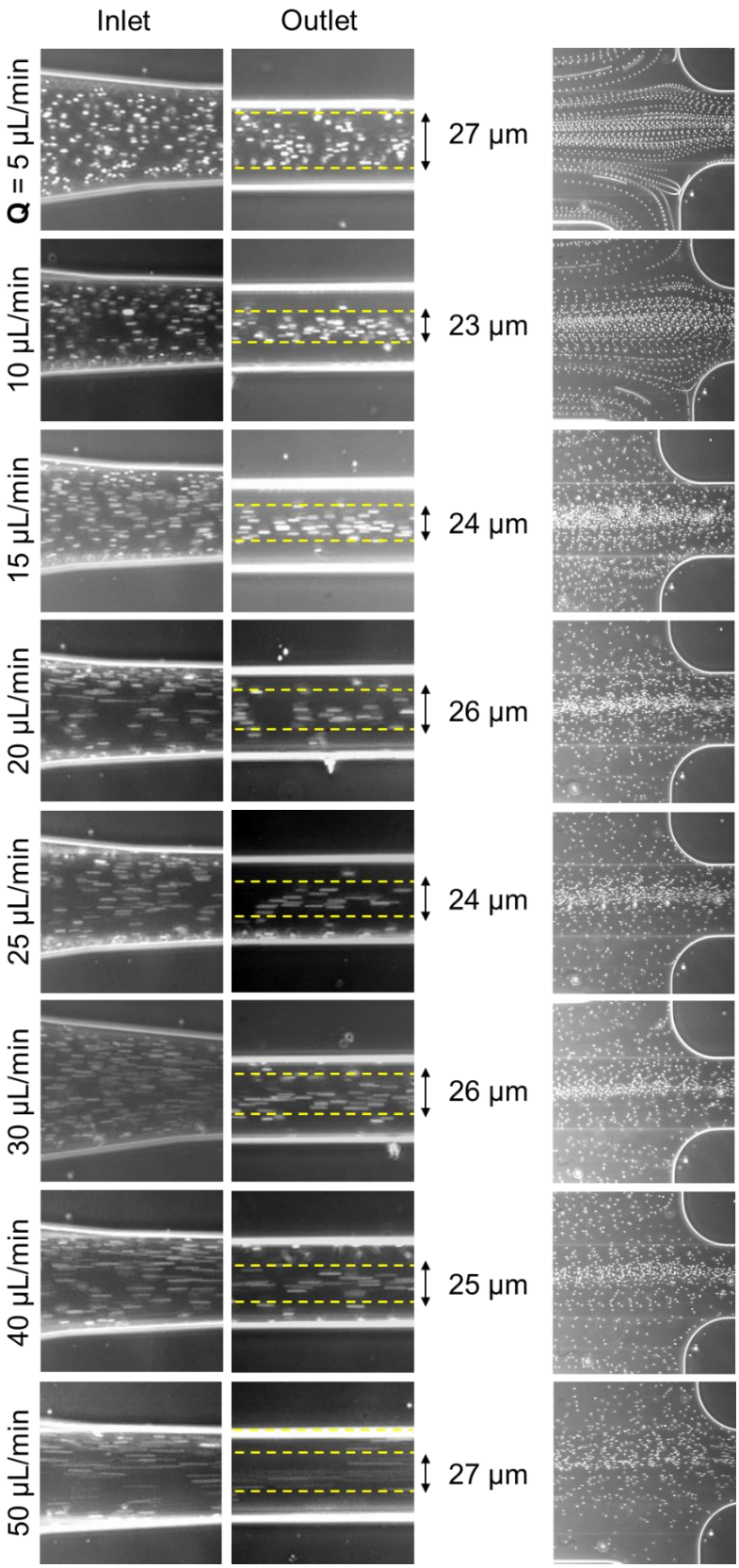

Figure 33 *- Bright-field images in phase contrast of seminal fluid diluted in 1000ppm PEO in PBS solution in 50 µm x 30 µm channel at the different flow rates tested; the width of the equilibrium bandwidth is reported along with some of the bright-field in phase contrast expansion images.*

In figure 34 are reported the bright-field images of the non-treated seminal fluid diluted in the viscoelastic solution; all the pictures were acquired with phase-contrast for each flow rate in the 75µm x 30µm channel at both inlet and outlet this time. We were able to measure the width of the distribution of the cells along the width of the channel and, since it was not possible to define a precise equilibrium position once again, all the expansion images were captured too to study how the different flow rates can cause a very different allocation in this area. Once more, all the inlet images show a homogeneous distribution of the cells in the channel width and the change of shape and sharpness as the flow rate increases is appreciable.

From 5µL/min till 20µL/min, as the flow rate increases, the area of spermatozoa distribution diminishes; in particular, it reaches the smaller zone of 31µm at 20µL/min. For all these conditions, at the expansion is possible to observe how the majority of sperm cells can be collected in the central outlet and how some of the cells near the wall can be deviated and still collected at the center. From 25µL/min to 50µL/min, as the flow rate increases, the width of the equilibrium position zone increases. In general, the width occupied by the spermatozoa remains about 35µm for all the flow rates but 50µL/min. In this latter case, as happened in the experiments explained before, the distribution area increases and in this specific case become 45µm, so there is no longer a specific focusing but rather a more homogeneous allocation of cells in the channel. Also, at this flow rate, we can see how the deviation of some of the cells does not occur anymore, and thus it is possible to say that a significant part of spermatozoa is lost in the side outlets.

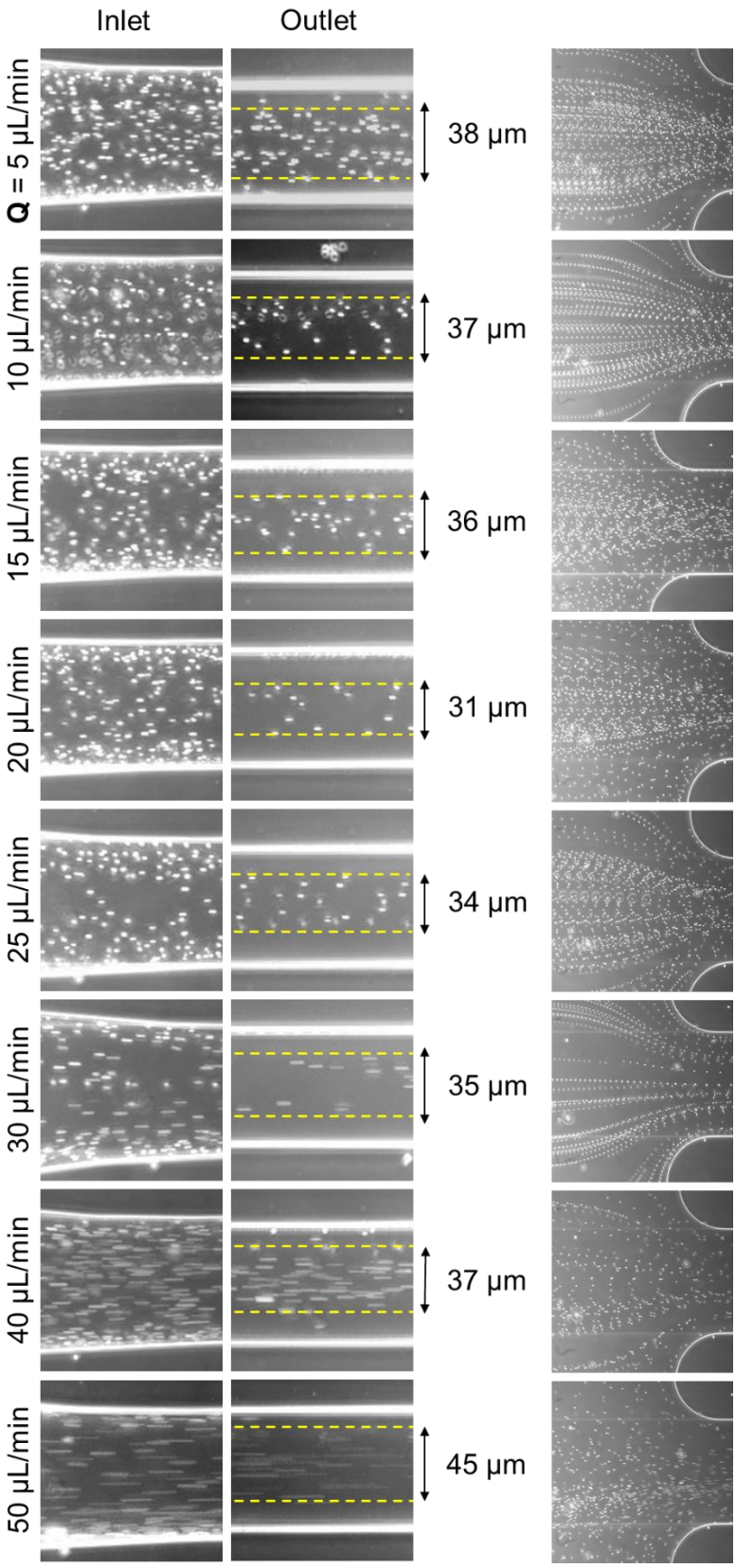

Figure 34 *- Bright-field images in phase contrast of seminal fluid diluted in 1000ppm PEO in PBS solution in 75 µm x 30 µm channel at the different flow rates tested; the width of the equilibrium bandwidth is reported along with some of the bright-field in phase contrast expansion images.*

3.4.3 Experiments with Erythrocytes

In figure 35 are reported the bright-field images of the erythrocytes obtained with the gradient centrifugation method; the pictures were acquired with phase-contrast for each flow rate in the 50µm x 30µm channel at both inlet and outlet. Since sharp streamlines were not observable, the measure of the width of the cells' distribution along the width of the channel was reported. It is possible to observe how all the inlet images show a homogeneous distribution of the cells in the channel width, which guarantees a lack of bias in the further distribution. Another appreciable detail is the change of shape and sharpness of cells as the flow rate increases: the lower is the flux, the clearer is the discoid shape, the higher is the flux, the blurrier is the cell.

As we can observe, with the increasing flow rate, the width of the distribution area of the erythrocytes decreases. In particular, at 5µL/min and 10µL/min, almost two different focusing positions can be seen; both of them remain around the center of the channel in an area of 15µm. Between 15µL/min and 20µL/min, the different streamlines disappear but the main location of cells stays around 15µm of the central zone. From 25µL/min to 50µL/min the distribution zone diminish till 9µm; at 25µL/min and 30µL/min a spreading in that area can be observed but from 40µL/min till 50µL/min it almost seems that all the RBCs form a single and very sharp streamline at the center of the channel.

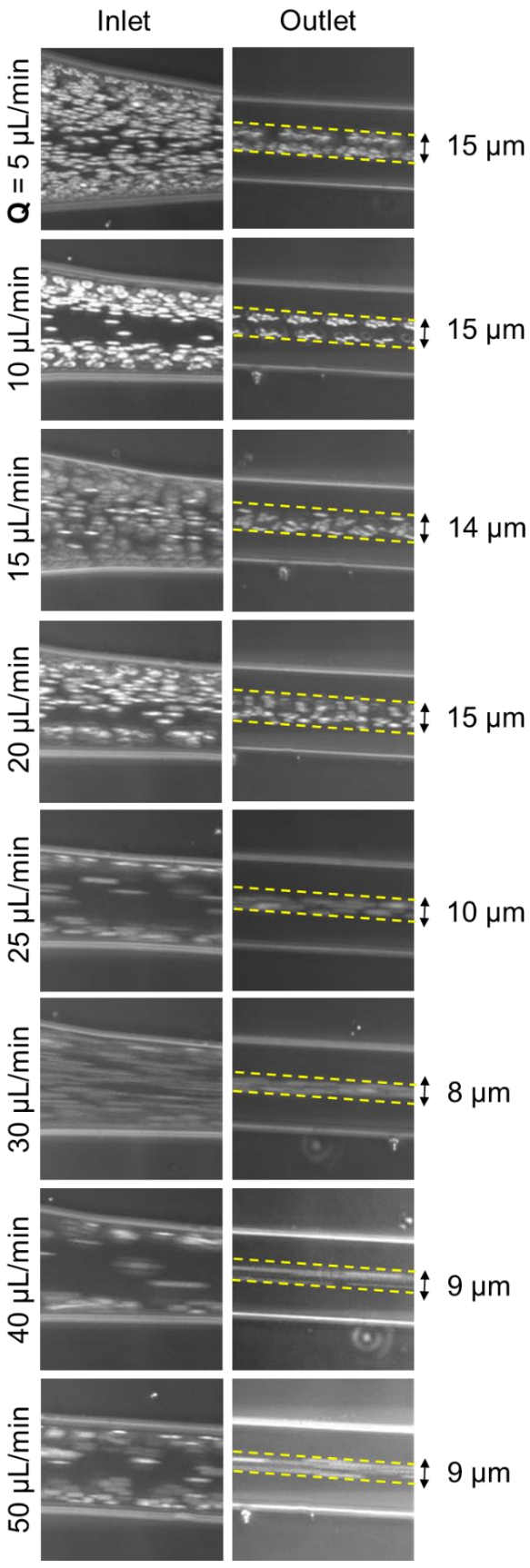

Figure 35 *- Bright-field images in phase contrast of erythrocytes diluted in 1000ppm PEO in PBS solution in 50 µm x 30 µm channel at the different flow rates tested; the width of the equilibrium bandwidth is reported.*

In figure 36 are reported the bright-field images of the erythrocytes obtained with the gradient centrifugation method; the pictures were acquired with phase-contrast for each flow rate in the 75µm x 30µm channel too at both inlet and outlet. Since sharp streamlines were not observable, the measure of the width of the cells' distribution along the width of the channel was reported. It is possible to observe how all the inlet images show a homogeneous distribution of the cells in the channel width, which guarantees a lack of bias in the further distribution; the only exceptions were at 25µL/min and 30µL/min where the RBCs can be seen only near the walls; this happened due to a central clogging of the inlet but, right after the images were taken, the device was unclogged and everything went back as described before. Another appreciable detail is the change of shape and sharpness of cells as the flow rate increases: the lower is the flux, the clearer is the discoid shape, the higher is the flux, the blurrier is the cell.

At 5µL/min the outlet cells' distribution is still quite random and located in 42µm of the central area; thus, cannot be seen as a focusing. But from 10µL/min to the higher flow rate the behavior improves and the zone where the RBCs are located tightens up. Specifically, from 10µL/min to 20µL/min the erythrocytes are found in about 29µm of the central width of the channel and it is possible to observe how the cells tend to form two different streamlines symmetrically from the center. At 25µL/min and 30µL/min, the two different equilibrium positions become sharper while from 40µL/min till 50µL/min a more random distribution in the central 24µm is visible.

As happened in the AR =1.67, even in the AR = 2.5 the higher the flow rate is, the tighter the focusing area becomes.

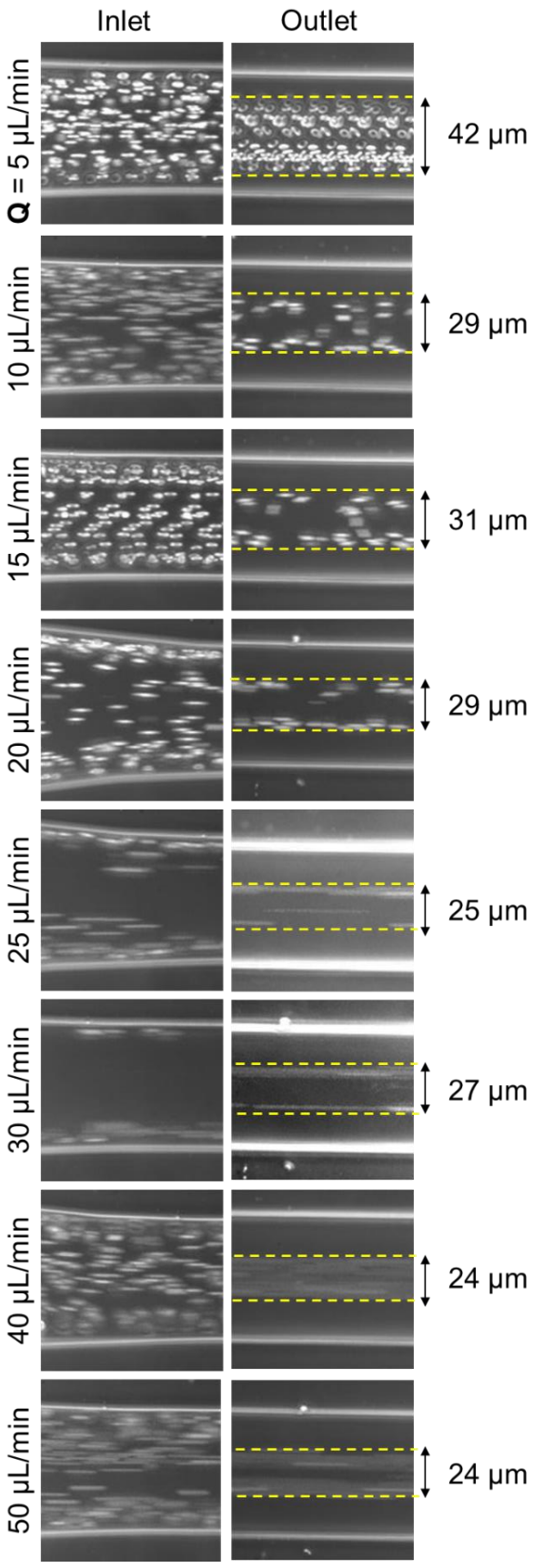

Figure 36 *- Bright-field images in phase contrast of erythrocytes diluted in 1000ppm PEO in PBS solution in 75 µm x 30 µm channel at the different flow rates tested; the width of the equilibrium bandwidth is reported.*

3.4.4 Experiments with Mixture of Sperm Cells and 15µm Particles

In figure 37 are reported the bright-field images of the mixture of spermatozoa and 15µm particles; the pictures were acquired in phase-contrast for each flow rate in the 50µm x 30µm channel at both configurations #1 and #2. The images show the behavior of the different corpuscles at the expansion area before they divide between the three different outlets. The whole figures were obtained by superimposing two different images of the same expansion captured with a 10X objective; this is why in some of the pictures the cells are not matching or neither does the illumination or their specific amount. In figure 38 are visible the separation efficiency and purity graphs; the values were calculated by counting the number of target cells present in each outlet, the total number of a certain type of cells in the expansion, and the number of total entities inside a specific outlet; then the formulas reported in the Materials & Method chapter were used. In our specific case, we consider the spermatozoa as the target entities for the central outlet and the 15µm particles as the target entities of the side ones.

In configuration #1, from 10µL/min to 25µL/min the corpuscles separation seems feasible: all the 15µm particles can be collected in the side outlets and a good amount of pure spermatozoa finishes in the central one. By looking at the separation efficiency and purity values it is clear that the separation efficiency of the 15µm beads from the spermatozoa is perfect, 100%; likewise, the purity of the sperm cells collected in the central outlet is 100%. The downside is that the efficiency values are all around 60% for the central outlet, and thus for the spermatozoa, and the purity values are way lower for the side outlets due to a large number of spermatozoa present when compared to the number of 15µm beads retrieved. At 30µL/min the values are pretty similar to the one just illustrated with a slight difference in the efficiency of the separation of the microbeads and the purity of the central outlets, which are still above 97% though; this is due to the presence of just a couple of 15µm particles in the central area.

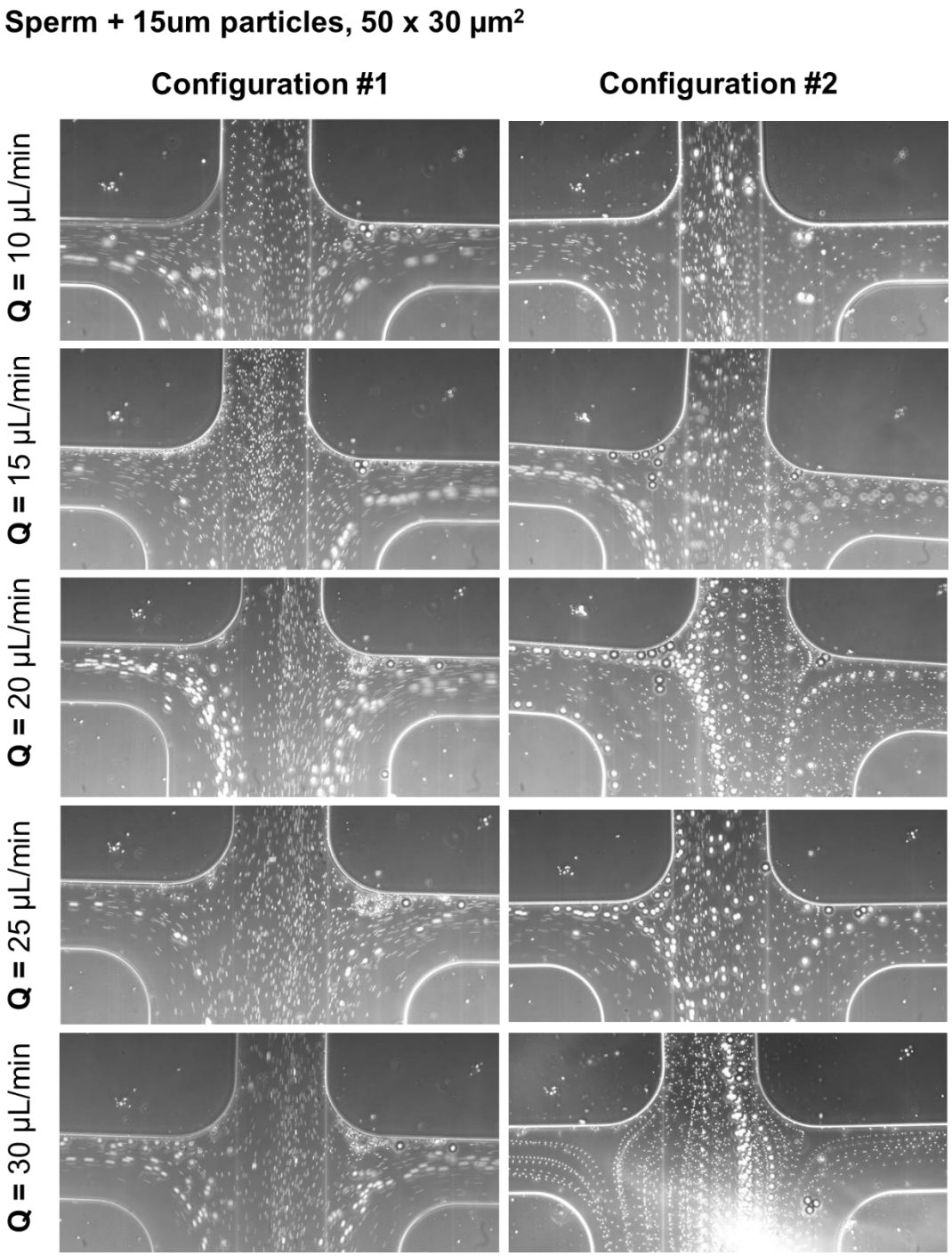

Figure 37 *- Bright-field images in phase contrast of the mixture of spermatozoa and 15µm particles diluted in 1000ppm PEO in PBS solution and tested in 50 µm x 30 µm channel at the different flow rates; the results of configurations #1 and #2 are reported.*

This latter phenomenon is enhanced in configuration #2; indeed, at 10µL/min almost none of the 15µm beads can be found in the side outlets and the few present are going into the central one, causing very low values of both separation efficiencies and purity in all the outlets, with the only exception of the purity of the central one, which is still above 90% due to the way higher number of spermatozoa present

with respect to the number of microbeads. From 15µL/min to 25µL/min the situation remains stable: some of the 15µm beads can be collected in the side outlets while a significant part of them finishes in the central one along with the majority of spermatozoa. Indeed, the separation efficiency values of the side outlets and central outlet are similar and around 50 and 70%, with higher values for the side ones; the purity values are higher than 80% for the central outlets but lower than 30% for the side ones, where a good number of both spermatozoa and microbeads can be seen. At 30µL/min an analogous situation to 10µL/min is present: the few particles finish in the central outlet while the spermatozoa are distributed all around the expansion and thus, the efficiency values of the side outlet are below ten, the efficiency of the central one is around 60% and the purity is almost perfect for the spermatozoa but almost non-existent for the 15µm beads in the side outlets.

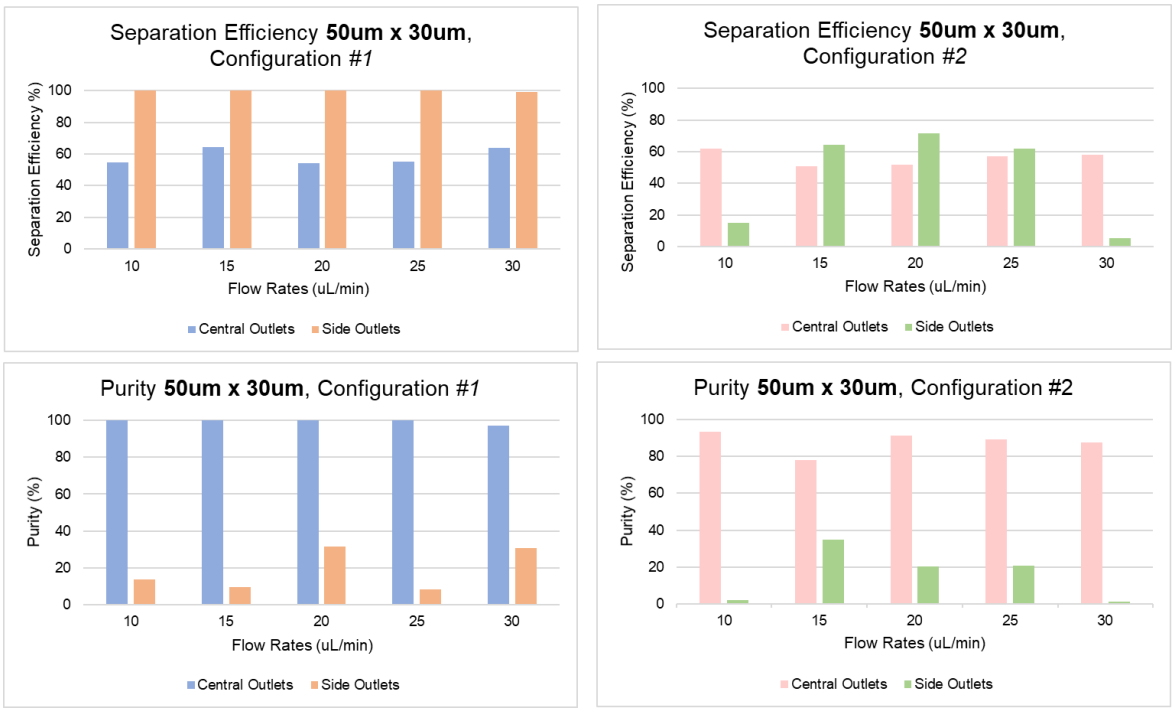

Figure 38 *– Separation Efficiency and Purity graphs for the mixture of sperm cells and 15µm particles diluted in 1000ppm PEO in PBS in the 50µm x 30µm channel; the results obtained from both the configurations #1 and #2 are reported. All the calculations were made considering the final aim of collecting the spermatozoa from the central outlet and the 15µm particles from the side ones.*

In figure 39 are reported the bright-field images of the mixture of spermatozoa and 15µm particles; the pictures were acquired in phase-contrast for each flow rate in the 75µm x 30µm channel at both configurations #1 and #2. The images show the behavior of the different corpuscles at the expansion area before they divide between the three different outlets. The whole figures were obtained as described

before and all the previous considerations are still valid. In figure 40 are visible the separation efficiency and purity graphs; the values were calculated by counting the number of target cells present in each outlet, the total number of a certain type of cells in the expansion, and the number of total entities inside a specific outlet; then the formulas reported in the Materials & Method chapter were used. In this specific case, the spermatozoa were still considered as the target entities for the central outlet and the 15µm particles as the target entities of the side ones.

Even though in this wider channel is harder to see the difference between the corpuscles, by squinting a bit the eyes, it is possible to observe the different behavior of cells and particles. In configuration #1, for all the flow rate tested, so from 10µL/min to 30µL/min, all the 15µm particles present were collected in the side outlets and a good part of spermatozoa was collected alone in the central one. This is testified by the efficiency values that are 100% for the side outlets and the perfect purity values as well for all the said flow rates. Once again, the separation efficiency values for the central outlets are between 40 and 60% while the purity values for the side ones are way lower due to the higher number of spermatozoa collected in them with respect to microbeads. In configuration #2 the situation is almost the ideal one at 10µL/min and 15µL/min, with 100% of efficiency values for the side outlets and purity values for the central one; in these cases, the efficiency values for the central outlet are a bit higher, all of them around 60%, and the purity values for the side outlets are a little better, almost 30%. From 20µL/min to 30µL/min the presence of just a couple of 15µm particles in the central outlet is visible but despite it, the separation efficiency values for the side outlets remain above 95% and the purity values for the central one are above 98%. Furthermore, the efficiency values for the central one increased when compared to the other configuration and reach a peak of over 60% at 30µL/min; at the same flow rate, the highest purity value for the side outlets is reached too at a value of about 50%.

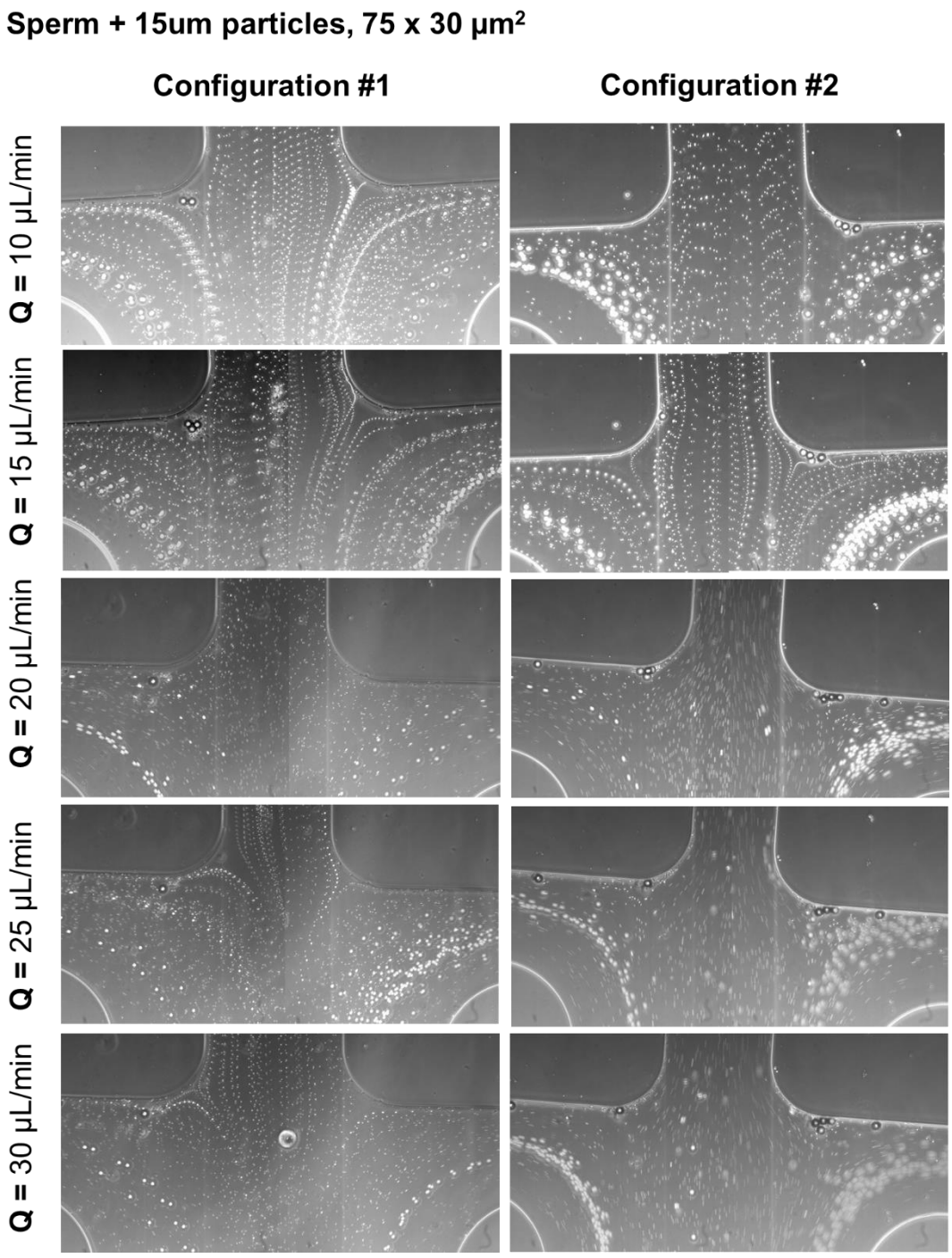

Figure 39 *- Bright-field images in phase contrast of the mixture of spermatozoa and 15μm particles diluted in 1000ppm PEO in PBS solution and tested in 75 μm x 30 μm channel at the different flow rates; the results of configurations #1 and #2 are reported.*

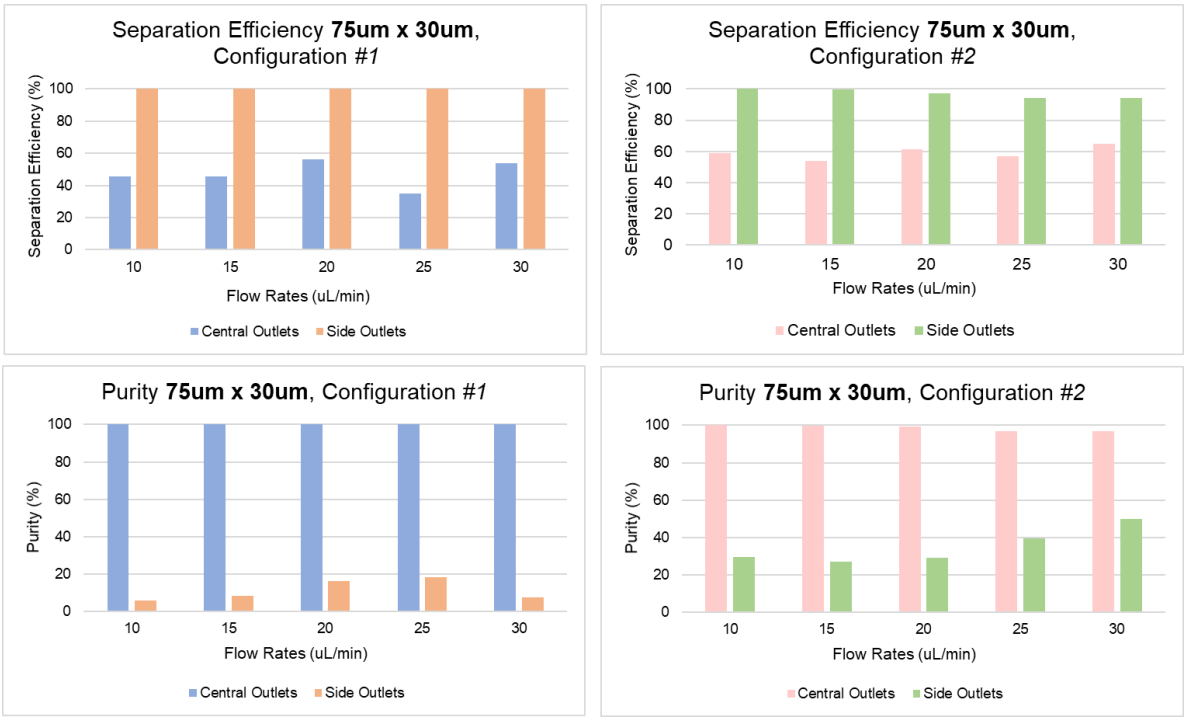

Figure 40 *- Separation Efficiency and Purity graphs for the mixture of sperm cells and 15µm particles diluted in 1000ppm PEO in PBS in the 75µm x 30µm channel; the results obtained from both the configurations #1 and #2 are reported. All the calculations were made considering the final aim of collecting the spermatozoa from the central outlet and the 15µm particles from the side ones.*

3.4.5 Experiments with Mixture of Sperm Cells and Erythrocytes

In figure 41 are reported the bright-field images of the mixture of spermatozoa and erythrocytes; the pictures were acquired in phase-contrast for each flow rate in the 50µm x 30µm channel at both configurations #1 and #2. The images show the behavior of the different cells at the expansion area before they divide between the three different outlets. The whole figures were obtained as described before and all the previous considerations are still valid. In figure 42 are visible the separation efficiency and purity graphs; the values were calculated by counting the number of target cells present in each outlet, the total number of a certain type of cells in the expansion, and the number of total entities inside a specific outlet; then the formulas reported in the Materials & Method chapter were used. In this specific case, the spermatozoa were considered as the target entities for the side outlets while the erythrocytes as the target entities of the central one; this switch was due to the major presence of RBCs in the center part of the expansion and the spermatozoa presence in both the central and side outlets.

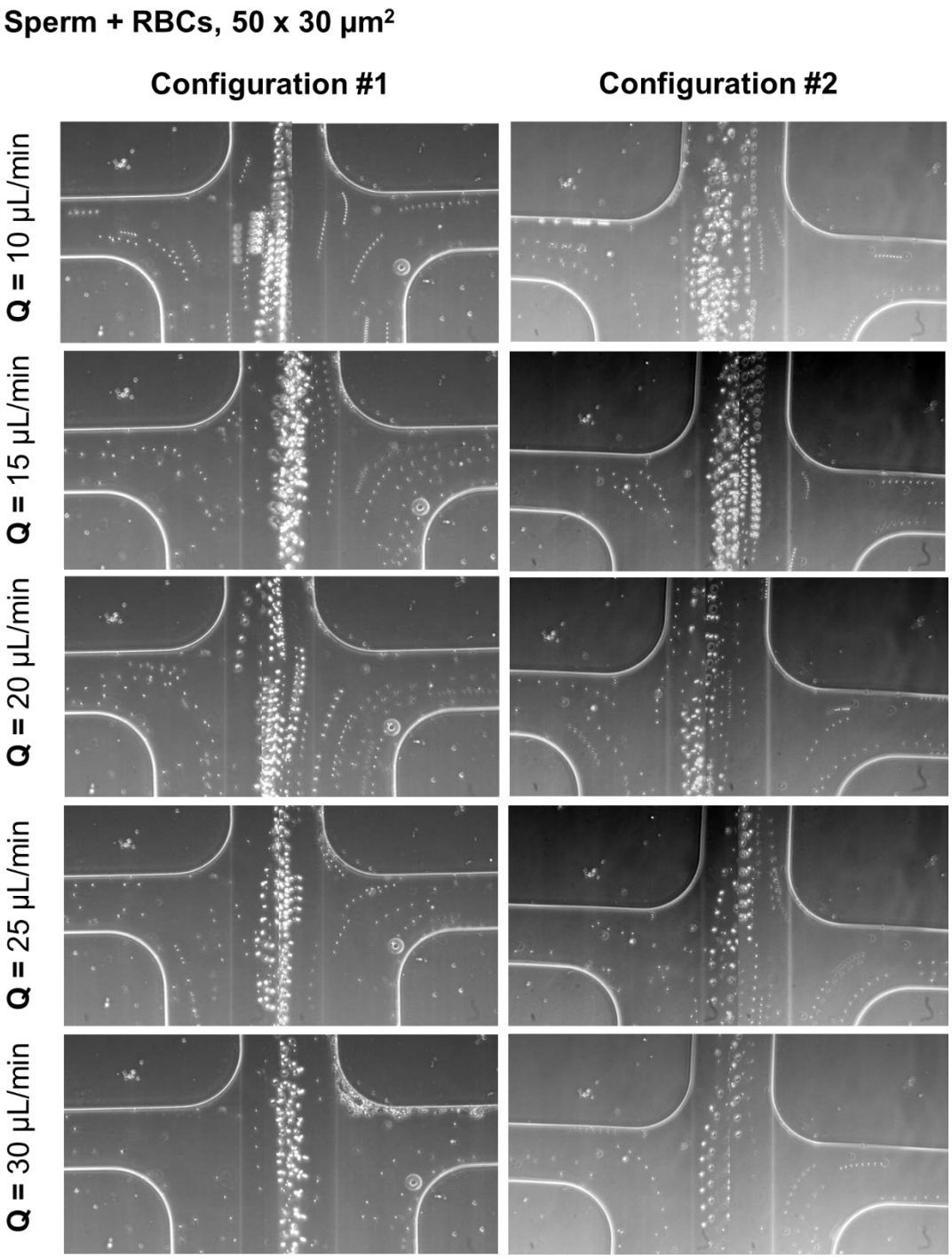

Figure 41 *- Bright-field images in phase contrast of the mixture of spermatozoa and erythrocytes diluted in 1000ppm PEO in PBS solution and tested in 50 µm x 30 µm channel at the different flow rates; the results of configurations #1 and #2 are reported.*

In configuration #1 for all the flow rates, so from 10µL/min to 30µL/min, all the RBCs were collected in the central outlets and a part of spermatozoa could be found in the side ones. Specifically, the separation efficiency values for the central outlet are 100% for all the conditions and the efficiency values for the side outlets are always between 55% and 70%. The purity values of the side outlets reach

100% for all the flow rates tested as well, and for the central one, they are almost always between 60% and 70%. The higher values are achieved at 15µL/min and 20µL/min.

A similar situation can be observed for configuration #2; the difference stays in the 10µL/min where some of the RBCs can be found in the side outlets too and this causes the lowering of the efficiency and purity values that remains above 90% and 80% for the central outlet and the side ones respectively. From 15µL/min to 30µL/min a perfect collection of all the erythrocytes in the central outlets and a pure sample of spermatozoa in the side ones is achieved. This is also confirmed by the graphs below, which show 100% for both efficiency values for the central outlet and purity values for the side ones. The remaining values have a similar pattern to configuration #1 but the values are slightly lower: between 45% and 65% for the separation efficiency of the side outlets and between 45% and 60% for the purity of the central one, except for 15µL/min in which the peak of above 70% is reached.

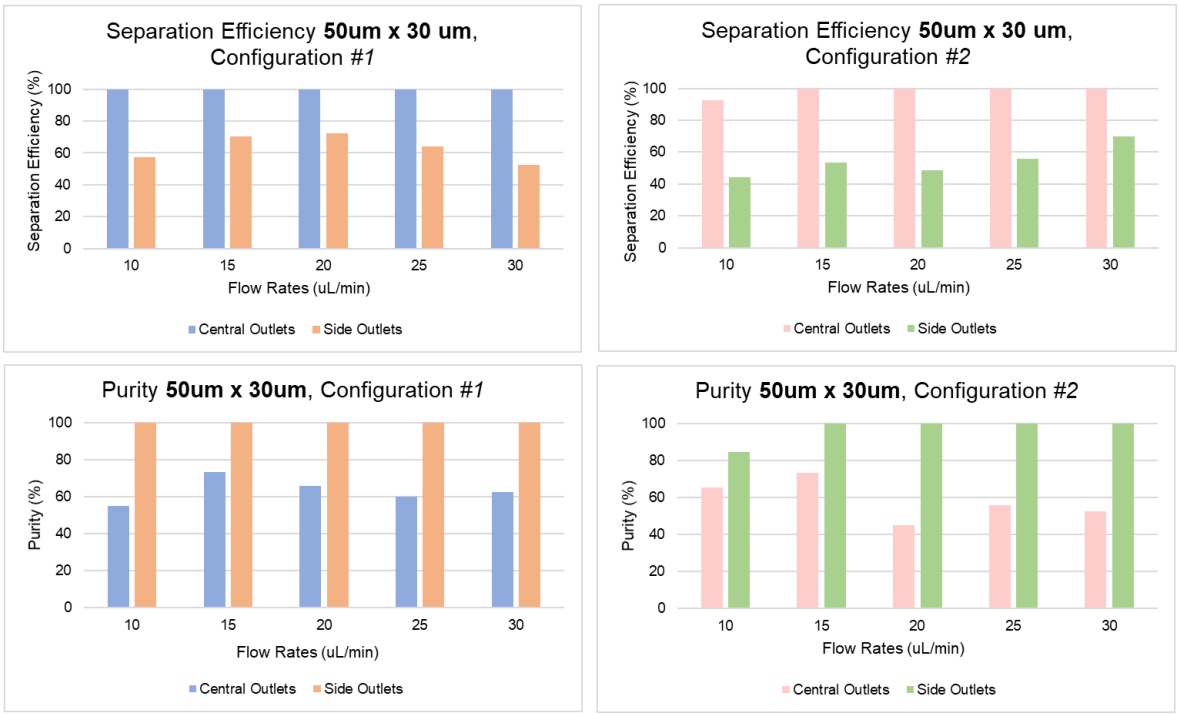

Figure 42 *- Separation Efficiency and Purity graphs for the mixture of sperm cells and RBCs diluted in 1000ppm PEO in PBS in the 50µm x 30µm channel; the results obtained from both the configurations #1 and #2 are reported. All the calculations were made considering the final aim of collecting the erythrocytes from the central outlet and the spermatozoa from the side ones.*

In figure 43 are reported the bright-field images of the mixture of spermatozoa and erythrocytes; the pictures were acquired in phase-contrast for each flow rate in the 75µm x 30µm channel at both

configurations #1 and #2. The images show the behavior of the different cells at the expansion area before they divide between the three different outlets. The whole figures were obtained as described before and all the previous considerations are still valid. In figure 44 are visible the separation efficiency and purity graphs; the values were calculated by counting the number of target cells present in each outlet, the total number of a certain type of cells in the expansion, and the number of total entities inside a specific outlet; then the formulas reported in the Materials & Method chapter were used. In this specific case, in configuration #1 the spermatozoa were considered as the target entities for the central outlet, like it was for the mixture of sperm cells and 15µm particles, while the erythrocytes as the target entities of the side ones; this choice was done because the RBCs seemed to tend to focus in two different streamlines and thus to be collected mainly into the side outlets. But in configuration #2 a switch of choice was done to the major presence of RBCs in the center part of the expansion and the spermatozoa presence in both the central and side outlets. Thus, the spermatozoa were considered as the target entities for the side outlets while the erythrocytes as the target entities of the central one. Without those changes in the target entities' consideration, the values would not have been open to interpretation.

In configuration #1, for all the flow rates tested the erythrocytes could be found in all three outlets, hence making the separation impossible. At 10µL/min indeed the separation efficiency values were below 65% in the side outlets and 20% for the central one. Besides, the purity values were below 60% for the side outlets and below 30% for the central one. Similarly happens at 15µL/min. From 20µL/min to 30µL/min all the values increase a little bit but none of them reaches the threshold of 85% required for a decent separation. The highest values can be found at 20µL/min where the separation efficiency is 85% for the side outlets and 60% for the central one, and the purity values are 80% for the central outlet and 60% for the side ones. But still, those values are lower and not sufficient when compared to the AR = 1.67 channel with the same mixture and configuration.

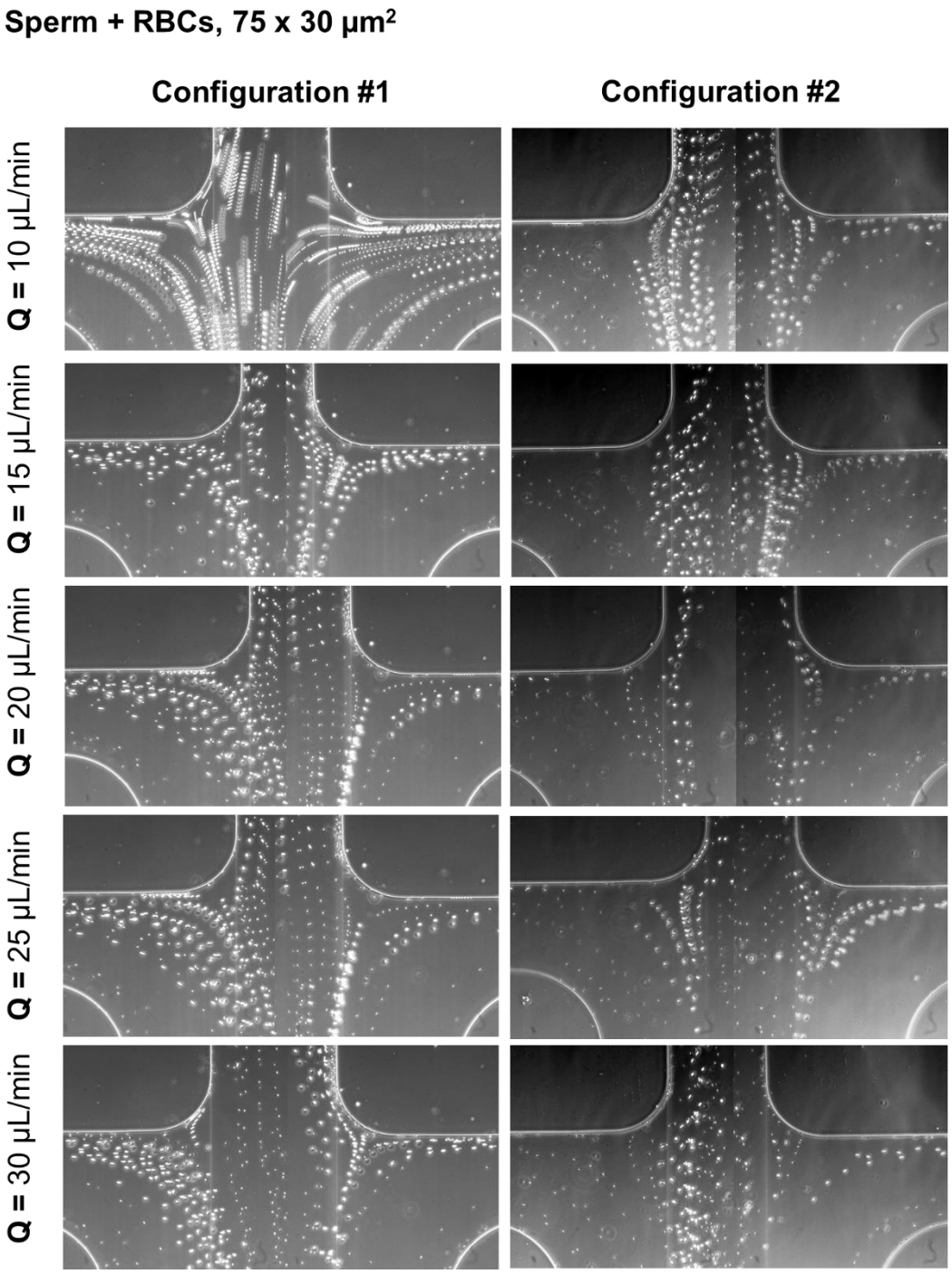

Figure 43 *- Bright-field images in phase contrast of the mixture of spermatozoa and erythrocytes diluted in 1000ppm PEO in PBS solution and tested in 75 µm x 30 µm channel at the different flow rates; the results of configurations #1 and #2 are reported.*

In configuration #2, since the majority of RBCs can be seen in the central area of the expansion, an inverted separation calculation like the one studied in the AR = 1.67 channel was performed. Specifically, here some of the erythrocytes could be still found in the right-side outlet but the majority of them were efficiently collected into the central outlet. The higher values of separation efficiency and

purity can be calculated between 10µL/min and 20µL/min; the efficiency values for the central outlets were above 80% and above 40% for the side ones. Purity values higher than 90% were reached for the side outlets at 15µL/min and 20µL/min and between 40 and 70% for the central one. At 25µL/min all the values calculated in the graphs were below 40%, while at 30µL/min a return to the previous trend can be observed: efficiency values of almost 90% for the central outlet and 40% for the side one and purity values of about 80% for the side outlet and 40% for the central one.

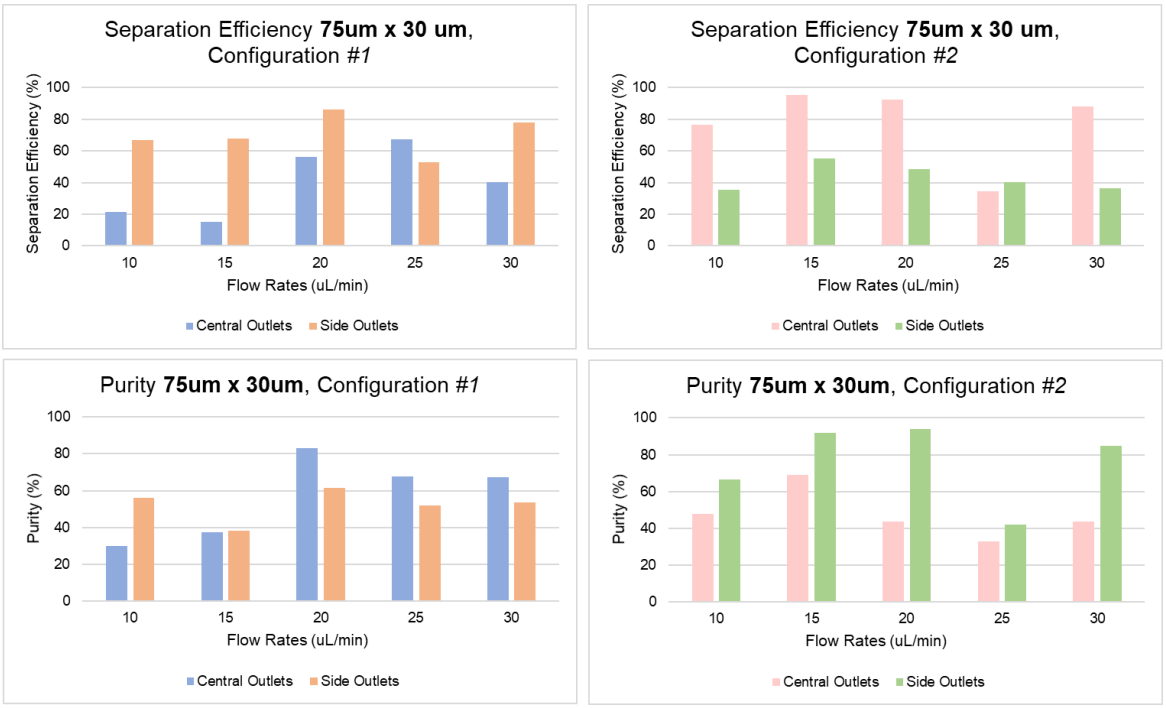

Figure 44 *- Separation Efficiency and Purity graphs for the mixture of sperm cells and RBCs diluted in 1000ppm PEO in PBS in the 75µm x 30µm channel; the results obtained from both the configurations #1 and #2 are reported. The calculations for configuration #1 were made considering the final aim of collecting the spermatozoa from the central outlet and the erythrocytes from the side ones, while the calculations for configuration #2 were made considering the opposite final aim; thus, collecting the erythrocytes from the central outlet and the spermatozoa from the side ones.*

CHAPTER 4

DISCUSSION

4.1 Expected Behavior

Analyzing all the data calculated in paragraph 3.2 and taking into consideration the formulas enunciated in paragraph 1.2.1, we can speculate and explain the expected behavior of the microbeads used in our research project. First of all, we know from the literature that the big particles will be focused near the sidewall while the smaller ones will find their equilibrium position near the centerline of the channel; this happens because, looking at the equations 4, 5, and 6 (inertial lift force, elastic force and drag force), all the forces are proportional to the particle's dimension and will have a different effect based on the diameter size of the microbead[56]. Specifically, since the inertial lift force is proportional to the power four of the particle diameter while the elastic force is proportional to the power three of the particles size, the larger would be the particle, the stronger would be the effect of the inertial lift force which will push the microbead in the equilibrium positions between the channel center and the channel sidewalls. On the other hand, if the diameter of the particles is smaller and the normal stress difference is prevalent, the particles will move inside the channel due to the elastic force effect and therefore will be pushed towards the centerline of the channel. Additionally, we expect to see the bigger particles focused tightly in less space in terms of length than the smaller one[46] because of the magnitude of the driving force, which is also diameter dependent[43]; meanwhile, we do not expect to achieve a perfect and tight focus of the smaller beads at the center, rather we expect to see them distributed around the centerline.

Analyzing the dimensions of our channel, we anticipate to observe a flatter velocity distribution along the width as the width itself of the channel increases[41,74]; so, we do expect to see how the different width of the streamlines increases going from the 50µm x 30µm channel to the 75µm x 30µm.

When the dimensionless numbers are taken into consideration, we must divide the expected behavior based on the flow rates contemplated: observing table 4, we anticipate that all the microbeads will be mainly focused near the centerline of the channel due to the synergic action of the elastic force and the wall-induced lift force for flow rates lower than 7µL/min for the 50µm x 30µm channel, and lower than 10µL/min for the 75µm x 30µm channel, as predicted by the studied literature[38]; and, the microbeads would more easily be focused between the channel centerline and the walls for flow rates higher than about 15µL/min in both channels. Besides, it was demonstrated that increasing the Re number particles generally move closer to walls due to inertial effects[46]. The elasticity number remains constant for every flow rate in the same channel but is quite different between the two channels: for the 50µm x 30µm channel El = 16.7 while for the 75µm x 30µm channel El = 9.7; this means that the smaller one would have a higher elastic effect acting on the particles and the focusing of them at the centerline would be tighter while for the bigger one we do expect to still obtain the separation of the particles by size because we still are in the elastic-inertial regime, but we do expect to see the particles less tightly focused and more randomly distributed at the center of the channel; please note that this would not be necessary a disadvantage, indeed in the previous research of Barilla L.[75], even though the focusing efficiency was fewer precise in the bigger channel, it turned out to have a better purity and efficiency of separation of particles because of the more space available for the specific retrieval of a single type of beads.

Finally, the comment on the blockage ratio values will confirm the previous speculations about the equilibrium positions of the particles: as we can observe from table 5, the 4µm particles have a $\beta = 0.14$ which matches the centerline equilibrium position of the literature, while the 7µm beads have a $\beta = 0.24$ which is still lower than the threshold values of 0.25 for the side focusing positions; this will probably mean that they will tend to focus at the channel centerline but, with the increase of the width of the channel, it is probable to find two different streamlines between the channel center and the side walls;

finally, the 15μm spheres have a $\beta = 0.51$ meaning that will surely and strongly tend to focus near the channel's walls.

The pressure drops values reported in table 6 were calculated to confirm the lack of any hazardous bursting point for our channels; indeed, all the values calculated for both channels and all the flow rates had a value not higher than 200 psi.

4.2 Microbeads Experiments

4.2.1 Particles inside 50 μm x 30 μm channel

From the conducted experiments we were able to validate some of the expected behaviors. Specifically, the 4μm particles in the 50μm x 30μm channel focused on the exact center of the device for every flow rate tested, from 5μL/min to 50μL/min. This was easily anticipated by both the blockage ratio value (about 0.14) and by the direct proportionality of the forces acting on the beads with the particles' diameter. The focusing efficiency values were almost perfect for flow rates between 15μL/min and 25μL/min and decreased with the increase of the flow rate, as predicted. Indeed, with the increasing flow rate, the inertial effect becomes dominant, and thus, the particles become more dispersed at the center of the channel. The 7μm beads showed a single focusing position at the center of the channel for all the flow rates too. However, this time the establishment of one single streamline was not so sure; the blockage ratio was 0.244 and the threshold for the change of focusing position has been established at 0.25[81] so I was not expecting such high focusing efficiency values, but I rather supposed to face a more uncertain behavior, as it happened with the previous research work done at the University of Illinois of Chicago, where at 5μL/min two different streamlines between the channel center and the side walls could be detected, while for all the other flow rates only one focusing position at the center was present. It has to be noticed, though, that the blockage ratio in that channel (50μm x 25μm) was higher, about 0.29. So, with our experiments, it is possible to say that by increasing of just 5μm the height of the channel, the center focusing behavior could be established and that 7μm beads have similar behavior with the 4μm particles. The blockage ratio threshold could be then considered valid, and the adjustment zone could be found for values higher than 0.25 but not lower. Lastly, the 15μm microbeads behaved

by the book: two different streamlines near the side walls could be detected for flow rates lower than 40μL/min and the focusing efficiency was almost perfect for every case tested. Only at 50μL/min, three different equilibrium position could be identified but, once again, this happens accordingly with the increasing of the inertial effect, in which we do expect to find five different equilibrium position that, from the bottom view, appears as one streamline at the exact center of the channel and other four superimposed streamlines near the sidewalls.

4.2.2 Particles inside 75 μm x 30 μm channel

All the particles were tested also in the 75μm x 30μm channel to understand if the wider channel would have allowed us a better separation between them. Before evaluating the sorting ability, the behavior of the single beads was studied: the smaller particles, as predicted, were less tightly focused a the center of the channel because of the dimensionless numbers, and in particular, the elasticity number, were lower than the ones in the 50μm x 30μm channel; indeed, the El in the AR = 2.5 channel is about 9.7 while it is about 16.7 in the AR = 1.67 channel; this means that the elastic force acting on the smaller particles is weaker and the small beads are rather dispersed along the center than focused in only one single streamline. Specifically, the images reported in paragraph 3.2.2 shows clearly how the 4μm beads have multiples streamlines gathered at the center of the channel; this affected the focusing efficiency values that were calculated, making them fluctuate between 60% and 90% but this could still provide the ground for the particles sorting since all of them are found in 30μm on the channel center. The 7μm beads have similar behavior, they can be found in the central 30-40μm and can form multiple streamlines. This time, the focusing efficiency is a bit improved, between 70% and 100%, due to the bigger size of the particles that affect positively the action of the different forces involved; in particular, since all the forces are directly proportional to the particles' size, the bigger are the particles, the higher is the magnitude of the forces and thus, the better is the focusing. This can be proved by looking at the behavior of the 15μm beads: they usually form two streamlines near the channel walls and three streamlines as the flow rate increases but their focusing efficiency values are between 75% and 100%, with the majority of the values around 90%.

4.2.3 Comparisons between particles behaviors

Since the main aims of this thesis project are about cell sorting, the different behavior of the different particles inside the same channel must be compared to find the best conditions that should be tested with the biological samples.

In the 50µm x 30µm channel, the separation between 15µm particles and the 4µm and 7µm bead is possible: as reported in the graphs in the paragraph 3.2.3, from 5µL/min to 30µL/min, with the only exception of 10µ/min, all the 15µm beads can be found near the sidewalls while all the 4µm and 7µm beads can be seen at the center of the channel. This makes us believe that at the expansion the difference between their equilibrium position would be enhanced and the collection of pure samples of different particles could be possible; specifically, 5µL/min, 15µL/min, and 20µL/min are the flow rates that we will confidently test with the biological samples because the space between the different streamlines is wider and thus, it could be possible to collect the 15µm beads from the side outlets and the 4µm and 7µm beads from the central one. An issue with these results is the lack of possibility of sorting the 4µm particles from the 7µm ones. This because both of them have a single equilibrium position at the center for each flow rate tested in the 50µm x 30µm channel.

For this reason, the 75µm x 30µm channel was also investigated; from the intensity value graphs in figure 26, it is possible to observe how the superimposition of the multiples streamlines of the different particles is a bit more complicated to interpret. At flow rates lower than 5µL/min sorting of any kind is not possible due to the lack of focusing of the smaller beads; from 10µL/min to 20µL/min, instead, the three-way separation seems possible: the 15µm particles streamlines are found near the sidewalls, the focusing positions of the 7µm beads are between the channel center and the side walls while the 4µm spheres can be seen distributed in the central area of the channel. Thus, the precise tuning of the fluid resistance and the finding of the optimal sorting cutoff could lead to a high purity and efficiency separation. From 25µL/min up, the purity and the efficiency of the separation could not be guaranteed because of the presence of a third equilibrium position of both 15µm and 7µm beads at the center of the

channel, like one of the smaller particles. For this reason, high flow rates would not be tested with the biological sample mixture.

4.2.4 Comparisons between the behaviors in different AR channels

A little comment about the reasons of the different behavior of the different particles inside the different AR channels is worth: as we can observe from figure 27, no matter the size of the particles, from the 50μm x 30μm to the 75μm x 30μm channel the number of the streamlines increases, as long as the width of each streamline, making the focusing efficiency less precise. Furthermore, the space between the double streamlines, when present, increased too. All these performances can be explained by the difference in the dimensionless number and by an increase in the width of the channel. As said before, not only the El number is smaller, but also the Re and Wi numbers have lower values in the wider channel, implying lower viscous contribution in the channel and thus, the less precise distribution of the particles inside the channel; the lower focusing efficiency can also be due to the flatter velocity distribution and to the increased inertial effect that causes a less tight focusing and a more random distribution along a certain area of the channel. But the larger space between the equilibrium positions could be an advantage and allow, as said before, a three-way separation and a further increase of separation if the optimal parameters of cutoff are chosen at the outlets.

4.2.5 Comparisons between different outlets configurations

Since it was demonstrated that in both channels some flow rates offered a good outcome for the particle separation, only the tuning of the resistance for the optimal cutoff had to be investigated. Indeed, given the fact that different equilibrium positions could be achieved for the different particles, those differences must be enhanced in the right way to collect only the wanted particles in the outlet desired. To do so, we exploited the open-outlets design, and we tested the mixture of 4μm and 15μm beads in three of the nine different configurations possible with our layout. Unfortunately, the other six configurations, in which also the distance of the punched central outlet was varying, were not tested due to the lack of time. Nevertheless, the three different configurations tested allowed us to disregard one of them and also to not consider suitable some of the channels and/or flow rates in each

configuration and thus giving us an idea of which optimal parameters should be further investigated with the biological samples.

The figures in paragraph 3.2.5 enable us to determine which setup could allow us the best purity and efficiency separation possible: the 50µm x 30µm channel at 10µL/min and 15µL/min in the configuration #1, and the 75µm x 30µm channel at 10µL/min in the configuration #1 and #2; indeed, we can clearly see only the 15µm particles (green) in the side outlets and the 4µm particles (blue) in the central one. Since for our final clinical application the final aim is to obtain a perfectly pure sample of spermatozoa to further process with the IVF procedure, even the loss of some of the sperm cells in the side outlets could be a good outcome anyway. Indeed, looking at the cells' concentration needed in these procedures, even a few spermatozoa but without contamination could be a great improvement of the gold standards nowadays used. Hereby we decided to take into consideration even the setups that would allow us an efficient separation of the other cells (big beads) from the spermatozoa (smaller beads), even if some of this latter could be lost in the side outlets. This seems possible only for the 75µm x 30µm channel from 15µL/min to 50µL/min in the configuration #1, and from 15µL/min to 25µL/min in configuration #2. But the results obtained from 30µL/min to 50µL/min in configuration #2 could be inaccurate due to the presence of particles clots at the beginning of the expansion on the right side and exactly on the bifurcation of the outlets; indeed, as we can observe from the images, those clots deviate a bit the natural trajectory of the particles and thus could change the real behavior of the beads inside our channel. For this reason, we think that could be of help testing these flow rates in this configuration anyway because they could turn out to be suitable for achieving the separation as well.

Ultimately, it is necessary to say that the last configuration, #3, must be disregarded in both channels and for every flow rate; in the 50µm x 30µm the focusing of the 4µm is better than in the other configurations since they are perfectly focused on the exact center and can be all collected in the central outlet, but the big issue is that the same thing could happen for the 15µm particles. These can be collected at the center as well, mining the purity of the central sample. Of course, this could be the optimal configuration if the retrieving was reversed and so the blood cells had to be recovered but unfortunately is not suitable for our final application. In the 75µm x 30µm channel a strange

phenomenon is visible: from 10μL/min to 25μL/min the particles are more attracted, without distinction in size, by the left side outlet; in particular, the 4μm beads could be collected only on the center and left side outlets at 10μ/min and 15μL/min, then from 20μL/min to 25μL/min all of them are only collected in the left side outlet; to let this happen, their initial focusing at the center is bent and a huge withdraw is visible, while the 15μm particles could be found in every outlet. For this reason, I decided to change the device in case a defect of fabrication was present and the unsymmetric withdrawal was caused by some imperfection of the setting. However, despite the change made, from 30μL/min to 50μL/min an analogous situation was observable, and the same thing happened with the right-side outlets: 4μm beads could be collected on the center and the right-side outlets while 15μm particles were collected in all three outlets. Considering the exclusion of design and setup issues, the leading conclusion was that the fluid resistance created with this particular configuration caused the unsymmetric attraction and withdrawal of the different particles, making it unsuitable for the corpuscles sorting that we aim to realize.

4.3 Biological Experiments

4.3.1 Experiments with Centrifuged Sperm Cells

The experiments with the spermatozoa showed us how their particular shape differs them from the microbeads and, thus, makes their behavior much more unpredictable. Indeed, their elongated head does not behave as a 4μm beads and the presence of the long tail could affect the movement inside the channel. To our knowledge there are no studies available about the real behavior of sperm cells inside a microchannel and how their particular shape allows them to move in their specific way in a pre-fixed flux; but with our experiments, we understood that they tend to follow the flux imposed by our syringe pump and, mainly, swim forwards or backward inside the channel. We used the word “swim” because, by observing the images taken for the erythrocytes (figure 35 and 36) and the ones taken for the spermatozoa (figures from 31 to 34), an increase in the cells’ blurring can be seen; since the setup was identical for all the experiments, the only plausible explanation for this increase of velocity is the fact

that the motile spermatozoa are moving along the fluid. Arguably the difference in the predicted behavior lies not only in the different shape but also in their viability and ability to move independently.

Overall, the spermatozoa can be found in the central area of the channel and their different focusing could tell us that they do not lie on the same plane but are distributed evenly along with the height of the channel. The zone occupied by them varies based on the channel width, but the relative percentage is always between 40% and 60% of the whole width of the channel. Even though this is not a tight focusing as it happens with the PS microbeads, it is still a promising result since it can signify having the major collection of this type of cells in the central outlet. The images acquired at the expansion (Figures 31 and 32) confirmed our assumptions. An alleged drawback is that some of the spermatozoa can be lost and collected also in the side outlet, diminishing the overall number of cells gathered for the future application but later I will be demonstrated how this is not a problem for our final application, but it can also become an advantage!

4.3.2 Experiments with Non-Treated Seminal Fluid

The experiments performed with the simply dilute seminal fluid were performed to demonstrate that our channel is able to operate even with the plain sample taken from the patients without requiring complicated steps and/or procedure before introducing it into our device, as it is instead required for all the gold standards methods nowadays used and enumerated in the introduction chapter. These trials turned out to be even better than the centrifuged samples: the width of the equilibrium zones was lower in both different AR channels. In particular, the values remained between 24µm and 27µm for the 50µm x 30µm channel, and between 31µm and 38µm for the 75µm x 30µm channel; this is 3-4µm lower than the results obtained with centrifuged sperm in the AR = 1.67 channel and 8µm lower for the AR = 2.5. Additionally, the other cell presence did not affect the final separation procedure or did not change the focusing tendency of the simple sperm cells. Besides, the few round cells present in the solution could be efficiently separated by the spermatozoa. The only other observations that must be taken into account are the fact that, as happened before, some of the spermatozoa were lost in the side outlets, even though the majority of them could be collected in the central one, and the fact that the smaller cellular debris,

such as epithelium remains, could be seen and collected in the central outlet. But this should not be considered a problem since those are demonstrated to not negatively affect the fertilization potential of the spermatozoa and they are, indeed, not even considered as harmful presence in the seminal fluid.

4.3.3 Experiments with Erythrocytes

The experiments with the erythrocytes gave us the expected results; indeed, their discoid shape is not that different from the spherical one of the PS particles used to predict their behavior. Additionally, the RBCs do not have an intrinsic capacity for movement and thus can be focused just like the 7µm beads. In figure 35 and 36 firstly two streamlines and then a central focusing could be observed; in particular, the apparent streamlines, and the space by them occupied, increased with the increasing of the width of the channel. In the 50µm x 30µm channel the mean central area occupied was about 11µm while in the 75µm x 30µm channel it was 28µm. So, it was 22% in the AR = 1.67 channel and 37% for the AR = 2.5 channel. Due to their quite tight focusing in the middle of the channel, we do expect to collect the majority of them in the central outlet for the smaller channel and maybe in all the outlets for the bigger one.

4.3.4 Experiments with Mixture of Sperm Cells and 15µm Particles

As said in all the chapters above, unfortunately, we were not able to retrieve the leukocytes from the whole blood samples, and thus, we were obliged to use the 15µm particles instead. However, the shape of WBCs is almost perfectly spherical and their dimension has a mean diameter of 15µm[79], just like the PS microbeads that we used. For these reasons, we still hold valid all of our results and we are pretty confident that they will not be any different from the real biological cells. Besides, all the cited papers in the introduction chapter, specifically in the paragraph about other microfluidic devices for corpuscles separation, used the same escamotage to predict the behavior of leukocytes in their experiments. Another important piece of information to consider, before going through the analysis of the results, is that the separation was attempted by collecting the 15µm particles in the side outlets and the spermatozoa from the central one.

From figure 37, it is obvious that the only possible configuration for the separation of sperm cells and 15µm particles with perfect purity values of the spermatozoa retrieval is the #1 for the 50µm x 30µm channel. Indeed, from figure 38, the separation efficiency values and purity values of 100% for respectively the side outlets and central one was achieved with configuration #1 in all the flow rates tested. This means discarding all the results obtained with configuration #2. By looking at the quantitative values, an important parameter to check is the separation efficiency of the central outlet; this represents the percentage of spermatozoa retrieved in the central outlet with respect to the initial amount present in the solution. This value is therefore important to count the number of spermatozoa retrieved and do all the calculations necessary to understand if the number of cells retrieved is enough for further processes, such as IVF procedures. For this reason, we would like it to be the highest possible and by looking at figure 38 it is possible to say that the best conditions are obtained at 15µL/min, where 64.2% is the exact value of the separation efficiency for the central outlet. The values of the purity of the side outlets are not important if the final purpose of our project is considered: the purity of the 15µm, or better leukocytes, retrieved is does not matter because they would not be used in the further procedures, but the only important thing is to get rid of them, which our device is able to do.

By considering the experiments conducted in the 75µm x 30µm channel, both configurations gave us promising results; specifically, the optimal achievement was obtained, as shown in figure 40, for all the flow rates in configuration #1 and 10µL/min in the configuration #2. For the conditions just cited the separation efficiency values and purity values for the side outlets and central outlets respectively were 100%. To decide the best condition, the separation efficiency of the central outlet must be considered, and similar values were obtained at 20µL/min in configuration #1 and 10µL/min in configuration #2, with a 56.1% in the first case and 58.7% in the second one.

Since our final aim is to retrieved pure samples of spermatozoa to use them in IVF procedure, it is important to consider the number of sperm cells needed for the application and thus, to do some calculation to demonstrate the beneficial use of our device: the number of spermatozoa needed in IVF procedure is between 100 000 and 10 000 spermatozoa per oocyte[82,83]; since the initial concentration of our solution is 3 x 10^6 sperm cells/mL and our separation efficiency is between 56% and 64% in the

best cases this would mean being able to recover about 1.68-1.92 x 10^6 sperm cells/mL. Considering the highest values of 1 x 10^6 spermatozoa needed for the IVF, this means pushing through our device between 0.60 and 0.52mL of the initial sample; given that our best results could be reached within 10μL/min and 20μL/min, the right spermatozoa amount would be retrieved in less than 30 minutes! In the worst-case scenario, 35 minutes would be needed, which would still be a great improvement in gold-standards methods nowadays used, which requires more than 3 hours!

4.3.5 Experiments with Mixture of Sperm Cells and Erythrocytes

Differently from what was tried with the mixture of spermatozoa and 15μm particles, with the solution of sperm cells and erythrocytes the separation between them was attempted by collecting the RBCs in the central outlet and the spermatozoa from the side ones for the 50μm x 30μm channel. This change in the sorting setup was dictated by the fact that most of the erythrocytes were focused on the center of the channel and thus could only be eliminated from the sperm cells if were collected from the central outlet. In this case, the inability of the sperm cells to focus on the exact center of the channel turned out to be essential for the successful outcome of our sorting!

Specifically, for configuration #1 the separation efficiency values, and the purity values of the central and side outlets respectively were 100%; the same thing happened between 15μL/min and 30μL/min in configuration #2. As before, what allows us to choose the best conditions possible is the value of the separation efficiency of the side outlets; those values represent the percentage of pure spermatozoa that can be retrieved from the initial sample. The highest value is obtained at 20μL/min in configuration #1 with a percentage of 72.4%; another similarly high value can be reached at 30μL/min in configuration #2, with 70.1%.

In the 75μm x 30μm channel the situation very different: the erythrocytes, no matter the configuration, can always be found in all the three outlets, making their separation from spermatozoa almost impossible. This is also demonstrated in figure 44 where the separation efficiency and purity values are reported; the maximum values for the efficiency of the RBCs retrieval are 95% at 15μL/min while the purity of sperm cells reaches the value of 93.8% at 20μL/min, in both cases in configuration #2.

Configuration #1 is not working well and we could observe it by looking at the values in figure 44: all the percentages calculated do not overcome 80%. Hence, the 75µm x 30µm channel must be discarded as a sorting option for erythrocytes and spermatozoa.

Since our final aim is always to retrieved pure samples of spermatozoa to use in IVF procedure, it is important to consider the number of sperm cells needed for the application and thus, to do the same calculation as before to demonstrate the beneficial use of our device: the number of spermatozoa needed in IVF procedure is always between 100 000 and 10 000 spermatozoa per oocyte[82,83] and we consider the highest value as the threshold since it could allow more chances for the fertilization. The initial concentration of our solution is always 3×10^6 sperm cells/mL, and our separation efficiency is between 70% and 72% in the best cases this would mean being able to recover about $2.10\text{-}2.17 \times 10^6$ sperm cells/mL. Considering the highest values of 1×10^6 spermatozoa needed for the IVF, this means pushing through our device between 0.48 and 0.46mL of the initial sample; given that our best results could be reached within 20µL/min and 30µL/min, the right amount of spermatozoa would be retrieved between 23 and 16 minutes, which is even faster than the retrieval of sperm from leukocytes! This still remains a superlative improvement in respect to the gold-standards methods used, which, as a reminder, requires more than 3 hours!

CHAPTER 5

CONCLUSIONS

5.1 Summary

The main purpose of this thesis project is the creation of a passive microfluidic device made of a straight channel with a rectangular cross-section that is able to perform the separation between spermatozoa and the other cells, such as leukocytes and erythrocytes, that can be found in the semen of pathologic patients. Specifically, we wanted to achieve the retrieval of a pure sperm cells sample to use for further in vitro fertilization procedures, to allow fatherhood even to men that has a pathology that, in the past, precluded the possibility of having babies.

This main purpose can be divided into three sub-aims; the first one was to find the optimal conditions needed to achieve the microbeads sorting. Indeed, the particles could be used to get a general idea of the flow rates, channel dimensions, and specific configurations to employ. To do so we started by testing the single type of particles in our channel. The microbeads chosen were 4μm, 7μm, and 15μm because we needed to mimic the spermatozoa, the erythrocytes, and the leukocytes, respectively. With the experiments, we understood that the smaller particles, 4μm, and 7μm beads, could be collected at the center of the channel while the bigger ones, 15μm, could be retrieved from the side outlets since they formed two different streamlines near the side walls. We tested different flow rates from 5μl/min till 50μL/min; by evaluating the focusing efficiency values we establish that the best results could be achieved within 30μL/min while for higher flow rates a decrease in the focusing and a particles dispersion could be observed. When the different AR channels' performances were compared, an increase in the number of streamlines and space occupied by the cells was noticed. Nevertheless, the

results were still both valid and promising; indeed, the main thing that count is the sorting potential, not the sharpness of focusing. The best results for the 50µm x 30µm channel were: for the 4µm beads between 15µL/min and 25µL/min, reaching a focusing efficiency always higher than 95%; the very same outcome was reached for the 7µm beads from 10µL/min till 30µL/min; finally, for the 15µm particles, 100% of focusing efficiency was obtained for two different streamlines for 5, 15-30µL/min. In the 75µm x 30µm channel the 4µm beads reached a central focusing with an efficiency of above 70% between 10µL/min and 20µL/min, and in particular, in this latter flow rate, the value reached was 90%. The 7µm particles were always focused in two of four streamlines near the center of the channel and from 5µL/min to 25µL/min the focusing efficiency was always higher than 93%, at 20µL/min it went down to 80%. In the end, the 15µm beads were able to focus perfectly in two different streamlines near the sidewalls from 5µL/min till 25µL/min with a focusing efficiency always higher than 85% and reaching, in some cases, 100%. Afterward, experiments with a mixture of 4µm and 15µm beads were performed. This time not only both the AR channels were tested but also different configurations were examined: configuration #1 with the central outlet at 1.5cm and the side ones at 0.5cm, configuration #2 with the central outlet at 1.5cm, and the side ones at 1cm, lastly, configuration #3 with the central outlet at 1.5cm and the side ones at 1.5cm too. From these tests, we discovered that the third configuration was not suitable for our application since it allowed the recovery of the 15µm beads in all three outlets and thus, it was discarded. On the other hand, configurations #1 and #2 turned out to be the right choice to obtain a feasible sorting. Specifically, configuration #1 had great outcomes for flow rates between 10µL/min and 25µL/min for the AR = 1.67 channel and all the flow rates in the AR = 2.5 channel. Configuration #2 allow us to achieve a good separation between the particles from 30µL/min to 50µL/min for the 50µm x 30µm channel and between 10µL/min and 40µL/min in the 75µm x 30µm channel. Those results were just qualitative.

The second sub-aim was to achieve the separation between the spermatozoa and the leucocytes but to do so, we had to first test one type of cells at the time in our device to check if the predicted behavior could be accomplished. For this reason, we tested firstly the spermatozoa alone, then the diluted seminal fluid, and finally the erythrocytes. As one can notice, no leukocytes were tested; this happened because

of the lack of capability and maybe expertise in retrieving the WBCs from whole blood samples that were provided. But, given the fact that those cells are perfectly round, very regular in dimension, and have a mean diameter of 15μm beads, we considered this latter as substitutes of the real white blood cells. The spermatozoa could be focused in a central area of about 28μm in the AR = 1.67 channel and of about 43μm in the AR = 2.5 channel. The location of sperm cells became tighter when diluted semen was used; in particular, the area occupied by the cells was 3μm smaller for the 50μm x 30μm channel and 8μm smaller for the 75μm x 30μm channel. It must be noticed that, due to the very different shape from the 4μm beads, a perfect focusing was not reachable but still the outcome was worth it. Moreover, the fact that some of the spermatozoa could be lost in the side outlets will turn out to be essential for the coming sorting step. Without spoiling anything yet, the RBCs behaved exactly as predicted by the 7μm beads: they focused in a central area of the channel and were even able to form two different streamlines in some cases. Overall, the focusing zone became smaller with the increasing of the flow rate and the mean values attained were 12μm for the AR = 1.67 channel and 29 μm for the AR = 2.5 channel. To accomplish the second sub-aim, a mixture of spermatozoa and 15μm particles was tested in both the AR channel and in configurations #1 and #2. In general, a successful outcome was achieved for all the condition tested but only the main accomplishment will be reported: the best conditions were at 15μL/min, with configuration #1 in the 50μm x 30μm channel and at 20μL/min, always in configuration #1 in the 75μm x 30μm channel. In both cases the separation efficiency for the 15μm beads and the purity of the spermatozoa sample was 100%; the only thing that changed was the separation efficiency for the spermatozoa, which means the number of spermatozoa retrieved with respect to the total number of sperm in the initial sample, that was 64% for the first case and 56% for the second one. Both of these conditions allow the acquisition of 1×10^6 sperm cells/mL from the initial sample within 30 minutes. This exact value of cells considered is the exact number of spermatozoa required in the IVF procedure to achieve successful fertilization of one oocyte. Thus, we can claim to have completed the second sub-aim with an outstanding result if compare to the performances of the gold-standards procedures for the spermatozoa retrieval, which requires several steps, the addition of enzymes or solvents, and at least a couple of hours of work.

The last sub-aim has the goal to separate the spermatozoa from other cells that could be found in the seminal fluid of pathologic patients or biopsy samples, such as erythrocytes. For this reason, a mixture of spermatozoa and RBCs was also tested in both our channels and in both valid configurations. In the beginning, we did not expect to achieve this separation because both sperm and red blood cells focused on the central area of the channel. But, luckily, what we considered to be a disadvantage at first, turned out to be the only option for separation. Indeed, as said before, while the erythrocytes were tightly focused on the center of the channel and could even form streamlines, the spermatozoa were more randomly distributed in a central area and some of them would escape the central outlet and be collected by the side ones. When the separation between these types of cells is attempted, the fact that some spermatozoa finish in the side outlets could allow us to retrieve them pure and without the presence of the other cells. The best conditions found were only in the 50µm x 30µm channel; in configuration #1 at 20µL/min the separation efficiency of RBCs and the purity of the spermatozoa collected were 100% and the separation efficiency of the spermatozoa, thus the number of spermatozoa retrieved from the initial values, was 72%. Analogously happened in configuration #2 at 30µL/min; the only difference is the separation efficiency for the spermatozoa that reached 70%. The 75µm x 30µm channel was discarded because the presence of two streamlines of RBCs caused their collection in all the three outlets and thus made the separation impossible to be achieved. However, the results obtained with the AR = 1.67 channel were higher performing than the ones obtained for the leukocytes separation: when the previously described calculations about the number of spermatozoa retrieved and the number needed for the IVF procedure, the required amount could be sorted and collected by less than 0.5mL of the initial sample and between 23 and 16 minutes!

5.2 Future Developments

Undoubtedly, in every research worth this name, the greater the final goal is, the more improvements can be found and, I must add, the more experiments are done, the more problems pop up. Therefore, future developments are always needed. Hereafter are reported the main issues encountered in our research project along with some improvements proposals.

First of all, the adherence of both particles and cells to the bottom wall of the channel occurred. The plausible explanation for this phenomenon is probably the fact that the plasma bonding does make the bottom wall of the channel sticky and thus, since it does not come in contact with anything after the device assembly, it can keep attached all the corpuscles that pass right onto it. This occurrence could become a problem not because of the bad image acquisition but mostly because it can cause clogs in the channel that could deviate the original trajectories of the corpuscles, creating bias in the results or reducing the efficiency of these. Likewise, clotting problems could also happen at the beginning, at the end, or even at the expansion. Indeed, even though the design of the channel was carefully studied to avoid these situations, it did not prevent completely this phenomenon. At the expansion, the smoother edges do allow a better slide of aggregates, if compared to the previous work done at the University of Illinois at Chicago, but the formation still happens due to the creation of floating clogs in the fluid. These can form at the inlet of the channel where, after few hours of usage, the accumulation of stacks of cells between pillars causes the formation of clusters. One possible solution could be the coating of the internal channel with a hydrophobic solution before the usage and maybe the addition of antiaggregants or surfactants in the solutions used.

Secondly, of course, the next step is necessary to test real leukocytes for the experiments to validate the performances obtained with our experiments. But most importantly, the usage of real pathologic samples or biopsies could really demonstrate the outstanding performances of our device for the spermatozoa retrieval and establish once and for all the use of microfluidics as a convenient alternative to the gold-standards methods used.

Among the other things that have to be investigated, the testing of the remaining configurations could be a start. Indeed, as explained before in the Materials and Methods chapter, only three of the nine possible configurations were tested. We chose to change the distance of the side outlets and keep constant the punched central outlet, but this could be changed too and maybe could allow the achievement of even better results in terms of separation efficiency and purity.

One disadvantage that was found in the previous research work done in the Papautsky Lab in Chicago and that was still present in this research project is the fact that in shear-thinning fluids, at high flow rates, the viscosity decreases, and the shear-gradient lift is enhanced, thus causing a defocusing of particles at such flow rates. To compensate for this effect, higher viscosity could be achieved by using a longer relaxation time (λ) as a rheological property of the fluid. In particular, longer λ can be obtained by using a higher molecular weight (M_w) or by increasing the polymer concentration[38]. Regardless, the maximum flow rate that allowed us to obtain efficient results was 30μL/min, which is not that high if compared to other flow rate achievements with other viscoelastic fluids. Indeed, the PEO has shown to work at 1-2 orders of magnitude slower flow speed than their inertial counterparts in similar channels and dimensions[38]; nevertheless, viscoelasticity remains the optimal choice for improving the throughput by balancing with the elasticity the shear-gradient lift that tends to drives the particles away from the centerline. A possible resolution would be trying to explore and change the type of polymer used as a viscoelastic fluid, maybe the λ-DNA solution, that would also be compatible with our supernatant fluid in which spermatozoa are naturally found or studying deeper the rheological parameters of this natural fluid and trying to enhance some of its useful characteristics.

Last but not least, we could not test the RBCs and WBCs together due to their different behavior and to the different setups for efficient sorting, which was the opposite for one another. A possible solution to achieve a three-way cells separation could be going back to use channels with a height of 25μm; this height allowed the formation of two different streamlines farther away from each other for the RBCs than the ones obtained in our current device; that happened because of the different blockage ratio value, which was > 0.25 and, thus, allowed the focusing of those cells more near the side walls. Besides, by our predictions, also the 15μm particles could behave like in our current device and form two different streamlines near the channels' walls, hopefully without forming a third one in the middle of the channel.

BUT, it must be considered that in all the pathological situations described in the Introduction chapter, in no case there was the simultaneous presence of more than an unwanted type of cells. In the leukocytospermia only the WBCs are present along with the spermatozoa, in the hematospermic patients there are only RBCs as intruders of semen, and lastly, in the biopsies of azoospermic patients,

a similar situation to the hematospermic ones happens. In addition, a lower count of spermatozoa is present but still, those cells are more than enough to be used in our device. Indeed, we must dilute a lot our physiological sample to obtain a final concentration of 3×10^6 cells/mL; the use of an azoospermic sample would only require less dilution. For all these reasons our device is still able to provide a feasible and outstanding solution for the spermatozoa sorting from all the different cell types and it may become a valid alternative to the current standards methods.

CITED LITERATURE

1. Cao, X. W., Lin, K., Li, C. Y. & Yuan, C. W. A review of WHO Laboratory Manual for the Examination and Processing of Human Semen (5th edition). *Zhonghua Nan Ke Xue* **17**, 1059–1063 (2011).

2. Jung, J. H. *et al.* Treatment of Leukocytospermia in Male Infertility: A Systematic Review. *World J. Mens. Health* **34**, 165 (2016).

3. Fariello, R. M. *et al.* Effect of leukocytospermia and processing by discontinuous density gradient on sperm nuclear DNA fragmentation and mitochondrial activity. *J. Assist. Reprod. Genet.* **26**, 151–157 (2009).

4. Soygur, B., Celik, S., Celik-Ozenci, C. & Sati, L. Effect of erythrocyte-sperm separation medium on nuclear, acrosomal, and membrane maturity parameters in human sperm. *J. Assist. Reprod. Genet.* **35**, 491–501 (2018).

5. Fathalla, M. F. Reproductive health: a global overview. *Early Hum. Dev.* **29**, 35–42 (1992).

6. Inhorn, M. C. & Patrizio, P. Infertility around the globe: New thinking on gender, reproductive technologies and global movements in the 21st century. *Hum. Reprod. Update* **21**, 411–426 (2014).

7. Ombelet, W., Cooke, I., Dyer, S., Serour, G. & Devroey, P. Infertility and the provision of infertility medical services in developing countries. *Hum. Reprod. Update* **14**, 605–621 (2008).

8. Lotti, F. & Maggi, M. Ultrasound of the male genital tract in relation to male reproductive health. *Hum. Reprod. Update* **21**, 56–83 (2015).

9. Khodamoradi, K. *et al.* Laboratory and clinical management of leukocytospermia and hematospermia: a review. *Ther. Adv. Reprod. Heal.* **14**, 263349412092251 (2020).

10. Ricci, G., Presani, G., Guaschino, S., Simeone, R. & Perticarari, S. Leukocyte detection in human semen using flow cytometry. *Hum. Reprod.* **15**, 1329–1337 (2000).

11. Sandoval, J. S., Raburn, D. & Muasher, S. Leukocytospermia: Overview of diagnosis, implications, and management of a controversial finding. *Middle East Fertil. Soc. J.* **18**, 129–134 (2013).

12. Lackner, J. E., Agarwal, A., Mahfouz, R., du Plessis, S. S. & Schatzl, G. The association between leukocytes and sperm quality is concentration dependent. *Reprod. Biol. Endocrinol.* **8**, 4–9 (2010).

13. Rodin, D. M., Larone, D. & Goldstein, M. Relationship between semen cultures, leukospermia, and semen analysis in men undergoing fertility evaluation. *Fertil. Steril.* **79**, 1555–1558 (2003).

14. De Bellabarba, G. A. *et al.* Nonsperm cells in human semen and their relationship with semen parameters. *Arch. Androl.* **45**, 131–136 (2000).

15. Whittington, K. & Ford, W. C. L. Relative contribution of leukocytes and of spermatozoa so reactive oxygen species production in human sperm suspensions. *Int. J. Androl.* **22**, 229–235 (1999).

16. Wolff, H. The biologic significance of white blood cells in semen. *Fertil. Steril.* **63**, 1143–1157 (1995).

17. Henkel, R. Sperm preparation: State-of-the-artphysiological aspects and application of advanced sperm preparation methods. *Asian J. Androl.* **14**, 260–269 (2012).

18. Cocuzza, M., Alvarenga, C. & Pagani, R. The epidemiology and etiology of azoospermia. *Clinics* **68**, 15–26 (2013).

19. Schlegel, P. N. Causes of azoospermia and their management. *Reprod. Fertil. Dev.* **16**, 561–572 (2004).

20. Jarvi, K. *et al.* CUA guideline: The workup and management of azoospermic males. *J. Can. Urol. Assoc.* **9**, 229–235 (2015).

21. Wosnitzer, M., Goldstein, M. & Hardy, M. P. Review of Azoospermia. *Spermatogenesis* **4**, e28218 (2014).

22. Oates, R. Evaluation of the azoospermic male. *Asian J. Androl.* **14**, 82–87 (2012).

23. Foresta, C., Ferlin, A., Bettella, A., Rossato, M. & Varotto, A. Diagnostic and clinical features in azoospermia. *Clin. Endocrinol. (Oxf).* **43**, 537–543 (1995).

24. Tüttelmann, F. *et al.* Clinical experience with azoospermia: Aetiology and chances for spermatozoa detection upon biopsy. *Int. J. Androl.* **34**, 291–298 (2011).

25. Gudeloglu, A. & Parekattil, S. J. Update in the evaluation of the azoospermic male. *Clinics* **68**, 27–34 (2013).

26. Popal, W. & Nagy, Z. P. Laboratory processing and intracytoplasmic sperm injection using epididymal and testicular spermatozoa: What can be done to improve outcomes? *Clinics* **68**, 125–130 (2013).

27. Berendsen, J. T. W., Eijkel, J. C. T., Wetzels, A. M. & Segerink, L. I. Separation of spermatozoa from erythrocytes using their tumbling mechanism in a pinch flow fractionation device. *Microsystems Nanoeng.* **5**, (2019).

28. Su, L. M. *et al.* Testicular sperm extraction with intracytoplasmic sperm injection for nonobstructive azoospermia: Testicular histology can predict success of sperm retrieval. *J. Urol.* **161**, 112–116 (1999).

29. Mathers, M. J., Degener, S., Sperling, H. & Roth, S. Hematospermia-a symptom with many possible causes. *Dtsch. Arztebl. Int.* **114**, 186–191 (2017).

30. Akhter, W., Khan, F. & Chinegwundoh, F. Should every patient with hematospermia be investigated? A critical review. *Cent. Eur. J. Urol.* **66**, 79–82 (2013).

31. Whitesides, G. M. The origins and the future of microfluidics. *Nature* **442**, (2006).

32. Samuel, R. *et al.* Microfluidic-based sperm sorting & analysis for treatment of male infertility. *Transl. Androl. Urol.* **7**, S336–S347 (2018).

33. Nguyen, N.-T., Wereley, S. T. & House, A. *Fundamentals and Applications of Microfluidics - Second Edition*. (2002).

34. Patrick Tabeling. *Introduction to Microfluidics*. (2007).

35. Fodor, S. P. A. *et al.* Light-Directed, Spatially Addressable Parallel Chemical Synthesis. 767–774 (1991).

36. Convery, N. & Gadegaard, N. 30 Years of Microfluidics. *Micro Nano Eng.* **2**, 76–91 (2019).

37. Ahn, S. W., Lee, S. S., Lee, S. J. & Kim, J. M. Microfluidic particle separator utilizing sheathless elasto-inertial focusing. *Chem. Eng. Sci.* **126**, 237–243 (2015).

38. Liu, C. *et al.* Size-Based Separation of Particles and Cells Utilizing Viscoelastic E ff ects in Straight Microchannels. *Anal. Chem.* (2015). doi:10.1021/acs.analchem.5b00516

39. Kim, B. & Kim, J. M. Elasto-inertial particle focusing under the viscoelastic flow of DNA solution in a square channel. *Biomicrofluidics* **10**, (2016).

40. Yuan, D. *et al.* Recent progress of particle migration in viscoelastic fluids. *Lab Chip* **18**, 551–567 (2018).

41. Yuan, D. *et al.* Sheathless separation of microalgae from bacteria using a simple straight channel based on viscoelastic microfluidics. *Lab Chip* **19**, (2019).

42. Li, D., Shao, X., Bostwick, J. B. & Xuan, X. Particle separation in xanthan gum solutions. *Microfluid. Nanofluidics* **23**, 1–11 (2019).

43. Fan, L. L. *et al.* Enhanced viscoelastic focusing of particle in microchannel. *Electrophoresis* 1–10 (2020). doi:10.1002/elps.201900397

44. Nam, J. *et al.* Microfluidic device for sheathless particle focusing and separation using a viscoelastic fluid. *J. Chromatogr. A* **1406**, 244–250 (2015).

45. Jian Zhou, Premkumar Vummidi Giridhar, S. K. and I. P. Modulation of aspect ratio for complete separation in an inertial microfluidic channel. *Lab Chip* 1919–1929 (2013). doi:10.1039/c3lc50101a

46. Zhou, J. & Papautsky, I. Fundamentals of inertial focusing in microchannels. *Lab Chip* 1121–1132 (2013). doi:10.1039/c2lc41248a

47. Go, T., Byeon, H. & Lee, S. J. Focusing and alignment of erythrocytes in a viscoelastic medium. *Sci. Rep.* **7**, 1–10 (2017).

48. Li, D., Lu, X. & Xuan, X. Viscoelastic separation of particles by size in straight rectangular microchannels: A parametric study for a refined understanding. *Anal. Chem.* **88**, 12303–12309 (2016).

49. Li Xiujun James and Zhou. *Microfluidic Devices for Biomedical Applications*. (woodhead publishing, 2013). doi:10.1533/9780857097040.4.445

50. Luz Yolanda Toro Suarez. *Micro- and Nanoscale fluid mechanics: transport in microfluidics devices*. (2015).

51. Qi, H. & Xu, M. Stokes' first problem for a viscoelastic fluid with the generalized Oldroyd-B model. *Acta Mech. Sin. Xuebao* **23**, 463–469 (2007).

52. Razavi Bazaz, S. *et al.* Computational inertial microfluidics: a review. *Lab Chip* **20**, 1023–1048 (2020).

53. Yang, S., Kim, Y., Lee, J., Lee, S. & Min, J. Sheathless elasto-inertial particle focusing and continuous separation in a straight rectangular microchannel. *Lab Chip* **1**, 266–273 (2011).

54. Yuan, D., Zhao, Q., Yan, S. & Yuan, D. Recent progress of particle migration in viscoelastic fluids. *Lab Chip* 551–567 (2018). doi:10.1039/c7lc01076a

55. Lim, H. *et al.* Sheathless high-throughput circulating tumor cell separation using viscoelastic non-Newtonian fluid. *Micromachines* **10**, (2019).

56. Nam, J., Lim, H., Kim, D., Jung, H. & Shin, S. Continuous separation of microparticles in a microfluidic channel via the elasto-inertial effect of non-Newtonian fluid. *Lab Chip* **12**, 1347–1354 (2012).

57. Dino Di Carlo. Inertial microfluidics Dino. *Lab Chip* 3038–3046 (2009). doi:10.1039/c2lc41248a

58. Ali Asgar S. Bhagat, S. S. K. Inertial microfluidics for continuous particle filtration and extraction. *Microfluid Nanofluid* 217–226 (2009). doi:10.1007/s10404-008-0377-2

59. Asmolov, E. S. The inertial lift on a spherical particle in a plane poiseuille flow at large channel Reynolds number. *J. Fluid Mech.* **381**, 63–87 (1999).

60. Jeonghun Nam, Hyunjung Lim, Dookon Kim, H. J. and S. S. Continuous separation of microparticles in a microfluidic channel via the elasto-inertial effect of non-Newtonian fluid. *Lab Chip* 1347–1354 (2012). doi:10.1039/c2lc21304d

61. Qin, D., Xia, Y. & Whitesides, G. M. Soft lithography for micro- and nanoscale patterning. *Nat. Protoc.* **5**, 491–502 (2010).

62. Mukherjee, P., Nebuloni, F., Gao, H. & Zhou, J. Rapid Prototyping of Soft Lithography Masters for Microfluidic Devices Using Dry Film Photoresist in a Non-Cleanroom Setting. *Micromachines* (2019). doi:10.3390/mi10030192

63. Krogh, M. *My Little Guide to Soft Lithography*. (2003).

64. Son, J., Samuel, R., Gale, B. K., Carrell, D. T. & Hotaling, J. M. Separation of sperm cells from samples containing high concentrations of white blood cells using a spiral channel. *Biomicrofluidics* **11**, 1–11 (2017).

65. Son, J. *et al.* Non-motile sperm cell separation using a spiral channel. *Anal. Methods* **7**, 8041–8047 (2015).

66. Xiang, N. *et al.* Fundamentals of elasto-inertial particle focusing in curved microfluidic channels. *Lab Chip* **16**, 2626–2635 (2016).

67. Lee, D. J., Brenner, H., Youn, J. R. & Song, Y. S. Multiplex particle focusing via hydrodynamic force in Viscoelastic Fluids. *Sci. Rep.* **3**, 3–10 (2013).

68. Liu, C. *et al.* Sheathless focusing and separation of diverse nanoparticles in viscoelastic solutions with minimized shear thinning. *Anal. Chem.* **88**, 12547–12553 (2016).

69. Feng, H., Magda, J. J. & Gale, B. K. Viscoelastic second normal stress difference dominated multiple-stream particle focusing in microfluidic channels. *Appl. Phys. Lett.* **115**, (2019).

70. Xiang, N., Ni, Z. & Yi, H. Concentration-controlled particle focusing in spiral elasto-inertial microfluidic devices. *Electrophoresis* **39**, 417–424 (2018).

71. Nam, J., Jang, W. S. & Lim, C. S. Non-electrical powered continuous cell concentration for enumeration of residual white blood cells in WBC-depleted blood using a viscoelastic fluid. *Talanta* **197**, 12–19 (2019).

72. Nam, J., Jang, W. S., Hong, D. H. & Lim, C. S. Viscoelastic Separation and Concentration of Fungi from Blood for Highly Sensitive Molecular Diagnostics. *Sci. Rep.* **9**, 1–12 (2019).

73. Lim, E. J. *et al.* Inertio-elastic focusing of bioparticles in microchannels at high throughput. *Nat. Commun.* **5**, (2014).

74. Nam, J. *et al.* High-throughput malaria parasite separation using a viscoelastic fluid for ultrasensitive PCR detection. *Lab Chip* **16**, 2086–2092 (2016).

75. Barilla, L. Viscoelastic Focusing and Sorting of Particles and Asymmetric Cells in Straight Microfluidic Channels. (University of Illinois at Chicago, 2020). doi:https://doi.org/10.25417/uic.13476156.v1

76. Lu, X., Zhu, L., Hua, R. mao & Xuan, X. Continuous sheath-free separation of particles by shape in viscoelastic fluids. *Appl. Phys. Lett.* **107**, (2015).

77. Kuntaegowdanahalli, S. S., Bhagat, A. A. S., Kumar, G. & Papautsky, I. Inertial microfluidics for continuous particle separation in spiral microchannels. *Lab Chip* **9**, 2973–2980 (2009).

78. Diez-Silva, M., Dao, M., Han, J., Lim, C. T. & Suresh, S. Shape and biomechanics characteristics of human red blood cells in health and disease. *MRS Bull.* **35**, 382–388 (2010).

79. Putzu, L. & Ruberto, C. Di. White Blood Cells Identification and Classification from Leukemic Blood Image. *Proc. IWBBIO Int. Work …* **7**, 18–20 (2013).

80. Bellastella, G. *et al.* Dimensions of human ejaculated spermatozoa in Papanicolaou-stained seminal and swim-up smears obtained from the Integrated Semen Analysis System (ISAS®). *Asian J. Androl.* **12**, 871–879 (2010).

81. Seo, K. W., Byeon, H. J., Huh, H. K. & Lee, S. J. Particle migration and single-line particle focusing in microscale pipe flow of viscoelastic fluids. *RSC Adv.* **4**, 3512–3520 (2014).

82. Schlegel, P. N. & Girardi, S. K. In vitro fertilization for male factor infertility. *J. Clin. Endocrinol. Metab.* **82**, 709–716 (1997).

83. Kim, Y. Y. *et al.* Use of the total motile sperm count to predict pregnancy outcomes in in vitro fertilization. *Fertil. Steril.* **100**, S448 (2013).

APPENDIX

MatLab Codes:

```
clear all
close all
clc

w_1 = 50*10^-6; h_1 = 30*10^-6; %50x30
w_2 = 75*10^-6; h_2 = 30*10^-6; %75x30
L = 0.03;
mu_1000 = 2.3*10^-3; %1000ppm
lambda_1000 = 6.8*10^-3; %1000ppm

Q = [1.66667E-11 8.33333E-11 1.16667E-10 1.66667E-10 2.5E-10 3.33333E-10 4.16667E-
10 5E-10 5.83333E-10 6.66667E-10 7.5E-10 8.33333E-10 0.000000001 1.16667E-09
1.33333E-09 1.5E-09 1.66667E-09];

Dh_1 = 2*w_1*h_1/(w_1+h_1)
Dh_2 = 2*w_2*h_2/(w_2+h_2)

ap_4 = 4.19*10^-6;
ap_7 = 7.32*10^-6;
ap_15 = 15.25*10^-6;

W = 0.010; % x Bangs Lab
ro = 1.06; % x Bangs Lab

%% Reynolds

Re_1000_1 = 2*1000*Q/(mu_1000*(w_1+h_1))
Re_1000_2 = 2*1000*Q/(mu_1000*(w_2+h_2))

%% Weissenberg

Wi_1000_1 = 2*lambda_1000*Q/(w_1^2 * h_1)
Wi_1000_2 = 2*lambda_1000*Q/(w_2^2 * h_2)

%% Elasticity

El_1000_1 = Wi_1000_1/Re_1000_1
El_1000_2 = Wi_1000_2/Re_1000_2

%% Pressure Drop

deltaP_psi_1 = [128*mu_1000*L*Q/(pi*Dh_1^4)]/6894.76
deltaP_psi_2 = [128*mu_1000*L*Q/(pi*Dh_2^4)]/6894.76

%% Blocakge ratio

beta1_4 = ap_4 / h_1
beta1_7 = ap_7 / h_1
beta1_15 = ap_15 / h_1

beta2_4 = ap_4 / h_2
beta2_7 = ap_7 / h_2
beta2_15 = ap_15 / h_2

%% Plots

figure (1);
hold on
plot (Q, Re_1000_1)
plot (Q, Re_1000_2)
legend ("Reynolds 50um x 30um","Reynolds 75um x 30um")

figure (2);
hold on
```

```
plot (Q, Wi_1000_1)
plot (Q, Wi_1000_2)
legend ("Weissemberg 50um x 30um","Weissemberg 75um x 30um")

%% Particles concentration

C_4 = (6 * W * 10^12)/(ro * pi * ap_4^3)
C_7 = (6 * W * 10^12)/(ro * pi * ap_7^3)
C_15 = (6 * W * 10^12)/(ro * pi * ap_15^3)

V1_4 = (1*10^6 * 10)/C_4
V1_7 = (1*10^6 * 10)/C_7
V1_15 = (1*10^6 * 2.5)/C_15

%% Particles concentration for 4 + 15 um

V1_4 = (1*10^6 * 2.5)/C_4
V1_15 = (0.5*10^6 * 2.5)/C_15
```

R codes:

```
library(ggplot2)
library(ggpubr)
library(dplyr)
library(tidyverse)
db <- Focusing_efficiencies

p4 <- db[db$part_dim=="4",]
p4.50 <- p4[p4$diameter=="50x30mm",]
ggplot(p4.50, aes(x=q, y=s1)) + geom_line(linetype = 4, color = "darkblue") +
geom_point(size=2, color = "darkblue") + xlab("Flow Rate (uL/min)") +
ylab("Focusing Efficiency (%)") + ggtitle("4um particles in a 50x30mm channel")
+theme_pubr(border=T) + theme(plot.title = element_text(size = 12))
ggplot(p4.50, aes(x=q, y=s1)) + geom_line(linetype = 4, color = "darkblue") +
geom_point(size=2, color = "darkblue") + xlab("Flow Rate (uL/min)") +
ylab("Focusing Efficiency (%)") + ggtitle("4um particles in a 50um x 30um channel")
+theme_pubr(border=T) + theme(plot.title = element_text(size = 12)) +
scale_x_continuous(breaks = c(5,10,15,20,25,30,40,50)) + scale_y_continuous(breaks
= c(50,60,70,80,90,100), limits = c(50, 100))

p4 <- db[db$part_dim=="4",]
p4.75 <- p4[p4$diameter=="75x30mm",]
ggplot(p4.75) + geom_line(aes(x=q, y=mean), linetype = 4, color = "darkblue") +
geom_point(aes(x=q, y=mean), size = 2, color = "darkblue") + geom_point(aes(x=q,
y=s1), size = 2, shape = 1, color = "darkblue") + geom_point(aes(x=q, y=s1a), size
= 2, shape = 1, color = "black") + geom_point(aes(x=q, y=s2), size = 2, shape = 2,
color = "darkblue") + geom_point(aes(x=q, y=s2a), size = 2, shape = 2, color =
"black") + geom_point(aes(x=q, y=s3), size = 2, shape = 3, color = "darkblue") +
geom_point(aes(x=q, y=s3a), size = 2, shape = 3, color = "black") +
geom_point(aes(x=q, y=s4), size = 2, shape = 4, color = "darkblue") +
geom_point(aes(x=q, y=s4a), size = 2, shape = 4, color = "black") +
geom_point(aes(x=q, y=s5), size = 2, shape = 5, color = "darkblue") +
geom_point(aes(x=q, y=s5a), size = 2, shape = 5, color = "black") + xlab("Flow Rate
(uL/min)") + ylab("Focusing Efficiency (%)") + ggtitle("4um particles in a 75um x
30um channel") +theme_pubr(border=T) + theme(plot.title = element_text(size = 12))
+ scale_x_continuous(breaks = c(5,10,15,20,25,30,40,50)) +
scale_y_continuous(breaks = c(50,60,70,80,90,100), limits = c(50, 100))

p7 <- db[db$part_dim=="7",]
p7.c.50 <- p7[p7$diameter=="50x30mm",]
ggplot(p7.c.50, aes(x=q, y=s1)) + geom_line(linetype = 4, color = "darkred") +
geom_point(size=2, color = "darkred") + xlab("Flow Rate (uL/min)") + ylab("Focusing
Efficiency (%)") + ggtitle("7um particles in a 50um x 30um channel")
+theme_pubr(border=T) + theme(plot.title = element_text(size = 12)) +
scale_x_continuous(breaks = c(5,10,15,20,25,30,40,50)) + scale_y_continuous(breaks
```

```
= c(50,60,70,80,90,100), limits = c(70, 100))

p7 <- db[db$part_dim=="7",]
p7.c.75 <- p7[p7$diameter=="75x30mm",]
ggplot(p7.c.75) + geom_line(aes(x=q, y=mean), linetype = 4, color = "darkred") +
geom_point(aes(x=q, y=mean), shape=16, color = "darkred") + geom_point(aes(x=q,
y=s1), shape=1, size=2, color = "darkred") + geom_point(aes(x=q, y=s2), shape=2,
size=2, color = "darkred") + geom_point(aes(x=q, y=s3), shape=3, size=2, color =
"darkred") + geom_point(aes(x=q, y=s3a), shape=3, size=2, color = "black") +
geom_point(aes(x=q, y=s4), shape=5, size=2, color = "darkred") + xlab("Flow Rate
(uL/min)") + ylab("Focusing Efficiency (%)") + ggtitle("7um particles in a 75um x
30um channel") +theme_pubr(border=T) + theme(plot.title = element_text(size = 12))
+ scale_x_continuous(breaks = c(5,10,15,20,25,30,40,50)) +
scale_y_continuous(breaks = c(50,60,70,80,90,100), limits = c(60, 100))

p15 <- db[db$part_dim=="15",]
p.15.c.75 <- p15[p15$diameter=="75x30mm",]
ggplot(p.15.c.75) + geom_line(aes(x=q, y=mean), linetype = 4, color = "darkgreen")
+ geom_point(aes(x=q, y=s1), size=2, shape = 1, color = "darkgreen") +
geom_point(aes(x=q, y=s2), size=2, shape = 2, color = "darkgreen") +
geom_point(aes(x=q, y=s3), size=2, shape = 3, color = "darkgreen") +
geom_point(aes(x=q, y=s3a), size=2, shape = 3, color = "black") +
geom_point(aes(x=q, y=s4), size=2, shape = 6, color = "darkgreen") +
geom_point(aes(x=q, y=mean), size=2, shape = 16, color = "darkgreen") + xlab("Flow
Rate (uL/min)") + ylab("Focusing Efficiency (%)") + ggtitle("15um particles in a
75um x 30um channel") +theme_pubr(border=T) + theme(plot.title = element_text(size
= 12)) + scale_x_continuous(breaks = c(5,10,15,20,25,30,40,50)) +
scale_y_continuous(breaks = c(50,60,70,80,90,100), limits = c(70, 100))
ggplot(p.15.c.75) + geom_line(aes(x=q, y=mean), linetype = 4, color = "darkgreen")
+ geom_point(aes(x=q, y=s1), size=2, shape = 1, color = "darkgreen") +
geom_point(aes(x=q, y=s2), size=2, shape = 2, color = "darkgreen") +
geom_point(aes(x=q, y=s2a), size=2, shape = 5, color = "black") +
geom_point(aes(x=q, y=s2b), size=2, shape = 17, color = "black") +
geom_point(aes(x=q, y=s3), size=2, shape = 10, color = "darkgreen") +
geom_point(aes(x=q, y=mean), size=2, shape = 16, color = "darkgreen") + xlab("Flow
Rate (uL/min)") + ylab("Focusing Efficiency (%)") + ggtitle("15um particles in a
75um x 30um channel") +theme_pubr(border=T) + theme(plot.title = element_text(size
= 12)) + scale_x_continuous(breaks = c(5,10,15,20,25,30,40,50)) +
scale_y_continuous(breaks = c(50,60,70,80,90,100), limits = c(70, 100))

p15 <- db[db$part_dim=="15",]
p.15.c.50 <- p15[p15$diameter=="50x30mm",]
ggplot(p.15.c.50) + geom_line(aes(x=q, y=mean), linetype = 4, color = "darkgreen")
+ geom_point(aes(x=q, y=s1), size=2, shape = 1, color = "darkgreen") +
geom_point(aes(x=q, y=s2), size=2, shape = 2, color = "darkgreen") +
geom_point(aes(x=q, y=s3), size=2, shape = 5, alpha = 0.2, color = "darkgreen")+
geom_point(aes(x=q, y=mean), size=2, shape = 16, color = "darkgreen") + xlab("Flow
Rate (uL/min)") + ylab("Focusing Efficiency (%)") + ggtitle("15um particles in a
50um x 30um channel") +theme_pubr(border=T) + theme(plot.title = element_text(size
= 12)) + scale_x_continuous(breaks = c(5,10,15,20,25,30,40,50)) +
scale_y_continuous(breaks = c(90,100), limits = c(90, 100))

#prova fica

db.long <- db %>% pivot_longer(-c(part_dim, diameter, q), names_to = "streamlines",
values_to = "efficiency")
db.long %>% group_by(part_dim, diameter, q) %>% get_summary_stats(efficiency)
db.long %>% ggplot(aes(x = q, y = efficiency)) + geom_point(aes(color =
as.factor(part_dim), size = diameter, shape = as.factor(q)))
```